Master's thesis
Geology
Petrology and Economic Geology

GEOCHEMICAL AND PALEOMAGNETIC CONSTRAINTS ON MID-PROTEROZOIC MAFIC DYKE EMPLACEMENT EVENTS IN SOUTHERN FINLAND

Katja Bohm

2018

Supervisors:
Arto Luttinen, Johanna Salminen

UNIVERSITY OF HELSINKI
FACULTY OF SCIENCE
DEPARTMENT OF GEOSCIENCES AND GEOGRAPHY

PL 64 (Gustaf Hällströmin katu 2)
00014 Helsingin yliopisto

HELSINGIN YLIOPISTO
HELSINGFORS UNIVERSITET
UNIVERSITY OF HELSINKI

Tiedekunta/Osasto – Fakultet/Sektion – Faculty Faculty of Science	Laitos/Institution– Department Department of Geosciences and Geography	
Tekijä/Författare – Author Katja Bohm		
Työn nimi / Arbetets titel – Title Geochemical and paleomagnetic constraints on mid-Proterozoic mafic dyke emplacement events in southern Finland		
Oppiaine /Läroämne – Subject Geology		
Työn laji/Arbetets art – Level Master's Thesis	Aika/Datum – Month and year 10/2018	Sivumäärä/ Sidoantal – Number of pages 86

Tiivistelmä/Referat – Abstract

Mid-Proterozoic mafic dyke swarms in southern Finland are associated with rapakivi magmatism. The dyke swarms are commonly referred to as "Subjotnian" (1.64–1.54 Ga), being older than the rift-filling Jotnian sandstones. Mafic rocks from five dyke swarms located in Åland, Satakunta, Häme, Suomenniemi and Sipoo were studied in this thesis.

An X-ray fluorescence (XRF) analysis was made of 110 rock samples from 101 mafic dykes and one mafic intrusion. The analyses were made of the same rock samples as previous paleomagnetic studies.

Overall, the Subjotnian mafic dykes in southern Finland are hyperstene-normative tholeiitic basalts or basaltic andesites with varying MgO contents (3–15 wt%). Some dykes show alkaline features with higher total alkali and/or Nb/Y values. They vary from quartz- to olivine-normative types. The dykes of the Åland swarm form two geohemical groups. The division is accompanied with a switch in magnetic polarity and distinct virtual geomagnetic pole positions. These observations imply that two separate magmatic events/pulses that have an age difference have taken place in Åland. The Satakunta dykes form two geochemical groups of which the other includes presumably Svecofennian dykes that show high Nb/Y values at given Zr/Y ratios. The dykes of the Häme swarm form three geochemical groups. Although some Suomenniemi dykes show geochemical and paleomagnetic affinities to Häme dykes, they probably represent a distinct igneous event of the event that formed the nearby Häme swarm. The Sipoo dykes are very homogeneous in their geochemistry and can be distinguished from the emplacement events that formed the other Subjotnian swarms.

The Subjotnian dyke swarms in southern Finland that are believed to have emplacement ages of >1.63 Ga (Häme, Suomenniemi and Sipoo swarms in S-SE Finland) generally have higher Nb/Y (and Zr/Y) values than the dyke swarms that are believed to record younger magmatic events at <1.58 Ga (Åland and Satakunta swarms in SW Finland). Some Satakunta dykes, however, have geochemical and/or paleomagnetic implications that suggest they have an older Subjotnian age than the dated 1.57 Ga dyke in Satakunta. Further chronological work on the Satakunta dyke swarm is needed to verify the age of the dykes.

Many of the Subjotnian dykes show a secondary magnetization component, called the "B-component", whose direction is always close to, but distinct of, the Present Earth Field (PEF) at the sampling location. There was no correlation between the B-component and the magma types of the dykes. The B-component occurs mostly in dykes that are very altered. Thus, the results support previous suggestions that the B-component formed due to hydrothermal alteration of the rocks and the subsequent formation of new magnetic minerals.

Avainsanat – Nyckelord – Keywords
Mid-Proterozoic, Subjotnian, Åland, Satakunta, Häme, Suomenniemi, Sipoo, Dyke swarm, Mafic dyke, Diabase, Rapakivi, Geochemistry, XRF, Paleomagnetism, Virtual geomagnetic pole

Säilytyspaikka – Förvaringställe – Where deposited
University of Helsinki

Muita tietoja – Övriga uppgifter – Additional information

HELSINGIN YLIOPISTO
HELSINGFORS UNIVERSITET
UNIVERSITY OF HELSINKI

Tiedekunta/Osasto – Fakultet/Sektion – Faculty Matemaattis-luonnontieteellinen tiedekunta	Laitos/Institution– Department Geotieteiden ja maantieteen laitos	
Tekijä/Författare – Author Katja Bohm		
Työn nimi / Arbetets titel – Title Geokemiallisia ja paleomagneettisia todisteita eteläisen Suomen keskiproterotsooisten mafisten juonien syntyvaiheisiin		
Oppiaine /Läroämne – Subject Geologia		
Työn laji/Arbetets art – Level Pro Gradu	Aika/Datum – Month and year 10/2018	Sivumäärä/ Sidoantal – Number of pages 86

Tiivistelmä/Referat – Abstract

Keskiproterotsooiset mafiset juoniparvet eteläisessä Suomessa liittyvät rapakivimagmatismiin. Näitä juoniparvia kutsutaan ”subjotunisiksi” (1,64–1,54 Ga), koska ne edeltävät jotunisia hiekkakiviä. Tässä työssä tutkittiin mafisia juonia viidestä eri juoniparvesta, jotka sijaitsevat Ahvenanmaalla, Satakunnassa, Hämeessä, Suomenniemellä ja Sipoossa.

Yhteensä 110 kivinäytteelle, jotka oli aiemmin kerätty 101 mafisesta juonesta ja yhdestä mafisesta intruusiosta, tehtiin röntgenfluoresenssianalyysi (XRF). Samoja näytteitä oli aiemmin käytetty paleomagneettisissa tutkimuksissa.

Yleistäen eteläisen Suomen subjotuniset mafiset juonet ovat hypersteeni-normatiivisia tholeiittisia basaltteia ja basalttisia andesiitteja. Joillakin juonilla on alkalisia piirteitä, jotka ilmenevät kohonneina alkalipitoisuuksina ja/tai Nb/Y-arvoina. Juonien MgO pitoisuudet ovat vaihtelevia (3–15 wt%), ja niiden normatiivinen koostumus vaihtelee kvartsinormatiivisista oliviininormatiivisiin tyyppeihin. Ahvenanmaan juonet jakautuvat kahteen geokemialliseen ryhmään, joilla on pääsääntöisesti myös erilaiset magneettiset polariteetit ja virtuaalisten geomagneettisten napojen sijainnit. Nämä havainnot viittaavat kahteen eri-ikäiseen magmaattiseen tapahtumaan Ahvenanmaalla. Satakunnan juonet muodostavat kaksi geokemiallista ryhmää. Toiseen ryhmään kuuluu oletettavasti svekofennisiä juonia, joilla on selkeästi korkeammat Nb/Y-arvot tietyillä Zr/Y-arvoilla kuin subjotunisilla juonilla. Hämeen juonet muodostavat kolme geokemiallista ryhmää. Joillakin Suomenniemen juonilla on geokemiallisia ja paleomagneettisia yhteneväisyyksiä Hämeen juonien kanssa, mutta todennäköisesti Suomenniemen juonet edustavat läheisen Hämeen juoniparven synnyttäneestä tapahtumasta erillistä magmaattista tapahtumaa. Sipoon juonet muodostavat hyvin homogeenisen geokemiallisen ryhmän, joka erottuu selkeästi muiden subjotunisten juonien geokemiasta. Sipoon juonien voidaan tässä mielessä ajatella edustavan magmaattista intruusiota, joka on erillinen niistä tapahtumista, jotka muodostivat muut tämän tutkimuksen juoniparvet.

Niillä eteläisen Suomen subjotunisilla juonilla, joiden on ajateltu muodostuneen >1,63 Ga (Hämeen, Suomenniemen ja Sipoon parvet Etelä- ja Kaakkois-Suomessa), on yleisesti ottaen korkeammat Nb/Y- ja Zr/Y-arvot kuin niillä juonilla, joiden on ajateltu kuuluvan nuorempiin, <1,58 Ga muodostuneisiin parviin (Ahvenanmaan ja Satakunnan juoniparvet Lounais-Suomessa). Osalla Satakunnan juonista on kuitenkin geokemiallisia ja/tai paleomagneettisia ominaisuuksia, jotka viittaavat niiden olevan vanhempia subjotunisia kuin Satakunnan iätetty 1,57 Ga juoni. Näiden juonien ikien varmistamiseksi tulisi kuitenkin tehdä uusia tarkkoja iänmäärityksiä Satakunnan juoniparvelle.

Monilla tämän tutkimuksen juonilla on havaittu sekundäärisen magnetoituman komponentti, ”B-komponentti”, jonka suunta on aina lähellä (mutta selkeästi eriävä) Maan magneettikentän tämänhetkistä suuntaa kullakin näytteenottopaikalla. Tässä tutkimuksessa ei havaittu yhteneväisyyksiä B-komponentin ja tietyn magmatyypin välillä. Sen sijaan B-komponentin havaittiin esiintyvän erityisesti hyvin muuttuneilla juonilla. Tämä tutkimus tukee aiempien tutkimusten havaintoja siitä, että B-komponentin synty liittyy kivien hydrotermiseen muuttumiseen ja siitä johtuvaan uusien magneettisten mineraalien syntyyn.

Avainsanat – Nyckelord – Keywords
Keskiproterotsooinen, Subjotuninen, Ahvenanmaa, Satakunta, Häme, Suomenniemi, Sipoo, Juoniparvi, Mafinen juoni, Diabaasi, Rapakivi, Geokemia, XRF, Paleomagnetismi, Virtuaalinen geomagneettinen napa

Säilytyspaikka – Förvaringställe – Where deposited
Helsingin yliopisto

Muita tietoja – Övriga uppgifter – Additional information

Table of contents

1. INTRODUCTION

Precambrian mafic dyke swarms are important sources of information when studying continental drift and magma systems related to crustal extension, mantle plumes and breakup of continents (e.g. Ernst and Buchan 1997; Bleeker and Ernst 2006). Mafic dyke swarms represent the plumbing system for the voluminous mantle-derived magmas that produce large igneous provinces (LIPs) (e.g. Ernst and Buchan 1997). LIPs are targets of multidisciplinary research by paleomagnetic, geochemical and geochronological methods. They can provide essential information not only on mantle plumes and mantle behaviour through Earth history but also on breakup of continents and supercontinent cycles (i.e. the cycles of continental crust aggregation and dispersal) (Courtillot et al. 1999; Ernst and Buchan 2001; Bleeker 2004; Bryan and Ernst 2008; Ernst et al. 2008). LIPs can also be used in constraining paleocontinental reconstructions (e.g. Bleeker and Ernst 2006). Furthermore, research on LIPs is necessary because they involve economic mineral deposits and have had a catastrophic impact on the climate and the biosphere (Bryan and Ernst 2008). Mafic dyke swarms are sometimes the only major remnants of LIPs of pre-Mesozoic age since erosion and tectonics have commonly removed most of the volcanic rocks of these events (Ernst and Buchan 1997). Mafic dyke swarms are thus essential components of the research on LIPs and their origin.

Mid-Proterozoic mafic dyke swarms in southern Finland from five different localities are studied in this thesis: the Åland, Satakunta, Häme, Suomenniemi and Sipoo swarms. These dyke swarms are associated with rapakivi granites (Laitakari 1969; Ehlers and Ehlers 1977; Laitala 1984; Pihlaja 1987; Rämö 1991) and they may be the early manifestations of rifting related to the attempted breakup of the 1.8–1.3 Ga Nuna (Columbia, Hudsonland; Meert 2002; Rogers and Santosh 2002; Zhao et al. 2004; Meert 2012; Evans 2013 and references therein) supercontinent (Salminen et al. 2014; 2016; 2017; 2018).

According to published age data, the five dyke swarms in southern Finland split into two age groups, so that the U-Pb ages of the Åland and Satakunta swarms in SW Finland range between 1576–1565 Ma (Lehtonen et al. 2003; Salminen et al. 2016 and references therein) and the U-Pb ages of the swarms in SE Finland, the Häme, Suomenniemi and Sipoo swarms, range between 1646–1633 Ma (Törnroos 1984; Laitakari 1987; Siivola

1987; Salminen et al. 2017). The recent paleomagnetic results of these dyke swarms challenge this chronological division, however, as one of the two paleomagnetic poles obtained from the Satakunta dykes (pole SK2; Salminen et al. 2014) shows a similar magnetization age to the Häme pole (Salminen et al. 2017). The other paleomagnetic pole from Satakunta (pole SK1; Salminen et al. 2014) is similar to paleomagnetic pole of Åland (Salminen et al. 2016) as is expected for the nearly coeval poles.

Among the dyke swarms in SE Finland, the roughly coeval paleomagnetic poles of Häme, Suomenniemi and Sipoo swarms are distinct (Mertanen and Pesonen 1995; Salminen et al. 2017; 2018). Possible explanations are age differences accompanied with continental drift and/or problems with the paleomagnetic data (Salminen et al. 2018).

Many paleomagnetic records of Precambrian Baltica also show a secondary paleomagnetic component (Mertanen and Pesonen 1995; Elming et al. 2009; Preeden et al. 2009; Lubnina et al. 2010; Salminen et al. 2014; 2016; 2017; 2018), which is always nearly parallel to the Present Earth Field direction (PEF) in the sampling area and which seems to come from the most altered dykes (e.g. Salminen et al. 2014). Later in this text, this component will be referred to as ‘B-component’ (Mertanen and Pesonen 1995) to distinguish it from other secondary components, such as PEF.

One aim of this work is to use geochemical analyses of the five mafic dyke swarms in southern Finland to recognize chemically different magma types that may represent distinct magmatic events. The geochemical data can enhance the interpretation of paleomagnetic data if some dykes can be added to or removed from paleomagnetic pole calculations. Distinguishing magmatic events by using the geochemical data can be done by critically evaluating the chemical compositions of the mafic dykes, especially their trace element ratios. Magmatic differentiation has a relatively strong effect on the major element contents of mafic dykes, but the ratios of incompatible elements remain relatively unchanged after these processes and can thus be used as geochemical fingerprints of the original magmas.

Rather few detailed studies on the geochemistry of the Finnish mid-Proterozoic mafic dyke swarms have been published (Rämö 1991; Eklund et al. 1994; Lehtonen et al. 2003; Lindholm 2010), and only one study (Salminen et al. 2014) has combined geochemical

and paleomagnetic data. Reliable high-precision geochronological data are also sparse. In this study, an X-ray fluorescence (XRF) analysis was made of 110 samples from 101 mafic dykes and one mafic intrusion of the five dyke swarms. The geochemistry was compared with the previously published paleomagnetic data (Mertanen and Pesonen 1995; Salminen et al. 2014; 2016; 2017; 2018) of the dyke swarms. The same rock samples were used for the geochemical (this study) and paleomagnetic (previous studies) studies.

There are several questions this study aims to address by using geochemical analyses: Does the variation in paleomagnetic data manifest itself also in geochemistry? Why the paleomagnetic pole of Häme dyke swarm is distinct from the roughly coeval poles of Sipoo and Suomenniemi dyke swarms? Are the Åland and Satakunta mafic dykes part of the same swarm with similar geochemical fingerprints? Are the Satakunta dyke swarm and the Häme dyke swarm consanguineous? Is the geographical division of the five dyke swarms thus also valid petrogenetically and/or chronologically? What is the reason for the pervasive overprinted magnetization component (the B-component) for some of the mafic dykes of these swarms?

2. MAFIC DYKES

2.1. Large igneous provinces and continental flood basalts

Continental flood basalts (CFBs) are one type of continental LIPs (Bryan and Ernst 2008). The definition of LIPs, according to Bryan and Ernst (2008), is as follows: LIPs "are magmatic provinces with areal extents >0.1 Mkm^2, igneous volumes >0.1 Mkm^3 and maximum lifespans of ~50 Myr that have intraplate tectonic settings or geochemical affinities, and are characterised by igneous pulse(s) of short duration (~1–5 Myr), during which a large proportion (>75%) of the total igneous volume has been emplaced." The Proterozoic LIPs are commonly deeply eroded, consisting of the plumbing system manifested by dyke swarms, sill provinces and layered intrusions and showing only minor remnants of the actual flood basalts (Ernst et al. 2008).

CFBs exist on every continent and form typically in extensional tectonic settings and by continental rifting (Winter 2001). While oceanic LIPs are often quite homogenic in their geochemistry, continental LIPs have more varieties (e.g. Bryan and Ernst 2008). Most continental LIPs are compositionally bimodal with mafic and silicic igneous rock occurrences that range from low-Ti to high-Ti magma types (e.g. Bryan and Ernst 2008). CFBs are commonly tholeiitic basalts, but alkaline types and evolved differentiates are also represented (Winter 2001). Generalized, CFBs are evolved with high Si, Fe, Ti and K contents, low (<60) Mg numbers [atomic 100*Mg/(Mg+Fe^{2+})] and low contents of compatible elements (Ni, Cr) relative to primary mantle-derived magmas (e.g. Winter 2001; Bryan and Ernst 2008).

The origin of CFBs is problematic. Variable isotope and trace element geochemistry suggests a diverse range of mantle sources for CFBs. Some CFBs have trace element geochemistry that resembles ocean island basalts (OIB) or enriched mid-ocean ridge basalts (E-MORB). They have relatively high concentrations of incompatible elements, such as large-ion lithophile elements (LIL) and light rare earth elements (LREE), and resemble plume-related magmatism in this respect (e.g. Winter 2001). Other CFBs have incompatible trace element ratios notably similar to those of island arc basalts (IAB) with, for example, low Nb and Ti and high La contents that could be due to crustal contamination (Heinonen et al. 2016; Luttinen 2018). Commonly observed enriched isotopic signatures point to crustal contamination (Arndt et al. 1993), subcontinental lithospheric mantle (SCLM) sources (Gallagher and Hawkesworth 1992) or subduction-modified mantle sources (Merle et al. 2014; Wang et al. 2015).

2.2. Geochemical research of mafic dykes

The chemical composition of magma differentiates as it goes through processes in the mantle and in the crust. Partial melting of the mantle peridotite generates primary magmas. The primary magmas subsequently evolve due to crystallization of some minerals (e.g. olivine), and the separation of these crystals from the melt. The process leads to the formation of evolved magmas that have differentiated chemical compositions when compared to the primary magma. Fractional crystallization of olivine for example, enriches the melt in K and Na and depletes it in Mg (e.g. Cox et al. 1981). Furthermore,

some elements (e.g. Sr, Rb, Nb, Zr, Ce, La) are more incompatible and prefer to stay in the liquid phase during crystallization, while some are compatible (e.g. Ni, Cr) and prefer the crystal structures of certain minerals (e.g. Cox et al. 1981). Thus, lower concentrations of compatible elements, for example, imply the magma has gone through fractional crystallization and is not a primary magma. Incompatible elements however are not affected by this differentiation as much as the compatible ones, although some incompatible elements may change to compatible during the magmatic evolution (Cox et al. 1981). The ratios of incompatible elements (such as Nb/Y or Zr/Y), however, are rather stable in the process of fractional crystallization.

Besides fractional crystallization and resultant accumulation of minerals, crustal contamination and hydrothermal alteration can also affect the composition of mafic magmas. Accumulation of e.g. olivine through gravitational settling produces a cumulate rock that is not representative of the original melt. Magmatic differentiation through crystallization does not significantly change the ratios of incompatible elements, which is why these ratios are commonly used when evaluating the mantle sources of mafic magmas. Crustal contamination in basalts on the other hand commonly changes the chemical element ratios so that, for example, La/Nb becomes higher and Ti/Zr becomes lower (Heinonen et al. 2016; Luttinen 2018). Hydrothermal alteration is indicated usually by the mobility of e.g. Na, K, Rb, Cs, Sr, Ba and P, but elements such as Ti, Zr, Nb, Y and the heavy rare earths are not affected by it (e.g. Pearce and Cann 1973; Winchester and Floyd 1976; Cox et al. 1981). Hydrothermal alteration depends not only on the mineralogy of the rocks, but also on the physical properties of the rock, such as vesicularity and volatile content.

Mafic dykes are good targets for geochemical studies because they are typically well-preserved compared to mafic lavas and have not been as strongly altered by subsolidus hydrothermal alteration as lavas due to lower vesicularity. The magmatic evolution of mafic dykes also tends to be relatively simple compared to felsic igneous rocks.

A combined set of major element, trace element, and isotopic data comprises a unique geochemical fingerprint of mafic dykes. By using geochemical fingerprints, it is theoretically possible to identify individual batches of magmas that have been derived from a magma plumbing system and that represent distinctive magmatic events of a single

period of intrusive activity. Geochemical fingerprinting is therefore a relatively economic method of grouping of numerous and widespread mafic dykes into provisional coeval magmatic suites. Such grouping is a prerequisite to petrological research of mafic dyke swarms and it can provide essential supportive information for geochronological and paleomagnetic research.

2.3. Paleomagnetic research of mafic dykes

The paleomagnetism of mafic dykes is based on 1) the magnetic minerals that block the direction of the Earth's magnetic field during the cooling of the magma and 2) the stable nature of the direction obtained from the dykes and its persistence through prolonged geological time. The primary magnetic minerals in mafic dykes often have small grain sizes which enhances the stability of the magnetization over big grain sizes (e.g. McElhinny 1973 and references therein). For mafic dykes, the direction of the Earth's magnetic field is locked in the magnetic minerals when their temperature decreases below the Curie point of each mineral (e.g. McElhinny 1973). This is called the primary magnetization component of the rock and it forms by thermoremanent magnetization (TRM). The primary component can last in the rocks over the geological time-scale if no extensive heating (TRM) or metamorphosis (chemical remanent magnetization, CRM; thermochemical remanent magnetization, TCRM) occurs (e.g. McElhinny 1973). Later geological events can overprint the primary magnetization direction.

Rocks are often partially remagnetized and show secondary magnetization components that form by CRM. By using adequate demagnetization methods, the magnetization components can be separated from the rock sample. Their primary nature can be verified with field tests. Commonly used field test in the case of mafic dykes is the baked contact test (Everitt and Clegg 1962). The contact zone of the host rock is heated (baked) by the mafic dyke near or above the Curie temperature of the magnetic minerals, which results in a similar magnetization direction for both the dyke and the contact zone of the host rock. Further away from the contact, the magnetization direction of the host rocks is different as these rocks were not heated by the dyke intrusion (TRM) (Everitt and Clegg 1962).

By using the direction of the remanent magnetization in addition to the coordinates of the sampling site, the location of a virtual geomagnetic pole (VGP) can be obtained. A pole calculated for one cooling unit (=one dyke) is called a virtual geomagnetic pole, because it does not average out the secular variation of the geomagnetic field (e.g. McElhinny 1973). A VGP shows the position of the pole of a geocentric dipole and its corresponding magnetic field direction at one location at one point in time (Butler 1992). Secular variation is the change in magnetic field with time and it occurs dominantly during $\leq 10^5$ years intervals, although any cyclicity cannot be assumed nor any predictions made (Butler 1992). If the secular variation is averaged out, the geocentric dipole coincides with the Earth's rotation axis, which is the basis of the Geocentric Axial Dipole (GAD) hypothesis (Hospers 1954) and the calculations of paleomagnetic poles. Paleomagnetic poles are calculated from the mean of VGPs.

VGPs can differ from the paleomagnetic poles as much as 15°–20° (e.g. McElhinny and McFadden 2000). Paleosecular variation during the last 5 m.y. shows that the amount of dispersion of VGPs depends on the site latitude, increasing from equator towards pole by almost a factor of two (Butler 1992). During the early Mesoproterozoic, Baltica was located in equatorial latitudes (e.g. Salminen et al. 2016).

Paleomagnetism is the only quantitative tool for paleocontinental reconstructions. Essential for the reconstructions is the concept of key paleomagnetic poles (Buchan et al. 2000; Buchan 2013). Key poles are the paleomagnetic poles that are precisely dated and the magnetization is proven primary by field tests (Buchan 2013). Only good quality poles, preferably key poles, should be used when constructing apparent polar wander paths (APWPs) and drift of continents.

The dipolar geomagnetic field also switches its polarity in unpredictable time intervals (e.g. Butler 1992). In Northern Hemisphere, normal (N) polarity is conventionally referred to as the downward north-seeking magnetization direction and reversed (R) polarity as the upward south-seeking direction. The time-averaged geomagnetic field direction differs by 180° between the two different polarities. The average duration of polarity intervals has been ~0.25 m.y. during the last 5 m.y., but there is much variation in the duration and the intervals are randomly distributed in the geological time scale

(Butler 1992). The duration of a transition is usually quick (probably <5000 years; Butler 1992).

Mafic dyke swarms comprise a target for the multidisciplinary research of paleocontinents and their reconstructions. Paleomagnetic data are essential for quantifying the ancient positions of continents and chronological data gives the absolute time frame for the reconstructions. Additional geochemical data can then enhance the interpretation of paleomagnetic data by allowing individual igneous events to be distinguished from others.

3. GEOLOGICAL SETTING AND BACKGROUND

3.1. Mid-Proterozoic rapakivi magmatism in southern Finland

Rapakivi granites occur on every continent (Rämö and Haapala 1995) and their temporal distribution worldwide may be coeval with supercontinent cycles (e.g. Rämö and Haapala 1995; Åhäll et al. 2000). In southern Finland, mid-Proterozoic mafic dyke swarms are associated with rapakivi granite batholiths in various places (Figure 1). The bimodal intrusions crosscut Paleoproterozoic (1.9–1.8 Ga) Svecofennian bedrock (Rämö and Haapala 2005). There are four large rapakivi batholiths (Wiborg, Åland, Laitila and Vehmaa) and a group of smaller plutons (e.g. Ahvenisto, Suomenniemi, Onas, Bodom, Obbnäs, Eurajoki) in Finland (e.g. Rämö and Haapala 2005).

The Finnish occurrences are part of a larger province of rapakivi granites that extends from central Sweden to the Salmi rapakivi intrusion in Russian Karelia and to Poland in the south. Available chronological data suggest that the Finnish rapakivi granites can be divided into two groups, where the older 1.65–1.62 Ga group is positioned between the younger 1.58–1.54 Ga group in SW Finland and the 1.54 Ma old (Neymark et al. 1994) Salmi batholith in Russian Karelia (Rämö and Haapala 2005). A study from the Vehmaa rapakivi batholith (Shebanov et al. 2000), however, suggests that the core of the ovoids typical of rapakivi granites has a U-Pb (zircon) age of 1630 Ma (error limits unavailable), while the matrix has a U-Pb (zircon) age of 1573 Ma (error limits unavailable). This connects the intrusive suite of SW Finland to the intrusions in SE Finland

geochronologically by indicating that magmatic activity existed also in SW Finland at roughly the same time as in SE Finland.

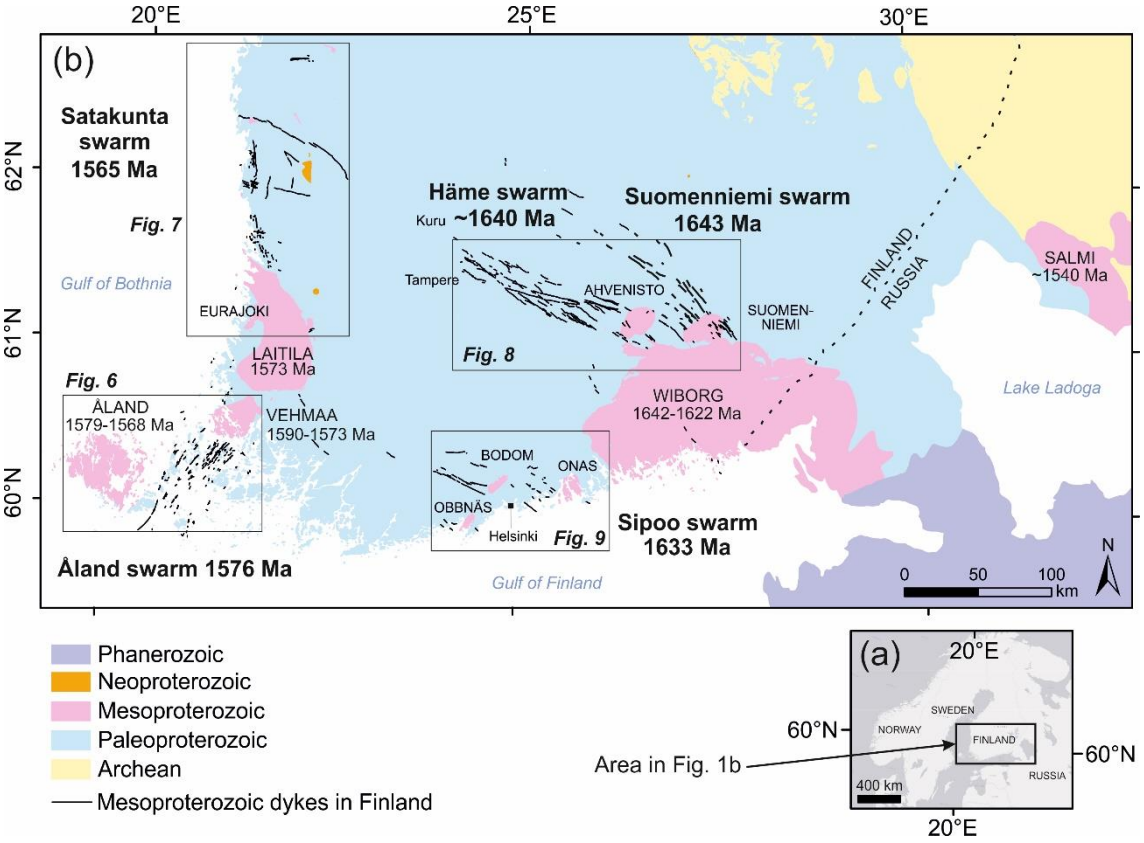

Figure 1. Generalized geological map of southern Finland and adjacent areas with the locations of the dyke swarms of this study. See text for age references.

The Finnish rapakivi granites occur as sheet-like bodies (Luosto et al. 1990) that have formed in several emplacement events (Rämö and Haapala 2005). According to the prevailing model, rapakivi magmatism in Finland was generated by the heating and melting of the Paleoproterozoic crust by underplating of partial melts from the mantle (e.g. Rämö and Haapala 2005). This mantle material is now manifested by the mafic dykes, plutons and minor volcanics of the bimodal association. The rapakivi granites were emplaced in an extensional tectonic environment where the associated dykes mostly intruded into previously formed cracks (Laitakari and Leino 1989). Mafic dykes are observed to cut the rapakivi granites in Åland (Bergman 1981) and in Suomenniemi (Rämö 1991), but this is not observed in the other dyke swarms of this study. Felsic dykes are also commonly present which, together with the rapakivi granites, mark the melting

of the Paleoproterozoic Svecofennian crust (e.g. Rämö 1991) with possible minor contribution from mantle-derived melts (Heinonen et al. 2010a). Based on Hf-isotopes, Heinonen et al. (2010a) suggest the primary origin for the gabbro-anorthositic rocks associated with southern Finnish rapakivi granites was an ambient depleted upper mantle and that the mafic magmas were modified by considerable crustal and/or sub-continental lithospheric mantle (SCLM) contamination.

3.2. Geochemical and paleomagnetic features of the Subjotnian dykes

The mid-Proterozoic dyke swarms in Fennoscandia are usually referred to as "Subjotnian" (ca. 1.65–1.54 Ga), being older than the rift-filling Jotnian sandstones in Satakunta. In this study, samples from five Subjotnian dyke swarms are analysed: the Åland, Satakunta, Häme, Suomenniemi and Sipoo swarms (Figure 1). The ages for the Satakunta and Åland mafic swarms range between 1576–1565 Ma (Lehtonen et al. 2003; Salminen et al. 2016 and references therein) and the ages for the Häme, Suomenniemi and Sipoo swarms between 1646–1633 Ma (Törnroos 1984; Laitakari 1987; Siivola 1987; Salminen et al. 2017).

3.2.1. Geochemical features

The Häme swarm is the largest and most studied of the Subjotnian dyke swarms (e.g. Laitakari 1969; 1987; Laitakari and Leino 1989; Lindholm 2010; Salminen et al. 2017). The geochemistry of the Suomenniemi swarm is also reported in considerable detail (Rämö 1991). In the case of the other swarms, geochemical studies are sparse. In Åland, the geochemical studies by Suominen (1991) and Eklund et al. (1994) are focused on the SW part of the dyke swarm around the island of Föglö (Figure 6). Older studies of the Åland swarm are limited to major element geochemistry (e.g. Ehlers and Ehlers 1977). One study of the Satakunta swarm focuses on the major elements (Pihlaja 1987). Lehtonen et al. (2003) reported also trace element geochemistry for Satakunta and Salminen et al. (2014) showed the Nb, Y and Pb-isotope compositions for the mafic dykes of Satakunta and Sipoo swarms.

The earlier geochemical studies show the Subjotnian mafic dykes in southern Finland are tholeiitic, subalkaline to alkaline basalts, basaltic andesites or andesites (Laitakari 1969; 1987; Pihlaja 1987; Rämö 1991; Eklund et al. 1994; Lehtonen et al. 2003; Lindholm 2010). They range from quartz tholeiites to olivine tholeiites in their normative composition and their MgO contents also vary. The Satakunta, Häme and Suomenniemi dykes are relatively Fe-rich for tholeiitic basalts (Rämö 1991; Lehtonen et al. 2003; Lindholm 2010).

Despite the similarities in major element compositions of the Subjotnian mafic dykes, Luttinen and Kosunen (2006) pointed out that the dyke swarms show notably variable Nb/Y values at given Nb content (Figure 2). They associated this with different magmatic evolution or mantle sources. For example, the Sipoo and some of the Häme dykes are characterized by high Nb/Y ratios at ~0.8–1.0, while the Åland dykes have relatively low Nb (~10–30 ppm) and Nb/Y (~0.2–0.4) (Figure 2; Luttinen and Kosunen 2006; Salminen et al. 2014). The data of the Suomenniemi dykes partly overlap with the data of those Satakunta dykes that have lower Nb/Y ratios (~0.3–0.5) at given Nb (Figure 2) than the Häme dykes (Figure 2; Luttinen and Kosunen 2006; Salminen et al. 2014).

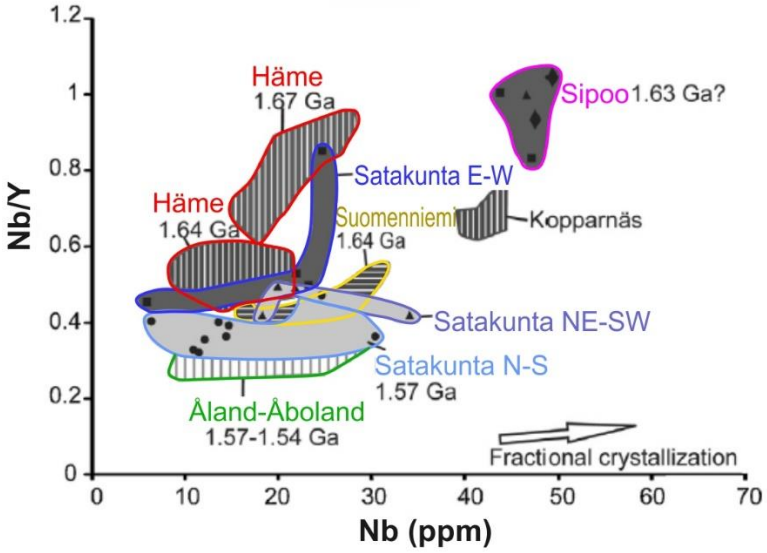

Figure 2. Trace element variation in the Subjotnian mafic dykes by Luttinen and Kosunen (2006) and Salminen et al. (2014). The Häme dykes were thought to include two separate age groups with different strike directions and chemical compositions at the time of the making of the diagram. The Satakunta dykes are grouped based on their strike directions (E-W, NE-SW and N-S). Modified from Salminen et al. (2014).

The area that covers the mid-Proterozoic dyke swarms in southern Finland (~0.14 Mkm^2) can readily be thought as a scene of one or several CFB events. The separate swarms may represent fragmented continental LIPs (Bryan and Ernst 2008) that have been separated by erosion. According to current knowledge, however, the time span for the formation of the mafic dyke swarms in Finland is ~80 Ma which is longer than the definition of LIPs (~50 Ma; Bryan and Ernst 2008) permits. The pulsed character stated in the definition of LIPs (Bryan and Ernst 2008) has, however, been proven either by geochemical (e.g. Lindholm 2010), mineralogical (e.g. Lehtonen et al. 2003) or other petrological observations for the southern Finnish Subjotnian dyke swarms. For example, composite dykes consisting of two mafic dykes are found at least in Åland (Ehlers and Ehlers 1977; Eklund et al. 1994). In Suomenniemi, two kinds of composite bimodal dykes are found: 1) dykes where the mafic dyke is younger than its felsic counterpart and 2) where the felsic dyke is younger than its mafic counterpart (Rämö 1991).

3.2.2. Paleomagnetic features

Figure 3 shows some of the paleomagnetic poles of Proterozoic Baltica, including the Subjotnian poles. The Subjotnian poles include data not only from the mafic dykes that are the targets of this study, but also from felsic rocks. The Satakunta paleomagnetic pole SK1 was calculated from the data of the N-S and NE-SW trending dykes and the paleomagnetic pole SK2 from the E-W trending dykes of Satakunta (Salminen et al. 2014). Salminen et al. (2014) suggested the pole SK2 is older than the SK1 pole due to its position near older (1.9–1.8 Ga Svecofennian aged) paleomagnetic key poles. A previous petrological study has also suggested that some of the E-W trending dykes in Satakunta are continuations of the (~1.64 Ga) Häme dyke swarm based on their strike directions and locations on the continuation of the Häme fracture zone (Pihlaja 1987). The presumably younger SK1 pole of Satakunta is similar to the pole of the Åland dykes (Salminen et al. 2014; 2016), which implies they may belong to the same swarm or simply that they are coeval. They can also be of different age if the continent has not moved. One dyke in Satakunta (dyke S11SL in this study) showed a Svecofennian paleomagnetic direction and was not included in the Subjotnian pole calculations by Salminen et al. (2014).

As shown in Figure 3, the roughly coeval (~1.63–1.64 Ga) Häme, Suomenniemi and Sipoo poles are distinct, which is unexpected since coeval [in the range of <±20 Ma; Buchan (2013)] paleomagnetic poles from the same craton should have the same position. The position of the poles of Suomenniemi and Sipoo swarms show younger magnetization ages than the pole of Häme swarm (Salminen et al. 2018) (Figure 3). However, the data from the combined felsic and mafic N polarity dykes of Suomenniemi, Sipoo and Häme overlap, indicating a coeval magnetization age (Salminen et al. 2018). According to Salminen et al. (2018) the asymmetry between N and R polarity could imply problems in the quality of the paleomagnetic data, possibly due to an unremoved secondary component.

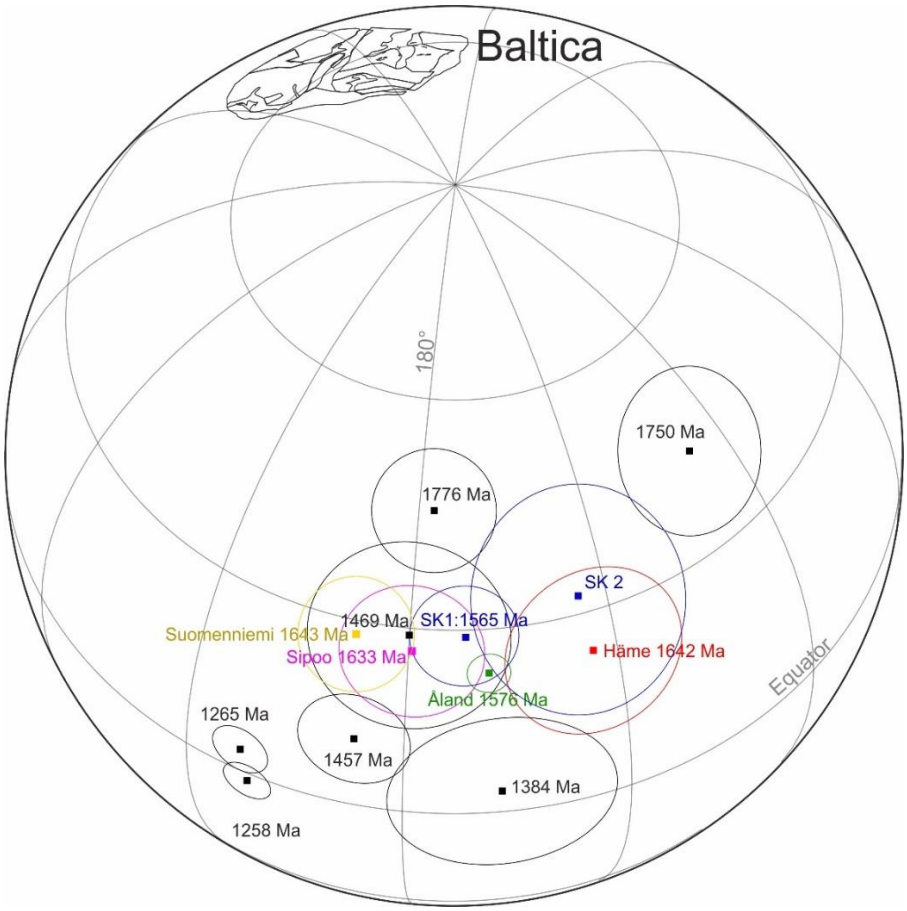

Figure 3. Some Proterozoic paleomagnetic poles for Baltica with A95 error circles. Baltica is at its present-day location. The poles of the dyke swarms in this study are indicated with colours. SK=Satakunta. The references of the poles: 1776 Ma Småland intrusion: Pisarevsky and Bylund (2010); 1750 Ma Hoting gabbro: Elming et al. (2009); 1642 Ma Häme dykes: Salminen et al. (2017); 1643 Ma Suomenniemi dykes: Salminen et al. (2018); 1633 Ma Sipoo dykes: Mertanen and Pesonen (1995); 1576 Ma Åland dykes: Salminen et al. (2016); SK1 1565 Ma Satakunta N-S and NE-SW trending dykes: Salminen et al. (2014); SK2 Satakunta E-W trending dykes: Salminen et al. (2014); 1469 Ma Bunkris-Glysjön-Öje dykes: Pisarevsky et al. (2014); 1457 Ma Lake Ladoga mafic rocks: Salminen and Pesonen (2007); Lubnina et al. (2010); 1384 Ma Mashak suite: Lubnina (2009); 1265 Ma Postjotnian intrusions: Pesonen et al. (2003); 1258 Ma Postjotnian intrusions: Pisarevsky et al. (2014).

For some of the Subjotnian dyke swarms, it is possible to define relative ages of the N and R polarity magnetization directions. In Åland archipelago, the R polarity dykes, which always occur on different islands or islets than the N polarity dykes, might be older than the N polarity dykes based on paleomagnetism (Salminen et al. 2016). The actual age difference, if present, is however unknown. In Sipoo, the R polarity mafic dykes are interpreted to be older than the N polarity quartz-porphyry dykes based on petrological studies by Laitala (1984) and Törnroos (1984) and on the paleomagnetic results by Mertanen and Pesonen (1995). According to Mertanen and Pesonen (1995), the R polarity mafic dykes showed secondary magnetization components of N polarity as thermochemical overprints that were produced by the hydrothermal fluids from the felsic intrusions. This has resulted in almost total remagnetization of one dyke (dyke SF in this study; Figure 9) (Mertanen and Pesonen 1995). In the Häme swarm, the N and R polarity dykes are coeval (J. Salminen, unpublished data). The geochronological resolution may not, however, be high enough to separate the different magma intrusions of different polarities. The polarity intervals can have durations of only some tens of thousands of years and the polarity transitions also happen in relatively short time intervals, probably <5000 years (Butler 1992).

Between the N and R polarity magnetization directions, an asymmetry in declination is observed in Häme (Salminen et al. 2017) and in inclination in Satakunta (Salminen et al. 2014) and Åland (Salminen et al. 2016) (Figure 4). The possible reasons for the asymmetry can be an unremoved secondary component, an unusual behaviour of the geomagnetic field in the Mesoproterozoic, crustal tilting or an age difference between the N and R polarity dykes associated with continental drift. For Åland and Satakunta, the symmetry enhanced after a secondary component (B-component) with an adjusted intensity was subtracted from the primary component (Salminen et al. 2017). For the Häme data, however, the asymmetry is in declination and the subtraction of an unremoved secondary component (B-component) did not enhance the symmetry (Salminen et al. 2017).

Many of the Subjotnian dykes as well as other Precambrian dykes in Baltica show a secondary magnetization component, the B-component, which in some dykes has completely overprinted the primary magnetization component (Mertanen and Pesonen 1995; Elming et al. 2009; Lubnina et al. 2010; Salminen et al. 2014; 2016; 2017; 2018).

Its direction is always close to the Present Earth Field direction (PEF) at the sampling area (Figure 5). Based on its paleomagnetic pole position, it is thought to be early Mesozoic and thus it may represent hydrothermal alteration (and the formation of new magnetic minerals such as hematite, maghemite or magnetite) related to the break-up of Pangea (Preeden et al. 2009; Salminen et al. 2014).

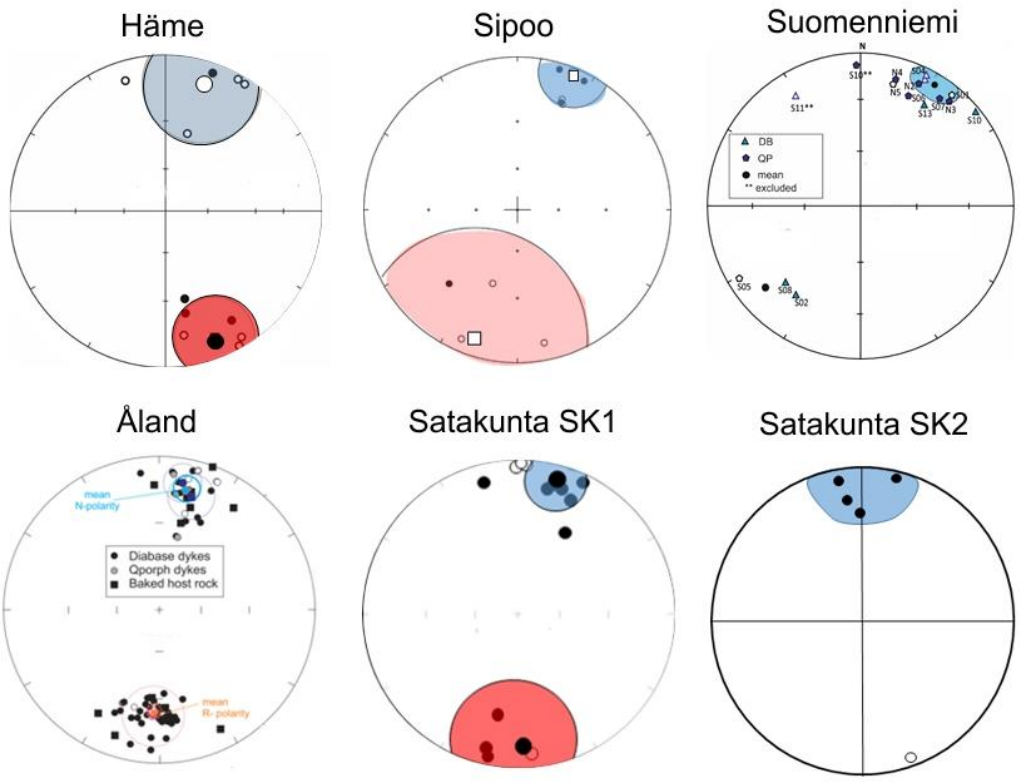

Figure 4. The normal (blue) and reversed (red) polarity magnetization components of the Subjotnian dykes shown in stereographic projections. Open (closed) symbol denotes downward (upward) directions. Modified from Salminen et al. (2014; 2016; 2017; 2018) and J. Salminen, personal communication (2018).

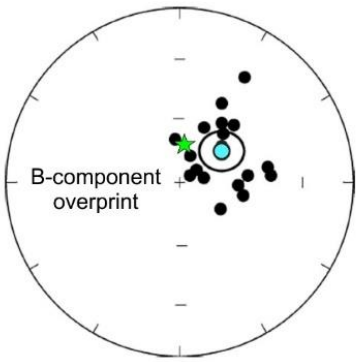

Figure 5. Site mean directions for the B-component in the Satakunta dyke swarm as reported by Salminen et al. (2014). Blue dot represents mean value. Closed symbols represent downward directions. Green star represents Present Earth's Field direction on the sampling area. Modified from Salminen et al. (2014).

3.3. The Åland dyke swarm

Åland archipelago is located in the southwestern Finland and the crystalline basement of the main island consists mainly of Mesoproterozoic rapakivi granite (Figures 1 and 6). The archipelago east of the Åland rapakivi intrusion consists of Paleoproterozoic Svecofennian rocks that are cut by Paleo- and Mesoproterozoic dykes. The U-Pb (zircon) ages of the Åland rapakivi granite units are between 1568 ± 10 Ma and 1579 ± 13 Ma (Suominen 1991).

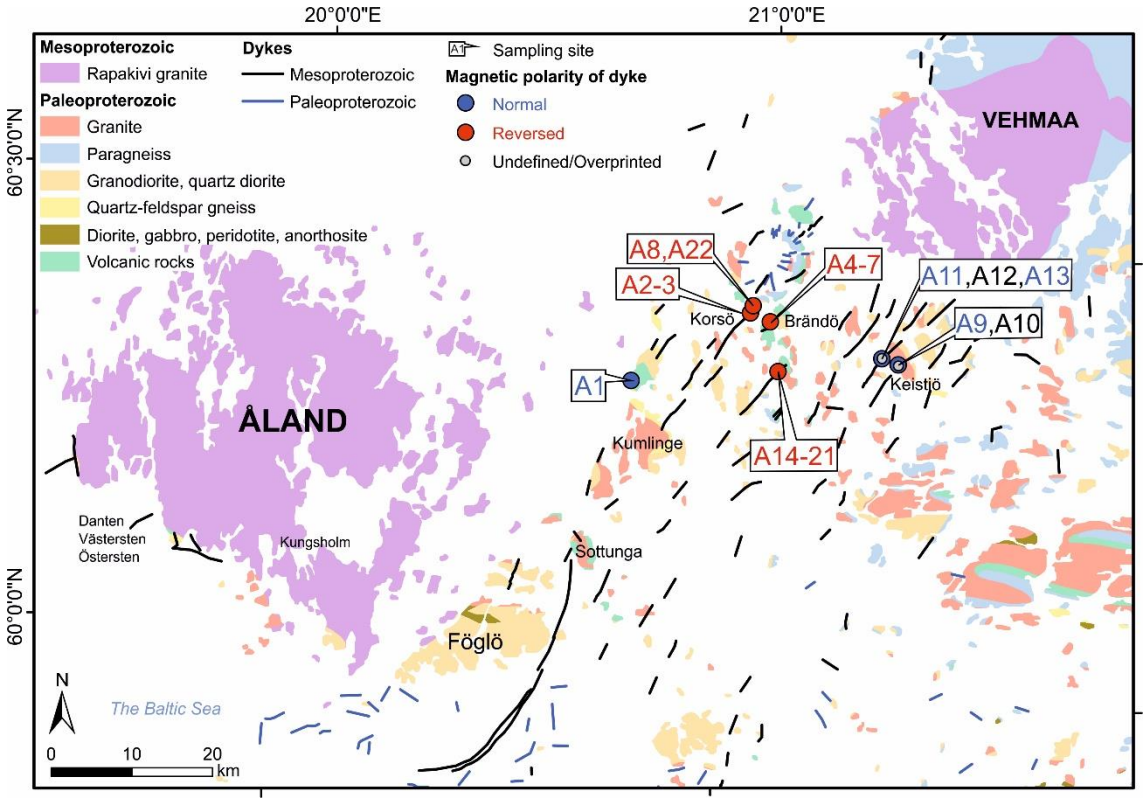

Figure 6. Generalized geological map of Åland. The sampling sites of this study are indicated.

The Subjotnian mafic dykes are spread around the SW part of the Åland rapakivi to the SE part and continue ~80 km to NE towards the Vehmaa rapakivi intrusion on the mainland Finland (Figure 6). However, mafic dykes do not occur in the vicinity of the Vehmaa intrusion, whereas quartz-porphyry dykes do (Karell et al. 2009). Additionally, the Åland and Vehmaa rapakivi granites are clearly separated from each other based on the steep structures that separate the Vehmaa rapakivi from the host rocks (Karell et al.

2009). This suggests the Åland rapakivi and associated dykes may have formed separately from those in mainland Finland. One U-Pb (zircon) age of Vehmaa rapakivi granite is 1590 ± 15 Ma (Vaasjoki 1977), although, as mentioned before, a study by Shebanov et al. (2000) showed that the core of the ovoid crystals has a U-Pb (zircon) age of 1630 Ma, while the matrix has a U-Pb (zircon) age of 1573 Ma. Since the prevailing model of rapakivi magmatism requires mafic underplating, the mafic magmatism may have occurred also in SW Finland as early as 1630 Ma.

The Åland dyke swarm is typified by vertically or subvertically dipping dykes with strikes generally in the SSW-NNE direction (e.g. Eklund et al. 1994). Their widths vary from a few millimetres to over 100 m (Salminen et al. 2016). In his study, Suominen (1991) divided the dykes in the SW part of the Åland swarm into three sets: the pyroxene diabase dykes of the Föglö island to the SE of Åland (Figure 6), the anorthositic varieties of these pyroxene diabase dykes on the islands to the SW of Åland (Västersten, Danten and Östersten; Figure 6), and the hornblende diabase dykes of the Kumlinge island (Figure 6). On the island of Föglö, the dykes show U-Pb (zircon) ages of 1577 ± 12 Ma and 1540 ± 12 Ma (Suominen 1991), although, according to Suominen (1991), the younger age may have been disturbed by tectonic movements along a fracture line near the site. To the SW of the Åland rapakivi area, the dykes are most likely of same age as the Föglö dykes (Suominen 1991). No U-Pb age was obtained from the dykes in Kumlinge by Suominen (1991).

In addition to the above-mentioned ages, a U-Pb (zircon) age of 1575.9 ± 3.0 Ma has been reported by Salminen et al. (2016) from a quartz-monzonitic part of a compositionally heterogeneous bimodal dyke (with width of ~200 m) on Korsö island (Figure 6). There is, however, evidence of mafic dykes of different ages, and the magmatic activity in Åland can be considered to have happened during 1570–1580 Ma ago. Evidence of magma mixing and mingling between basaltic and granitic magmas (Lindberg and Eklund 1992; Eklund et al. 1994) proves the rapakivi granites and mafic magmas are at least in some locations coeval. In Kungsholm, Jomala, one mafic dyke cuts the Åland rapakivi granite (Bergman 1981), proving some dykes are younger than the rapakivi granites. Ehlers and Ehlers (1977) also describe multiple intrusions in some of the mafic dykes, forming composite dykes. It remains speculative whether the possible 1630 Ma magmatism in Vehmaa (Shebanov et al. 2000) reached to Åland.

3.4. Satakunta dyke swarm

The Mesoproterozoic suite in the Satakunta area in SW Finland is located on the west coast of Finland, north of the Laitila and Eurajoki rapakivi batholiths (Figures 1 and 7). In the southern part of the area (Figure 7a), the Jotnian Satakunta sandstone and the Postjotnian mafic dykes separate the Subjotnian dykes from the 1573 ± 8 Ma [U-Pb (zircon); Vaasjoki (1977)] Laitila batholith. The Satakunta sandstone was deposited at ca. 1600–1270 Ma in an intracratonic rift basin during several stages (Pokki et al. 2013). The younger limit of this timeline is constrained by the intrusion of the Postjotnian olivine diabase dykes and sills that cut the sandstones and the Laitila rapakivi batholith.

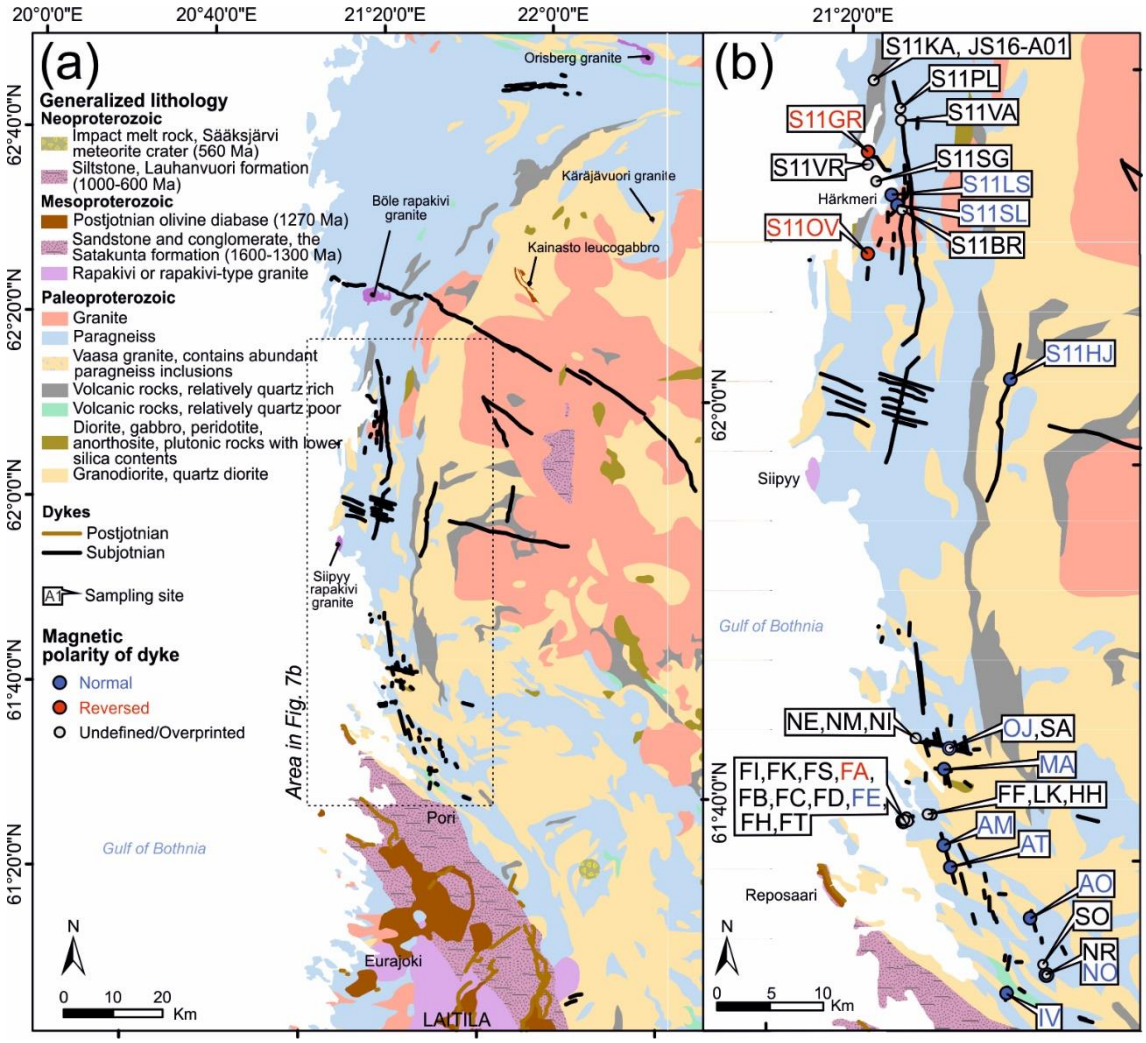

Figure 7. a) Generalized geological map of the Satakunta dyke swarm and adjacent areas. b) The sampling sites of this study. The Laitila rapakivi intrusion is indicated in a).

In the northern part of the Satakunta swarm area (Figure 7a), ~150 km to north of the Laitila batholith, there are smaller rapakivi or rapakivi-type intrusions (Lehtonen et al. 2003): Böle [U-Pb (zircon) age 1568 ± 6 Ma; Lehtonen et al. (2003)], Siipyy [U-Pb (zircon) age 1562 ± 14 Ma; Idman (1989)], Käräjävuori and Orisberg. In the Kainasto area (Figure 7a), there are also anorthositic leucogabbros/leucomonzogabbros, medium-grained gabbros and plagioclase porphyrites of which the plagioclase porphyrites resemble the Subjotnian mafic dykes in terms of texture, occurrence and chemical composition (Lehtonen et al. 2003). Postjotnian mafic dykes are also present (Lehtonen et al. 2003).

Lehtonen et al. (2003) divide the Subjotnian mafic dykes of Satakunta into N-S and E-W trending dykes that sometimes occur as swarms. Salminen et al. (2014) have additionally a NE-SW trending group. Pihlaja (1987) suggested the E-W trending dykes in the Pori area (Figure 7a) may belong to the same *en echelon* fracture system as the Häme dykes based on their strike direction and their location that seems to be on a continuous path from the Häme fracture zone.

According to Lehtonen et al. (2003), coarse-grained types of the Satakunta mafic dykes are gabbro-like with shorter and wider dimensions than fine-grained types. A U-Pb (baddeleyite) age of 1565 Ma (error limits unavailable) has been reported by Lehtonen et al. (2003) for a N-S trending coarse-grained dyke in Härkmeri (in this study, dyke S11LS). According to Lehtonen et al. (2003), the presence of spherical 1–2 cm sized quartz inclusions in one dyke is indicative of coeval felsic magmas (or crustal contamination).

3.5. The Häme dyke swarm

The Häme swarm is the most extensive of the Subjotnian dyke swarms, as it starts from the Ahvenisto complex near the city of Heinola and continues ~150 km to the ~NW direction to Kuru (Figures 1 and 8) (Laitakari 1969). The 1644–1629 Ma (Heinonen 2010) Ahvenisto complex that lies to the NW of the large Wiborg (1642–1622 Ma; Rämö et al. 2014) rapakivi batholith, is a anorthosite-mangerite-charnokite-granite complex that has

a rapakivi core partially surrounded by mafic rocks in a horseshoe-shaped zone (e.g. Heinonen et al. 2010b). The main mafic rock types in Ahvenisto are leucogabbronorite and olivine-bearing leucogabbro (Heinonen et al. 2010b). According to Laitakari and Leino (1989), the Ahvenisto gabbro-anorthosite may have been the magma chamber of the mafic dykes of Häme.

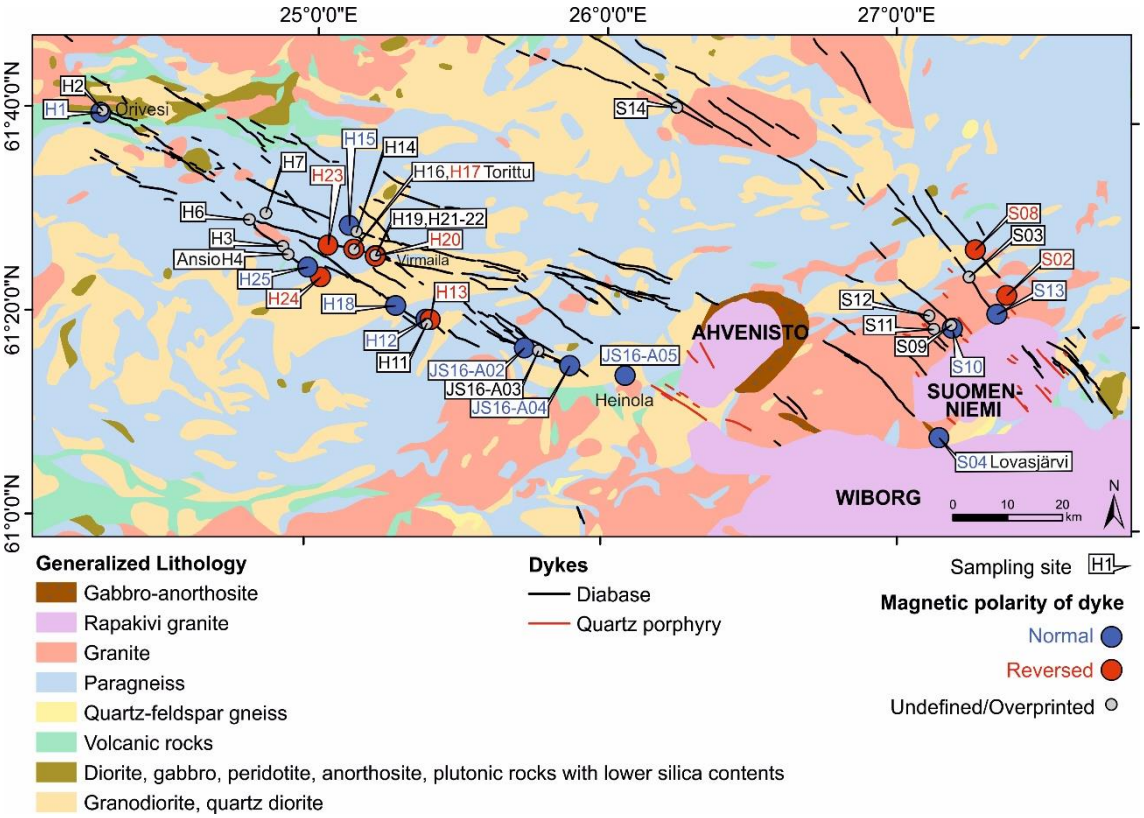

Figure 8. Generalized geological map of the areas of the Häme and Suomenniemi dyke swarms. The sampling sites of this study are indicated. The Ahvenisto, Suomenniemi and Wiborg rapakivi intrusions are also indicated.

The widths of the Subjotnian dykes of Häme swarm vary from a few centimetres possibly up to 250 m (Laitakari 1969). The widths get narrower the longer the distance is from the Ahvenisto complex (Laitakari 1969). The dykes dip vertically or subvertically with typically sharp contacts with the host rock (Laitakari 1969). In three locations, mafic dykes cut other mafic dykes (Laitakari 1969) which records multiple magma injections. Laitakari (1969) reports two strike direction maxima; 120°–135° and 095° plus several other dykes with trends between these limits (095°–120°). Previously the two main strike directions have been interpreted to correspond to compositionally and chronologically

distinctive phases (Laitakari 1969; 1987; Vaasjoki and Sakko 1989; Luttinen and Kosunen 2006), but a detailed geochemical study by Lindholm (2010) does not support this idea and suggests the major element variability is mainly caused by different cooling histories. Instead, Lindholm (2010) identifies three geochemically distinct groups that are independent of strike directions based on incompatible element ratios.

Based on the most reliable age determinations, the mafic dykes of Häme swarm intruded at 1635–1646 Ma. The precise ages are: a U-Pb (zircon) age of 1646 ± 6 Ma (Ansio; Laitakari 1987), a U-Pb (baddeleyite) age of 1642 ± 2 Ma (Virmaila; Salminen et al. 2017) and a U-Pb (zircon) age of 1640 ± 2 Ma (Ahvenisto; Heinonen et al. 2010b). Additionally, a U-Pb (baddeleyite) age of 1647 ± 14 Ma is obtained from Torittu (Salminen et al. 2017; site H17 in this study; Figure 8). Unpublished data (J. Salminen) from the dykes in this study (Figure 8: sites H12, H13, H14 and H25) give U-Pb (baddeleyite) ages of 1635–1640 Ma. A quartz porphyritic dyke from Ahvenisto complex has a U-Pb (zircon) age of 1636 ± 2 Ma (Heinonen et al. 2010b), suggesting a younger age for the felsic dykes.

3.6. The Suomenniemi dyke swarm

The Suomenniemi swarm lies ~60 km to the NE of the Häme swarm and is associated with the Suomenniemi rapakivi pluton to the north of the Wiborg rapakivi batholith (Figure 8). The main rapakivi granite series in Suomenniemi crystallized from a single parental magma at 1644 ± 4 Ma (U-Pb, zircon) and another granitic intrusion occurred some millions of years later (Rämö 1991; Rämö and Mänttäri 2015). Even later, at 1634 ± 4 Ma (U-Pb, zircon), the felsic dykes intruded the rapakivi granites and the Svecofennian bedrock (Rämö and Mänttäri 2015).

The ~40 mafic dykes that have been studied in the Suomenniemi swarm are vertical, trending towards NW, and cut sharply the surrounding bedrock (Rämö 1991). The mafic and felsic dykes have widths of a few centimetres to 50 m but are commonly 5–20 m wide (Rämö 1991).

The mafic dykes of Suomenniemi swarm are approximately the same age than the main rapakivi series: a U-Pb (zircon) age of 1643 ± 5 Ma (Siivola 1987) has been obtained from the Lovasjärvi intrusion (Figure 8). Vaasjoki et al. (1991) report that the intrusion of the mafic dykes in Suomenniemi continued until 1635 Ma, based on the U-Pb data from the felsic dykes in Suomenniemi and an observation of a composite dyke where the mafic part is younger than the felsic part. Composite dykes, where a felsic dyke has intruded the mafic dyke are also present (Rämö 1991 and references therein). Three mafic dykes are found to cut the rapakivi batholith, while the majority surrounds it (Rämö 1991). According to Haapala and Rämö (1990), the rapakivi granites in Suomenniemi originate from the Svecofennian crust based on Nd-isotopes. According to Rämö (1991), the mafic dykes as well as gabbroic and anorthositic rocks in Suomenniemi were derived from LREE-depleted mantle source and were contaminated by the Svecofennian crust, based on varying Nd isotopic compositions.

The Lovasjärvi intrusion (Figure 8; site S04 in this study) is a sheet-like, 5 km long and 800 m wide, NW trending and vertically dipping intrusion that is cut by rapakivi granites at both ends (Siivola 1987). The intrusion consists of melatroctolite and olivine diabase in the NW part, and medium- to coarse-grained olivine-free diabase in the middle and SE parts (Siivola 1987; Rämö 1991). Siivola (1987), Laitakari (1987) and Vaasjoki and Sakko (1989) group the intrusion as part of the Häme dyke swarm, while Rämö (1991) and Salminen et al. (2018) consider it to belong to the Suomenniemi complex. This study follows the latter way.

3.7. The Sipoo dyke swarm

The Sipoo dykes are associated with Onas rapakivi stock that lies ~20 km to the west from the large Wiborg rapakivi batholith (Figure 9). The age of the Onas rapakivi is 1630 ± 10 Ma [U-Pb (zircon); Laitala 1984]. Further to the west, there are two other smaller rapakivi complexes in Bodom and Obbnäs with associated dyke swarms (Figure 9). Both of these rapakivi granites have a U-Pb (zircon) age of 1645 ± 5 Ma (Vaasjoki 1977).
According to Mertanen and Pesonen (1995), the Sipoo dyke swarm consists of mafic and felsic dykes with vertical or subvertical dips. The width of the swarm is ~80 km and

length ~20 km. The mafic dykes seem to be striking in E-W directions while the felsic dykes strike mostly in NW-SE directions (Mertanen and Pesonen 1995). The widths of the mafic dykes range from a few centimetres to 3 m.

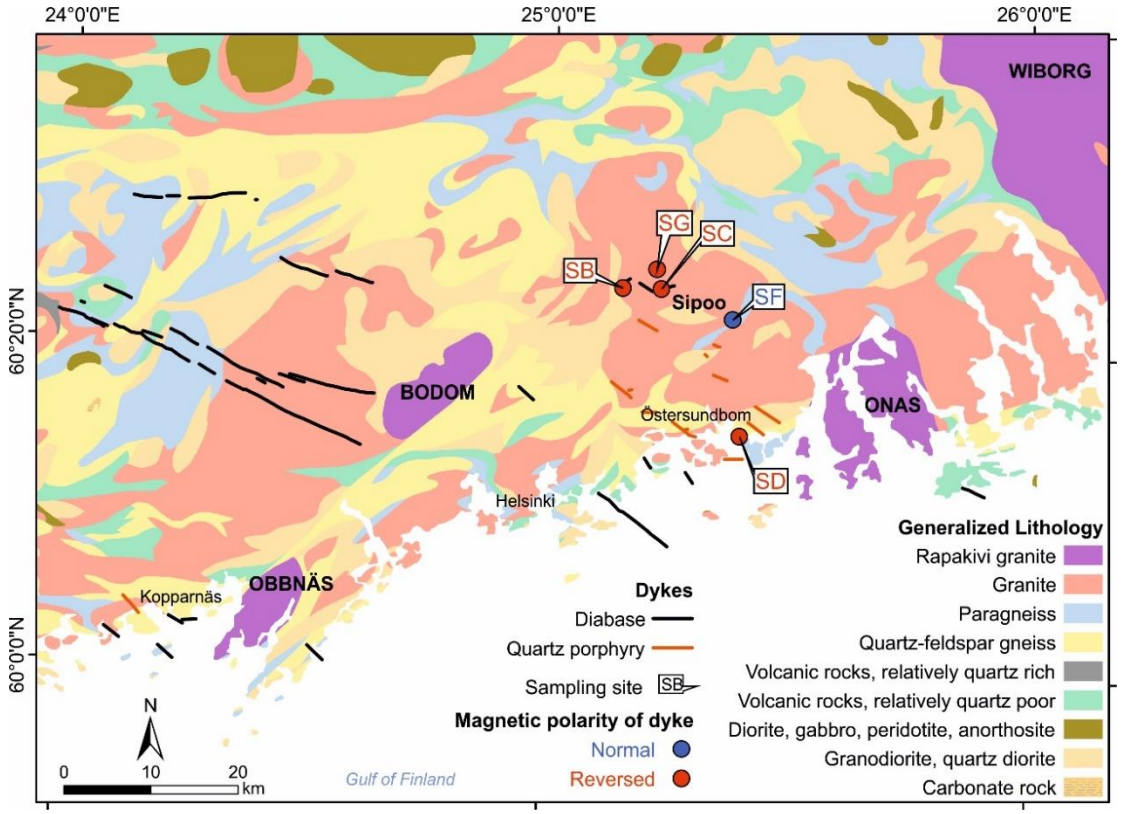

Figure 9. Generalized geological map of the Sipoo dyke swarm and adjacent areas. The sampling sites of this study are indicated (no geochemistry was made of the dyke SD).

A felsic dyke in Östersundbom has been dated 1633 Ma [error limits unavailable; U-Pb (zircon); Törnroos 1984]. The felsic dykes are older than the Onas granite (Törnroos 1984), but younger than the mafic dykes since composite dykes, where a felsic dyke cuts a mafic dyke, are present (Laitala 1984). The felsic dykes are altered, which may be related to the crystallization of the Onas granite (Törnroos 1984). The mafic dykes, on the other hand, are altered possibly due to the hydrothermal fluids from the felsic dykes and the Onas granite (Mertanen and Pesonen 1995).

4. MATERIALS AND METHODS

4.1. Materials

A total of 109 samples from 101 mafic dykes and one sample from a sheet-like mafic intrusion (site S04 from Lovasjärvi in Suomenniemi; Figure 8) were prepared for geochemical analysis. The sample collection was done previously for the purposes of paleomagnetic research (Mertanen and Pesonen 1995; Salminen et al. 2014; 2016; 2017; 2018). The sampling locations are plotted in Figures 6–9. The majority of the samples were collected by a portable water-cooled gasoline drill. Some samples from Sipoo were collected as block samples with a hammer. The diameters of the drill core samples are 2.54 cm and lengths vary (Figure 10). Most of the specimens used for this work have a mass of ~30 g. Sample selection was made, when possible, by avoiding weathered and fractured samples as well as samples containing phenocrysts. A table showing the coordinates of the dykes and other features of the samples is in Appendix I.

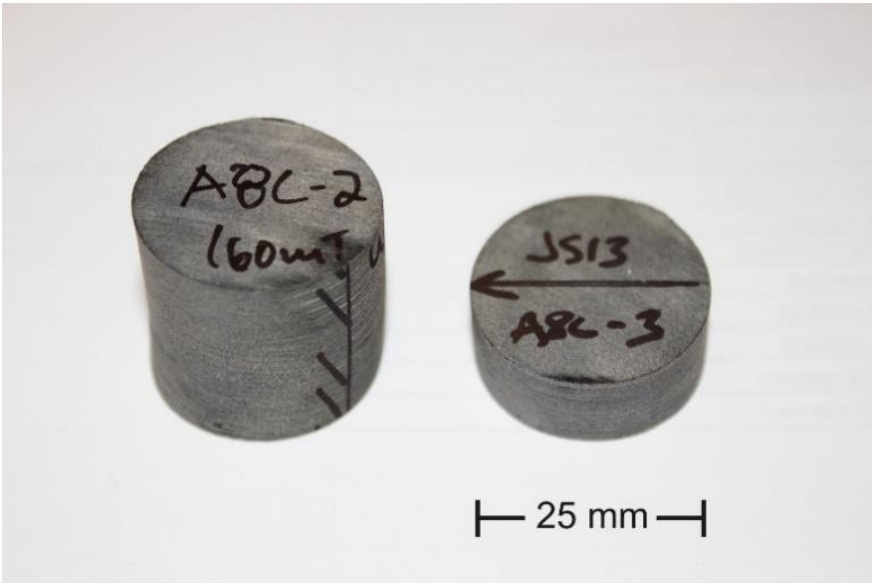

Figure 10. Some drill core samples from the dyke A8 from Åland. The sample A8C-2 was used for geochemical analysis and, in terms of its size that is standard for paleomagnetism, represents a typical sample for geochemistry in this study.

4.2. Geochemical and petrographical methods

The sample preparation for the geochemical analysis was done at the mineralogy laboratory at the Department of Geosciences and Geography, University of Helsinki. For the wavelength dispersive X-ray fluorescence (WD-XRF) analysis, the samples were first polished with a coarse (120 mm) diamond abrasive disc to remove ink marks, glue, paint (Sipoo samples), graphite pencil marks and fingerprints on the surfaces. Subsequently, they were crushed inside a plastic bag with additional tough packing plastic material using a rock splitting press and a hammer. The rock chips were then pulverized using a tungsten carbide ball mill (Fritsch Pulverisette 6). To produce a glass bead by fusing (Claisse M4 fluxer), 0.600 g of the sample powder was mixed with 6.000 g of flux mixture of lithium tetraborate (49.75%), lithium metaborate (49.75%) and lithium bromide (0.5%). The beads were analysed using PANalytical Axios mAX 4 kw WD-XRF spectrometer for the major (Si, Ti, Al, Fe, Mn, Mg, Ca, Na, K and P) and trace elements (Ba, Ce, Cr, Cu, La, Nb, Ni, Rb, Sr, U, V, Y, Zn and Zr).

At present, there are neither published accuracy nor precision estimates for the analyses performed at the mineralogy laboratory. Based on experiments with different calibrations of the XRF instrument, the detection limits have been obtained for each element (indicated in the Appendix II if the result was below the limit) (Pasi Heikkilä, personal communication 2018). The precision (2σ) for the major oxides was <0.1 wt.% and for the trace elements <10 ppm, except for Ce <20 ppm (Pasi Heikkilä, personal communication 2018).

Some samples showed low total values of the major oxides (down to 90.87 wt.%). A second bead was made of the powder for one sample (A9A-2, dyke A9 from Åland) to verify the results. The results of the second bead were similar to the first one (Table 1), which indicates the low values are due to other reasons than the sample preparation practice. The reasons for the low values are discussed in Chapter 5.1. and Section 5.2.1.

Table 1. Comparison of the results of sample A9A-2 (Åland) obtained from the beads fused from the same sample powder. The results of La and U for the original bead (A9A-2) are below detection limits (10 ppm for La and 2 ppm for U).

Major oxides	Sum	SiO_2, wt.%	TiO_2	Al_2O_3	FeO	MnO	MgO	CaO	Na_2O	K_2O	P_2O_5
A9A-2	90.87	46.10	1.98	13.94	13.33	0.17	6.53	4.76	1.38	2.23	0.45
A9A-2, new	91.88	46.43	1.98	14.06	13.39	0.17	6.99	4.80	1.38	2.24	0.44

Trace elements	Ba, ppm	Cu	Cr	Ni	Sr	Zn	Zr	Rb	Nb	Y	Ce	La	V	U
A9A-2	254	35	159	70	56	270	168	171	9	50	44	7	188	0
A9A-2, new	243	35	157	74	57	270	171	170	11	48	46	12	188	2

Fifty-two thin sections were examined using polarization microscope Nikon LABOPHOT2-POL. Samples for petrography were selected based on a preliminary geochemical grouping of the dykes and their previously reported paleomagnetic properties (Mertanen and Pesonen 1995; Salminen et al. 2014; 2016; 2017; 2018). Their textural and mineralogical features and their possible chemical alteration features were observed.

5. RESULTS

5.1. Petrography

Generalizing, most of the samples show nesophitic, subophitic or ophitic textures depending on the size of the interstitial clinopyroxene relative to the euhedral plagioclase laths. Twelve of the 52 samples are porphyritic with plagioclase microphenocrysts (<3mm). One sample (from dyke A5 from Åland) showed also clinopyroxene microphenocrysts (<1mm), which form glomerophyric clusters with plagioclase microphenocrysts (<2mm). Plagioclase (An_{30-60}) is mostly lath-shaped and less than 1 mm long. Largest plagioclase grains are up to 2 cm long in the sheet-like intrusion S04 from Lovasjärvi in Suomenniemi. Fifteen of the 52 samples include olivine, which occurs as subhedral grains and/or anhedral and interstitial between plagioclase laths. Primary opaque minerals are commonly anhedral and interstitial but occur also as euhedral

elongated or cubic grains. Sometimes they have been crystallized before clinopyroxene, which is indicated by euhedral opaque inclusions in clinopyroxene. Secondary opaque minerals are also present. A few samples have orthopyroxene as an interstitial mineral. Apatite is a common accessory mineral and zircons occur in some samples. Some dykes show rapid cooling with swallow tails and skeletal crystal shapes in plagioclase and the presence of vesicles (filled with carbonate, quartz, biotite, chlorite and occasional opaques) are suggestive of near-surface emplacement environment (Figures 11b–c). Preferred orientation of plagioclase and spherulitic textures are common in these cases (Figures 11b–c).

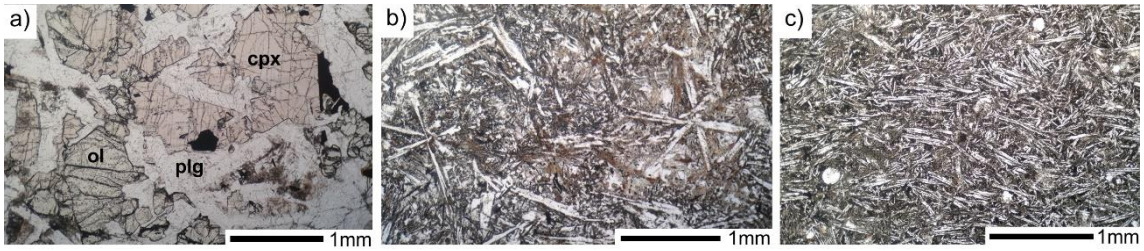

Figure 11. Photomicrographs of three thin sections showing different textures observed in the samples (plane polarized light). a) ophitic texture in dyke H24 (sample JS14-H24B-2; Häme), b) spherulitic texture in dyke H15 (Häme) and c) preferred orientation of plagioclase with vesicles in dyke A13 (Åland). ol=olivine, plg=plagioclase, cpx=clinopyroxene.

Secondary biotite is always present and occurs as an alteration product of opaque minerals and olivine. Biotite is often further altered to chlorite. Clinopyroxene has altered to chlorite and possibly metamorphosed to amphibole, in some cases almost completely. Olivine is in some cases altered to “iddingsite” and its cleavage spaces are often filled with opaque minerals, biotite and serpentine. Plagioclase shows variable alteration to sericite and saussurite but is generally the least altered primary mineral. In this study, the overall alteration level of the samples was described using a four-stage scale: *low* = very little alteration, *moderate* = some alteration, *high* = very altered, *very high* = totally altered (Figure 12). The low total %-values of the XRF analysis for some samples is explained by the high level or complete alteration of the samples which has increased the amount of volatiles in them.

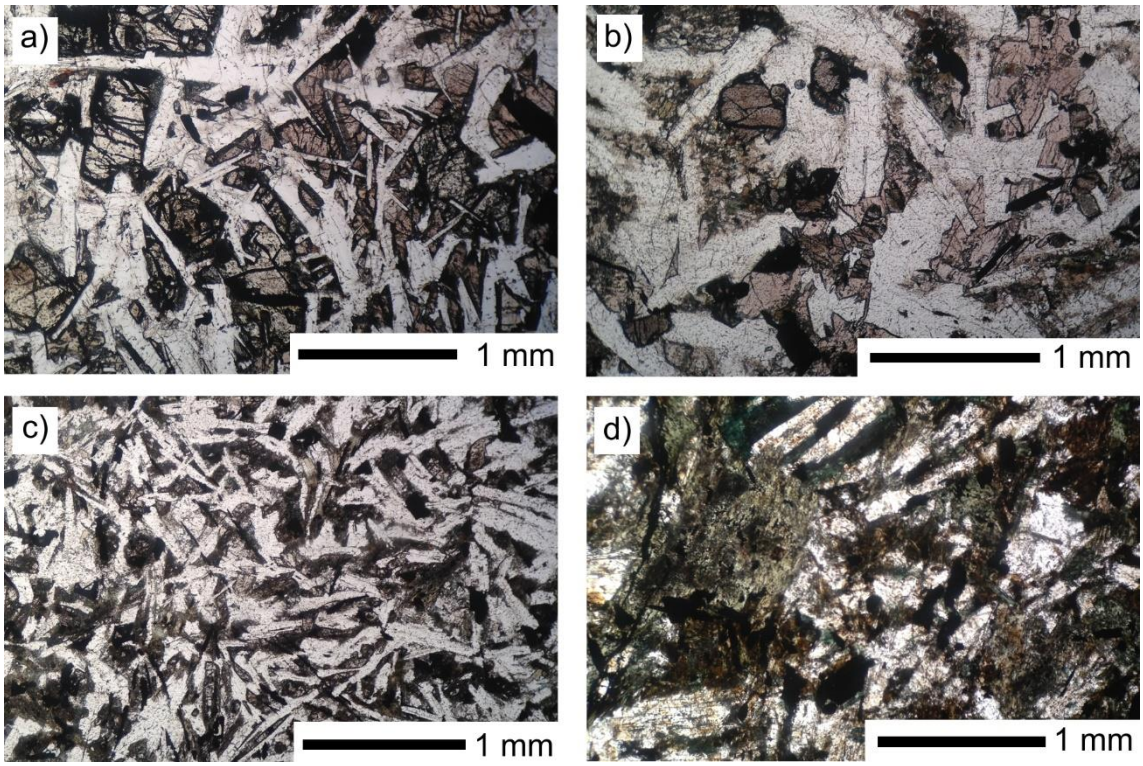

Figure 12. Photomicrographs of four thin sections showing degrees of alteration (plane polarized light). a) low degree alteration: dyke H13 (sample H13; Häme), b) moderate degree alteration: dyke S02 (Suomenniemi), c) high degree alteration: sample dyke H11 (Häme) and d) very high degree alteration: dyke SF (Sipoo).

The dykes H13 and H14 from Häme had anhedral and interstitial-type of plagioclase, that had formed from an adcumulus-type of crystal growth. The dyke S13 from Suomenniemi had a quartz-xenocryst and the dyke A3 from Åland a metasedimentary xenolith.

Examination of the samples which contain the overprinted paleomagnetic B-component shows them to exhibit mainly a "*high*" degree of alteration. Many of them contain vesicles and/or fractures. In these samples, the opaque minerals often occur in two varieties, indicating crystallization of magnetic minerals in at least two separate stages. This degree of alteration is compatible with previous studies (Preeden et al. 2009; Salminen et al. 2014).

Three of the thin section samples differ from igneous mafic intrusions in terms of mineralogy and/or texture. The sample A2F-3 (dyke A2) from Åland is andesitic which is also indicated by the geochemistry (Section 5.2.1; Figure 13). This sample is from a fine-grained dyke cutting a coarser-grained dyke. The sample A2G-1 is from the coarser-

grained part and is a somewhat typical (although altered) diabase with subophitic texture. Satakunta dykes NI and NO are totally recrystallized, metamorphosed at amphibolite facies and are amphibolites with foliated textures and abundant hornblende, biotite and plagioclase. The petrographical features are summarised in Appendix III.

5.2. Geochemistry

5.2.1. Subjotnian dykes in general

The results of the XRF analyses with C.I.P.W. norms are listed in Appendix II. The processing and interpretation of the data are done using major oxide normalization to 100% (i.e. volatile-free) whereas trace element data are not normalized. Solubility of water is low in tholeiitic basalts and normalized data probably correspond closely to the original magma compositions. As discussed in Chapter 5.1. (Appendix III), many of the samples contain abundant secondary water-bearing minerals. Thus, it can be assumed that the low totals in some samples result from alteration.

The dykes are grouped according to their locations in the geochemistry diagrams of Figures 13–16. All the dykes are hyperstene-normative (i.e. tholeiitic), which is typical of continental flood basalts. They vary from quartz- to olivine-normative types. In the total alkali vs. silica (TAS) diagram, the dykes plot mainly in the fields of basalts, basaltic andesites and basaltic trachyandesites (Le Bas et al. 1986; Figure 13). Sub-alkaline compositions are dominant, but many (31%) have alkaline affinity in Figure 13. Total alkalis are in the range of 2–6 wt.% and SiO_2 content between 46–55 wt.% for most of the samples. The Åland dykes and some of the Satakunta dykes plot at lower total alkali contents than most of the other dykes.

Many of the studied Subjotnian dykes have been altered. Classification diagram based on immobile Nb, Zr, Ti and Y is well-suited for altered samples (Figure 14). Generalizing, classification of the dykes based on Nb/Y and Zr/Ti is compatible with TAS classification. The data points group on the basalt field accompanied by groups of andesites/basaltic andesites and alkali basalts. Accumulation of phenocrysts (e.g. olivine) does not significantly affect the ratios of incompatible elements, so the picrobasalt dykes

JS16-A05 (Häme) and FF (Satakunta) (Figure 13) are classified as basalt and alkali basalt in Figure 14, respectively. However, while JS16-A05 seems to be fitting well among the other Häme dykes, FF is part of a minor group of Satakunta dykes that plot in the alkali basalt field. Sipoo, Åland and Häme dykes all form distinctive, relatively coherent groups, while the Suomenniemi dykes are scattered and the Satakunta dykes seem to form at least two groups. Dykes S11SG (Satakunta), SO (Satakunta) and FF (Satakunta) and sample A2F-2 from dyke A2 (Åland) are exceptional in Figures 13 and 14. These are interpreted as unrepresentative rock samples and are no longer discussed in this study.

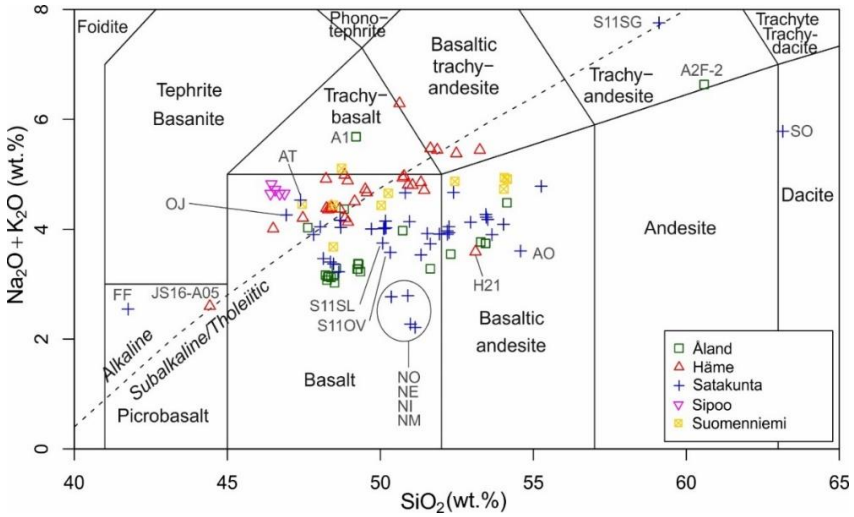

Figure 13. Total alkali–silica diagram for the classification of volcanic rocks (Le Bas et al. 1986). The diagram includes all the samples of this study (n=110). Exceptional dykes and sample are identified (see text).

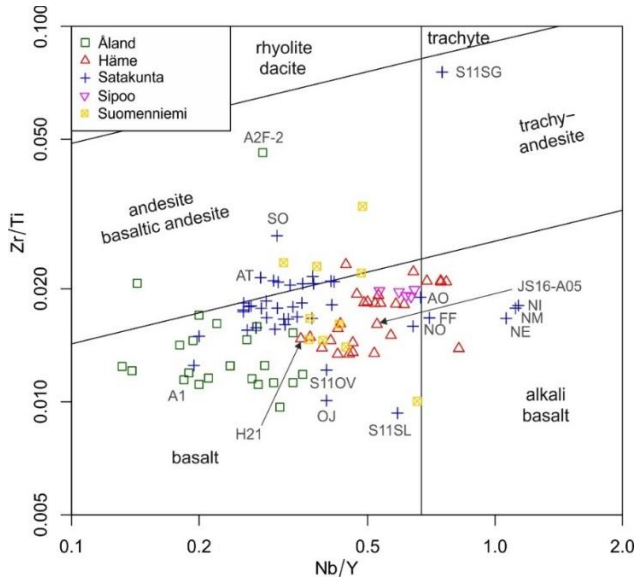

Figure 14. Classification diagram of basaltic rocks after Pearce (1996). The diagram includes all the samples of this study (n=110). Exceptional dykes and sample are identified (see text).

The Subjotnian dykes of this study exhibit a very wide range of MgO (3.1–15.4 wt.%) (Appendix II). Figures 15 and 16 show variations in major oxides and trace elements relative to Mg number [molar 100*Mg/(Mg+Fe^{2+}), where Fe^{2+}=0.9*total Fe], which is a widely used index of fractional crystallization. The dykes are all evolved to varying degree from a primary magma. The great majority of the dykes represent evolved magmas typified by high TiO_2 (0.7–4.5 wt.%) and lower Ni contents (12–249 ppm). A positive correlation can be seen in Al_2O_3 and CaO, while a negative correlation is seen in TiO_2, FeO, K_2O and P_2O_5 (Figure 15). The trace elements also show correlation with Mg number: the compatible elements Ni and Cu show positive correlation while the incompatible elements (Ba, Sr, Zn, Zr, Rb, Nb, Y, Ce and La) show negative correlation (Figure 16).

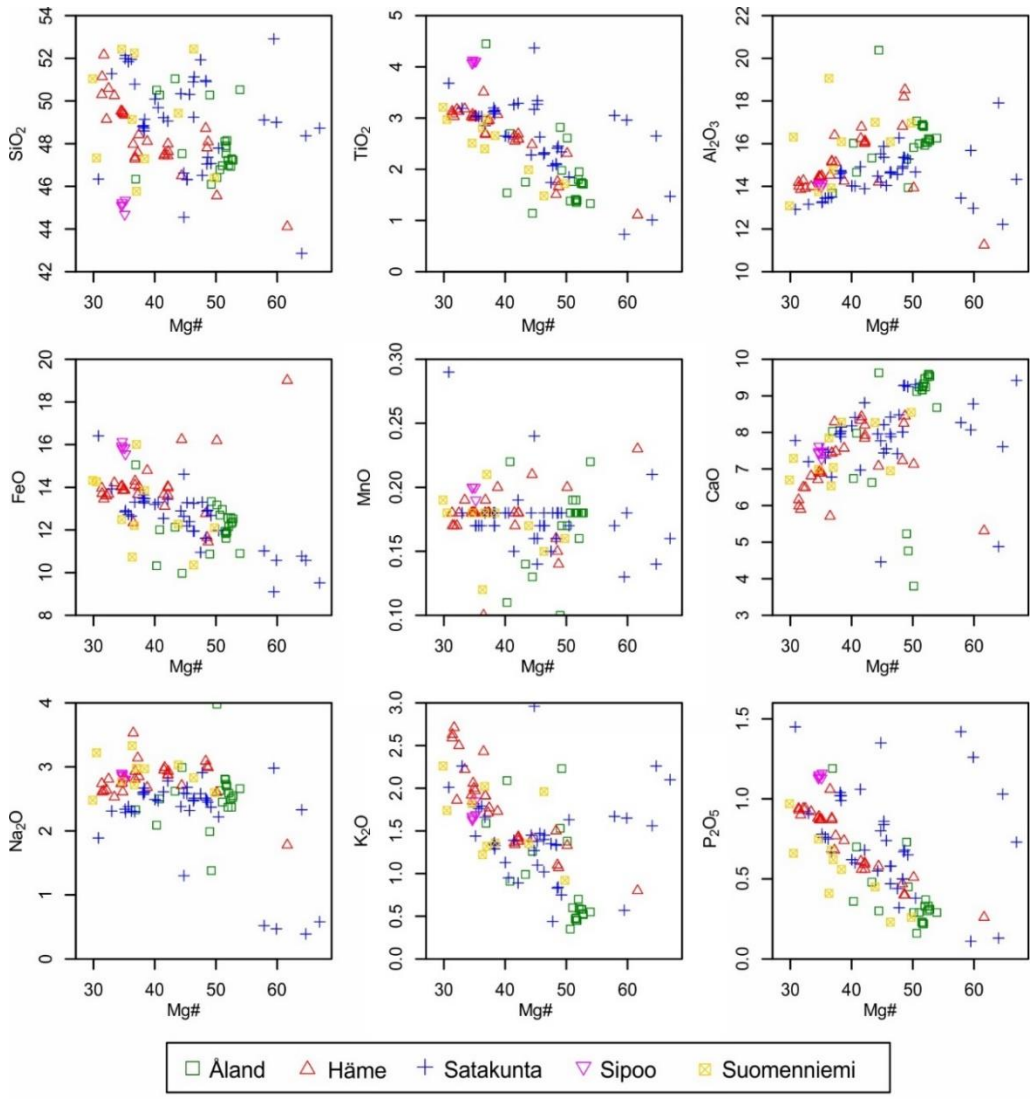

Figure 15. Mg number (Mg#) vs. major elements (in wt. %) variation diagrams for the Subjotnian dykes (n= 106).

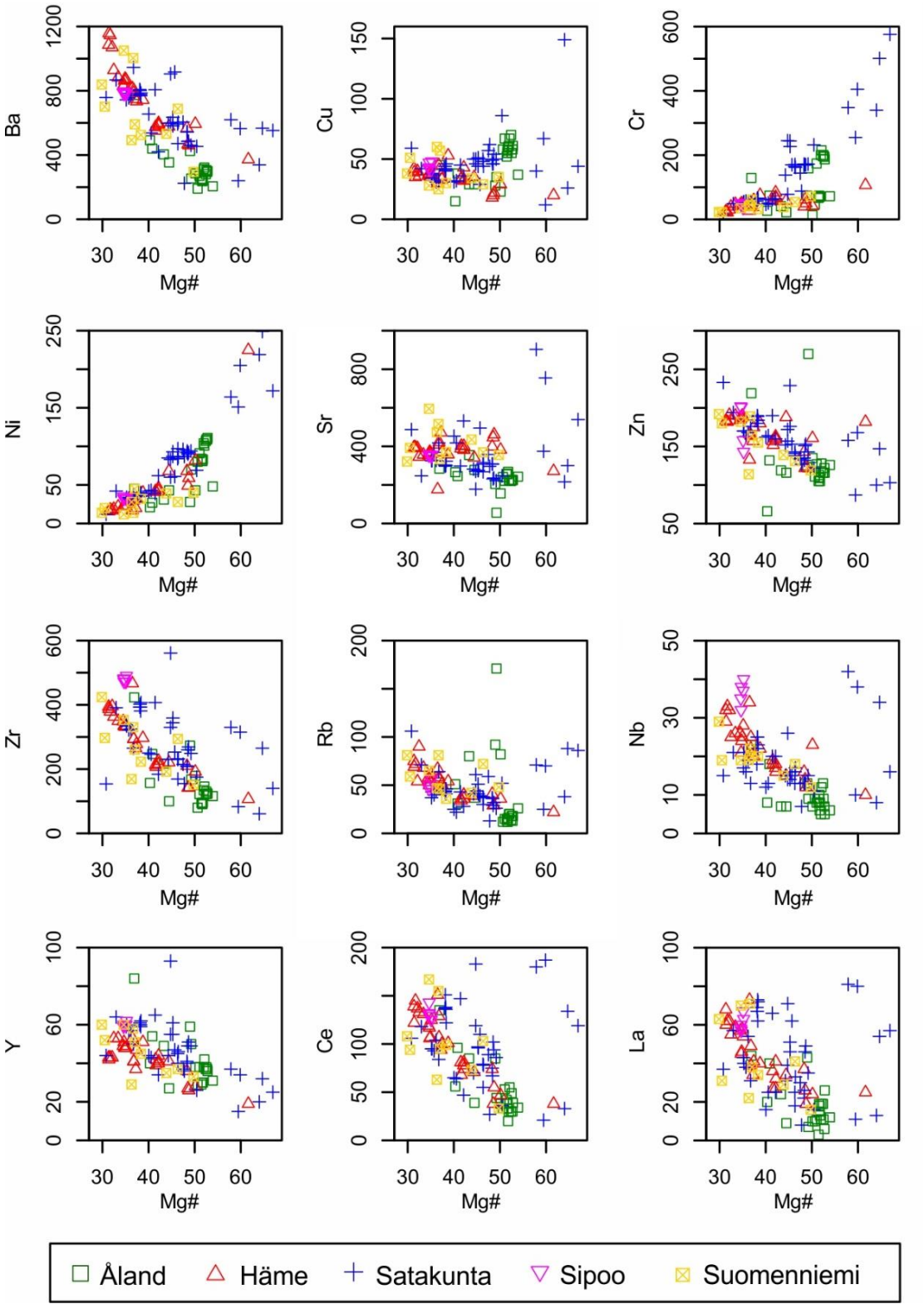

Figure 16. Mg number (Mg#) vs. trace elements (in ppm) variation diagrams for the Subjotnian dykes (n= 106).

5.2.2. Geochemistry of Åland dyke swarm

Fifteen of the 23 hyperstene-normative dykes of Åland are olivine-normative, while eight are quartz-normative. The Åland dykes are mainly subalkaline basalts in TAS diagram with low total alkalis (~3–4 wt.%.) (Figure 13). Dykes A10, A11, A12 and A13 are basaltic andesites and dyke A1, which is situated on a different island than other sampled dykes in Åland swarm (Figure 6), is a trachybasalt in TAS diagram (Figure 13) with a high total alkali value at ~5 wt.%.

Most of the Åland dykes in Figures 15 and 16 form a homogeneous group that is characterized by relatively low contents of incompatible elements (e.g. K_2O, P_2O_5, Ba, Zr, Rb, Nb, Ce and La) and high contents of CaO and Ni at Mg numbers of 42–51. Dykes A1 and A8–A13 differ from this group with slightly lower Mg numbers that range from 37 to 50, and with their generally higher K_2O, P_2O_5, Ba, Zr, Rb, Ce and La contents.

5.2.3. Geochemistry of Satakunta dyke swarm

Ten Satakunta samples (n=43) are olivine-normative while 33 are quartz-normative. Sample AM1-1AB/2AB (dyke AM) lacks normative diopside, was sampled close to chilled margin, and is discarded from further examination due to possible contamination from host rock (see Appendix I: sample AM7-1B is from the same dyke, 3 m from the dyke margin, and AM1-1AB/2AB is from close to contact.). The dyke OJ has a relatively high amount of normative olivine (24.40) compared to the other samples of Satakunta. The presumably Svecofennian aged dyke S11SL does not significantly differ from the whole Subjotnian assemblage in diagrams in Figures 13–16.

The majority of the Satakunta dykes plot in the subalkaline basalt and basaltic andesite fields in Figures 13 and 14 forming a coherent group with total alkalis at ~3.0–4.6 wt.%. Dykes OJ and AT plot in the alkaline basalt field in TAS diagram due to lower silica contents (Figure 13). Dyke AT is also different from the rest of the Satakunta dykes with its distinctively higher Ti, Zr, Y and Ce contents at the Mg number of 45. Most of the Satakunta dykes have Mg numbers between 31–50.

There is a group of four dykes (NO, NE, NI and NM) that have lower total alkalis (~2–3 wt.%) than the rest of the Satakunta dykes (Figure 13), plot in or near the alkaline basalt field in Figure 14, have high Mg numbers (58–65) and high contents of incompatible elements (TiO_2, K_2O, P_2O_5, Ba, Sr, Zr, Rb, Nb, Ce and La) as well as low Na_2O and FeO contents (Figures 15–16). The high contents of compatible elements (Ni, Cu) and high Mg numbers (59.5 and 64.7, respectively) suggest dykes AO and OJ might be part of this group. At least two dykes (NI and NO) in the group are metamorphic (Chapter 5.1; Appendix III).

5.2.4. Geochemistry of Häme dyke swarm

Twelve of the Häme dykes (n=29) are quartz-normative and 17 olivine-normative. In the TAS diagram (Figure 13), the Häme dykes plot on both sides of the alkaline-subalkaline boundary. They are characterized by relatively high contents of total alkali (~4.0–5.5 wt.%). Most of the Häme dykes are basalts, but a group of basaltic trachyandesites is also present. Apart from the picrobasalt dyke JS16-A05 (Mg number 62), the Häme dykes have Mg numbers between 31–50. Dyke JS16-A05 has a very high amount of normative olivine (40.99) and its magnetite norm is higher than ilmenite norm while the opposite occurs in the other Subjotnian dykes. It also shows a high content of olivine grains (Appendix III). The low-Mg Häme dykes are among the most incompatible element-enriched Subjotnian mafic intrusions. Dyke H21 is a basaltic andesite, highly anomalous relative to the other Häme dykes and has also a distinct strike direction and mode of occurrence (see Appendix I). This sample is therefore no longer discussed in this study.

5.2.5. Geochemistry of Suomenniemi dyke swarm

Four of the Suomenniemi dykes (n=10) are quartz-normative and six olivine-normative. The compositions of the Suomenniemi dykes are relatively scattered in all diagrams in Figures 13–16. In TAS diagram, they straddle the alkaline-subalkaline boundary and are basalts and basaltic andesites with total alkali contents in the range of ~3–5 wt.%. Their Mg numbers range between 30–50. Some of the Suomenniemi samples have slightly lower contents of incompatible elements at given Mg number than the rest of the Subjotnian samples.

5.2.6. Geochemistry of Sipoo dyke swarm

The samples (n=5) from the Sipoo dykes (n=4) show all olivine-normative compositions. The Sipoo dykes are geochemically homogeneous. In the TAS diagram (Figure 13), they plot in the alkaline basalt field with relatively high contents of total alkalis at ~4.6 wt.%. They are among the most evolved dykes with low Mg numbers (~35). The Sipoo dykes have slightly higher TiO_2, P_2O_5, Zr and Nb at given Mg numbers than the other Subjotnian dykes.

5.2.7. Geochemical grouping of the dykes

Geochemical compositions of mafic rocks reflect the net effect of several processes, including partial melting, fractional crystallization and crystal accumulation, magma mixing and contamination, degassing and secondary alteration. Nb/Y vs. Zr/Y diagram (Figure 17) eliminates the effects of fractional crystallization of mafic magmas and the ratios of the incompatible elements in this diagram are not affected by secondary alteration. The distribution coefficients of Nb, Zr and Y for the predominant mineral phases of mafic magmas, i.e. plagioclase, olivine and clinopyroxene, are similar (e.g. Aigner-Torres et al. 2007; Earthref.org, GERM Partition Coefficient (Kd) Database, site visited 02.10.2018). Thus, the ratios of these elements during fractional crystallization stay somewhat constant. Higher degree of partial melting results in decreasing Nb/Y and Zr/Y, because the distribution coefficients of Nb and Zr are similar, but they are lower than that of Y for the mantle peridotite minerals (olivine, orthopyroxene, clinopyroxene, garnet/spinel) (e.g. Salters and Longhi 1999; Earthref.org, GERM Partition Coefficient (Kd) Database, site visited 02.10.2018). Thus, variations in Nb/Y at given Zr/Y are very likely to indicate mantle source heterogeneity, because variable partial melting is typified by coupled variations in Nb/Y and Zr/Y (e.g. Luttinen 2018). Overall, the Nb/Y vs. Zr/Y plot (Figure 17) effectively summarises petrogenetically significant geochemical variation in the studied Subjotnian dykes. The same elements, Nb, Zr and Y were first used as a diagnostic feature of the Subjotnian dykes by Luttinen and Kosunen (2006) and were later also used by Salminen et al. (2014).

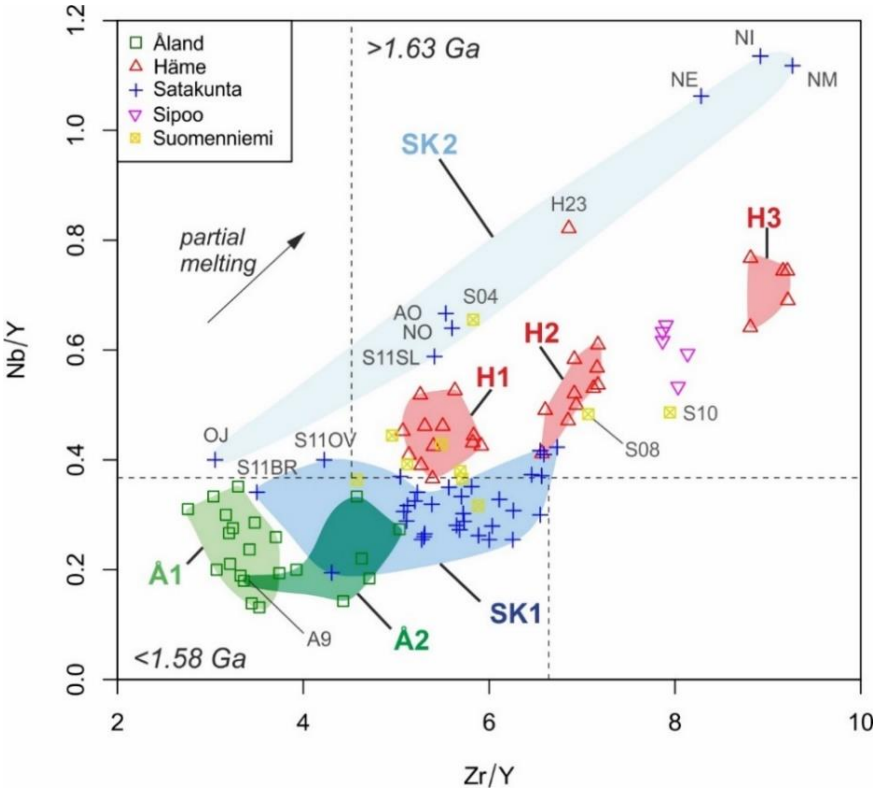

Figure 17. Variation of Nb/Y vs. Zr/Y for the Subjotnian dyke swarms (n=104). Exceptional dykes are indicated (see text). H1, H2 and H3 (Häme swarm), SK1 and SK2 (Satakunta swarm) and Å1 and Å2 (Åland swarm) refer to geochemical groups defined in this study. Dashed lines indicate compositional fields of older (>1.63 Ga) and younger (<1.58 Ga) swarms.

Table 2. Grouping of the Åland dykes according to their geochemistry as in Figure 17. N=normal polarity magnetization. R=reversed polarity magnetization.

ÅLAND SAMPLE/DYKE	LOCATION	POLARITY OF VGP	WIDTH OF DYKE (m)	STRIKE/ DIP (°)
GROUP Å1:				
A2G-2/**A2**	Korsö	R	100-300	170/-
A3C-2/**A3**	Korsö	R	>100	170/-
A4D-2/**A4**	Brändö-s-tip	R	0.2	045/60
A5C-2/**A5**	Brändö-s-tip	R	0.3	045/90
A6A-2/**A6**	Brändö-s-tip	R	0.05-0.1	045/90
A7C-2/**A7**	Brändö-s-tip	R	0.15	045/90
A14F-2/**A14**	Torsholma-Barkholm	R	1.5	040/85
A15F-2/**A15**	-"-	R	0.8	040/80
A16D-2/**A16**	-"-	R	0.5	040/80
A17B-2/**A17**	-"-	R	1.5	025/80
A18B-2/**A18**	-"-	R	1	040/90
A19C-2/**A19**	-"-	R	1.5	030/90
A20A-2/**A20**	-"-	R	1.5	025/85
A21C-2/**A21**	-"-	R	1.5	035/80
A22A-2/**A22**	Brändö-s-tip	R	>5	
GROUP Å2:				
A1E-2/**A1**	Enklinge	N	3	045/80
A8C-2/**A8**	Brändö-s-tip	R	0.3	045/90
A9A-2/**A9**	Keistiö	N	0.12	020/80
A10A-2/**A10**	Keistiö	-	0.1-0.6	
A11B-2/**A11**	Keistiö	N	0.35	035/ 80
A12C-2/**A12**	Keistiö	-	0.3	030/75
A13E-2/**A13**	Keistiö	N	5	025/ 85

The Åland dykes form two groups (Å1 and Å2; Figure 17; Table 2). Although its Zr/Y value is similar to Group Å1 (~3–4), dyke A9 is assigned to Group Å2 based on the geochemistry described in Section 5.2.2.

The Satakunta samples also form two groups (SK1 and SK2; Figure 17; Table 3), of which the Group SK1 includes most of the samples. Group SK1 is geochemically

Table 3. Grouping of the Satakunta dykes according to their geochemistry as in Figure 17. N=normal polarity magnetization. R=reversed polarity magnetization. SVF=Svecofennian.

SATAKUNTA SAMPLE/DYKE	LOCATION	POLARITY OF VGP	WIDTH OF DYKE (m)	STRIKE/ DIP (°)
GROUP SK1:				
AM7-1B/**AM**	Ämttöö	N	>20	000/90
S11HJ 10.1/**S11HJ**	Heikinjärvi	N	>6-10	020/90
S11HJ 14.1/**S11HJ**	Heikinjärvi	N	10	020/90
IV6-1A/**IV**	Ilvesmäki-Pori-Toukari	N	>20	170/90
IV15-1A/**IV**	Ilvesmäki-Pori-Toukari	N	>20	170/90
S11GR 4.1/**S11GR**	Grötgrund	R	1.5	000/60
S11LS 5.1/**S11LS**	Lillsund	N	>60	000/-
HH2-1B/**HH**	Holmberginhaka	-		005/80
S11KA 4.1/**S11KA**	Karlstrand	-	1.5	145/60
S11VA 1.1/**S11VA**	Västerängen	-	10-15	160/90
S11PL 1.1/**S11PL**	Powerline-Kristiinankaupunki	-	~4	165/70
S11VR 2.1/**S11VR**	Vargöskatan	-	0.5	160/-
S11OV 3.1/**S11OV**	Överträsket	R	<0.15	010/60
MA1-1D/**MA**	Mäntymäki	N	15	170/90
MA9-1D/**MA**	Mäntymäki	N	15	170/90
AT2-1B/**AT**	Ämttöö-Riisivilja	N	0.1	035/90
FB5-1B/**FB**	Fiskee	-	~1	060/-
FE-1AB/1B/**FE**	Fiskee	N	0.3	060/72
FI1-1B/**FI**	Fiskee	-	<0.3	040/90
FK2-3C/**FK**	Fiskee	-	0.7	058/90
FS3-1B/**FS**	Fiskee	-	0.35	050/ 90
FT10-1A/**FT**	Fiskee	-		047/90
FC1-1D/**FC**	Fiskee	-	~7	060/90
FC5-1A/**FC**	Fiskee	-	~7	060/90
FD6-1D/**FD**	Fiskee	-	<0.3	060/50
FH7-1AB/**FH**	Fiskee	-	0.3	060/ 80
LK8-1B/**LK**	Fläksholma	-		055/90
SA8-1B/**SA**	Salmela	-		090/75
FA9-1C/**FA**	Fiskee	R	0.35	090/90
NR6-1A/**NR**	Söörrmarkuntie	-	0.2	095/85
S11BR 5.1/**S11BR**	Brändön	-	<0.5	075/90
JS16-A01B-1/**JS16-A01**	Karlstrand	-	<2	130/90
GROUP SK2:				
NE1-1B/**NE**	Niemi	-		
NI6-1B/**NI**	Niemi	-		100/75
NM1-1C/**NM**	Niemi	-		
OJ2-2B/**OJ**	Ojala	N	0.1	090/90
NO2-1B/**NO**	Söörrmarkuntie	N	0.6	150/65
S11SL 5.1/**S11SL**	Strandlund	N (SVF)	1.5	090/90
AO3-1A/**AO**	Ämttöö-Riisivilja	N	0.25	115/60

relatively uniform and is typified by low Nb/Y at given Zr/Y. Based on the overall geochemistry, dykes S11BR and S11OV were assigned to Group SK1 despite their relatively low Zr/Y ratios when compared to the other dykes in Group SK1 (Figure 17).

Satakunta Group SK2 shows variable Zr/Y and Nb/Y and is distinguished from most of the Subjotnian dykes by high Nb/Y at given Zr/Y. Several dykes belonging to Group SK2 (NI, NO, AO, OJ) show evidence of metamorphism or very strong alteration (including low total values). Group SK2 includes also the presumably Svecofennian dyke S11SL. It is possible the dykes NE and NM in Group SK2 are metamorphosed since their chemistry is similar to that of the metamorphosed dyke NI (Figure 17).

The Häme dykes also show wide ranges of Zr/Y and they can be divided into three groups (Table 4). Group H1 includes the majority of the Häme dykes and shows the lowest Nb/Y (~0.4–0.5) and Zr/Y ratios (~5–6). Group H3 has the highest Nb/Y (~0.6–0.8) and Zr/Y ratios (~9) while Group H2 has Nb/Y in the range of ~0.4–0.6 and Zr/Y at ~7. Group H1 partly coincides with the Suomenniemi dykes and Group H2 with one dyke (S08) from Suomenniemi (Figure 17). Dyke H23 could not be assigned to these groups. This study supports the conclusion of Lindholm (2010) that the geochemical groups of Häme dykes do not correlate with the strike direction of the dykes (Table 4) as was earlier proposed by Laitakari (1969; 1987) and Vaasjoki and Sakko (1989).

The Suomenniemi samples cluster near the Häme Group H1 in Figure 17, but there is also variation within the swarm. Sample S04 of the Lovasjärvi intrusion has relatively high Nb/Y (~0.65) at Zr/Y of ~6, and dyke S10 relatively high Zr/Y (~8) at Nb/Y of ~0.5. The scatter in the Suomenniemi data implicates that the sample set may not be sufficient for a comprehensive picture of the compositional variability in the Suomenniemi swarm.

As in the previous diagrams in Chapter 5.2., the Sipoo dykes form their own, homogeneous geochemical group (Figure 17). They are characterized by relatively high Nb/Y (~0.5–0.6) and Zr/Y (~8).

Table 4. Grouping of the Häme dykes according to their geochemistry as in Figure 17. N=normal polarity magnetization. R=reversed polarity magnetization.

HÄME SAMPLE/DYKE	LOCATION	POLARITY OF VGP	WIDTH OF DYKE (m)	STRIKE/ DIP (°)
GROUP H1:				
JS16-A03F-1/**JS16-A03F**	Soidinkallio	-	8	125/-
JS16-A04A-1/**JS16-A04**	Kurjeniemi	N	24	140/90
JS16-A05C-1/**JS16-A05**	Heinola	N	>250	135/-
JS14-H3A-1/**H3**	Kasiniemi	-	20	120/-
JS14-H4B-1/2/**H4**	Kasiniemi/Ansio	-	30	120/-
JS14-H6C-1/**H6**	Karivuori	-	>70	100/-
JS14-H12A/**H12**	Hirtniemi	N	12	095/90
JS14-H13A1/**H13**	Hirtniemi	R	>60	135/90
JS14-H18A-1/**H18**	Tuomasvuori	N	~50	135/-
JS14-H18C-1/2/**H18**	Tuomasvuori	N	~50	135/-
JS14-H24A1/**H24**	Romo	R	>50	130/-
JS14-H25B/E-1/**H25**	Muorinkallio	N	>80	130/-
GROUP H2:				
JS16-A02C/D-1/**JS16-A02**	Iso Niinilammi	N	1.9	135/75
JS14-H1B-1/2/**H1**	Orivesi: Tre-Jklä road	N	5	090/90
JS14-H1E-1/2/**H1**	Orivesi: Tre-Jklä road	N	5	090/90
JS14-H2F-1/**H2**	Orivesi: Tre-Jklä road	-	1.5	100/-
JS14-H7B-1/**H7**	Vehkajärvi	-	3.1	100/90
JS14-H7L-1/**H7**	Vehkajärvi	-	3.1	100/90
JS14-H11A/**H11**	Hirtniemi	-	6-8	135/90
JS14-H14C-1/**H14**	Myllylahti	-	>40	140/ 00
JS14-H15C-1/2/**H15**	Harmoistenkaivo	N	45	140/90
JS14-H17A-1/**H17**	Torittu	R	~60	090/90
GROUP H3:				
JS14-H16E-1/2/**H16**	Torittu	-	0.6	100/90
JS14-H19A-3/**H19**	Koukkujärvi	-	24	130/-
JS14-H19H-2/**H19**	Koukkujärvi	-	24	130/-
JS14-H20F-1/2/**H20**	Koukkujärvi	R	2.5-3	110/90
JS14-H22B-1a/1d/**H22**	Koukkujärvi	-	>12	110/90
OTHER:				
JS14-H23A1/**H23**	Partakorpi	R	30	110/-

It is interesting to notice that the dyke swarms that are believed to have emplacement ages of >1.63 Ga plot almost exclusively at high Nb/Y (and Zr/Y) values in Figure 17. In contrast, the dyke swarms that probably record younger magmatic events at <1.58 Ga are typified by low Nb/Y and Zr/Y. This apparent transition from high Nb/Y to low Nb/Y compositions during Subjotnian magmatism is discussed in Chapter 6.3.

6. DISCUSSION

6.1. Geochemistry vs. magnetic polarity records in the dykes

The reversal of the geomagnetic field is manifested in the studied dykes by the existence of both N and R polarity magnetization directions. Mafic rocks with different polarity must have at least marginally different ages. Bearing in mind that the precision of even the best isotopic ages is on the order of 1% and that polarity intervals can be relatively short (>10^4 years; Butler 1992), comparison between magnetic polarity and geochemical variations can provide useful constraints for assessing the magmatic-tectonic evolution of mafic dyke swarms. Figure 18 shows the variation of Nb/Y vs. Zr/Y of all the dykes compared with the polarity of the primary magnetization direction. Most dyke swarms have formed slowly enough for the magnetic field reversal to have occurred at least once. The geochemistry of the N polarity dykes is different from that of the R polarity dykes within the Åland swarm and within Satakunta Group SK1.

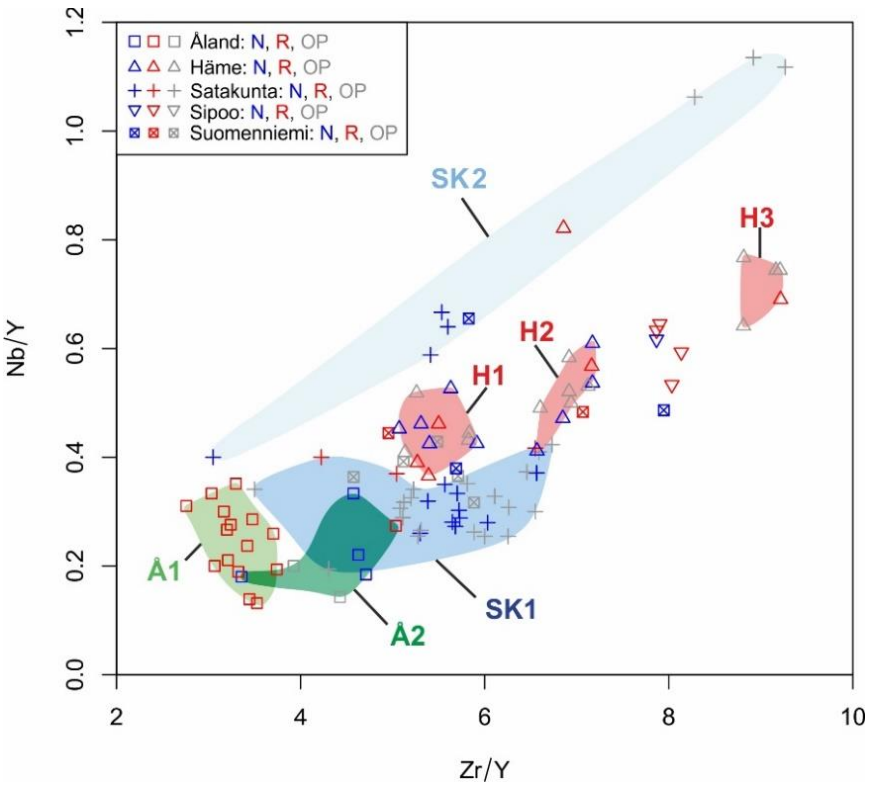

Figure 18. Variation of Nb/Y vs. Zr/Y of the studied dykes (n=104) compared with the magnetic polarity of the dykes. The geochemical groups (as in Figure 17) of Åland (Å1 and Å2), Satakunta (SK1 and SK2) and Häme (H1-H3) are indicated. N=normal polarity magnetization. R=reversed polarity magnetization. OP=overprinted (no primary component obtained).

The geochemical division of the Åland dykes is in line with the polarity directions (Figure 19). This correlation is clearly visible in the Nb/Y vs. Nb plot in Figure 19b. Group Å1 includes only dykes that show R polarity. Group Å2 includes the N polarity dykes and one R polarity dyke. The dykes that did not show a primary paleomagnetic component (dykes A10 and A12) are located in the same area as the N polarity dykes (Figure 6) and show geochemical affinity to Group Å2. Group Å2 differs from Group Å1 by higher Zr/Y ratios (Figure 19a). As reported in Section 5.2.2. for the dykes in Group Å2, they also have higher SiO_2, K_2O, P_2O_5, Ba, Zr, Nb, Rb, Ce and La contents and slightly lower Mg numbers than the dykes in Group Å1. The different magnetic polarities in the geochemically defined groups of mafic dykes in Åland imply there were two separate magmatic events/pulses that have an age difference.

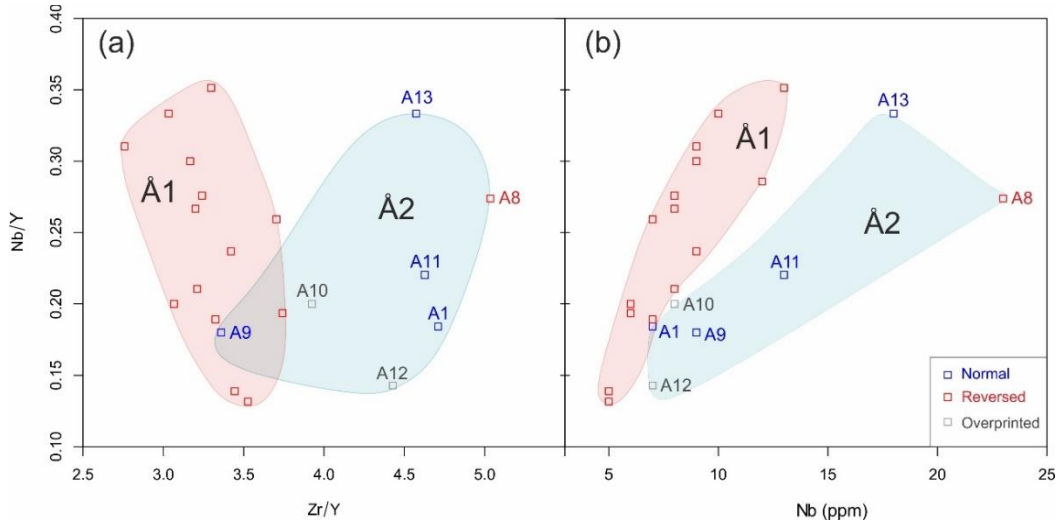

Figure 19. Variation of Nb/Y vs. a) Zr/Y and b) Nb of the normal and reversed polarity Åland dykes.

In Satakunta, Group SK1 shows mainly N polarity. Three dykes show R polarity. Within the Satakunta Group SK1, the N and R polarity dykes show a clear division in their Nb/Y ratios (Figure 20). The Nb/Y ratios of the R polarity dykes are higher at given Zr/Y ratios than those of the N polarity dykes. As in Åland, this could mean they have different magma sources that represent different magmatic events. However, the small number of R polarity dykes in Group SK1 may not be sufficient enough to reliably verify this conclusion.

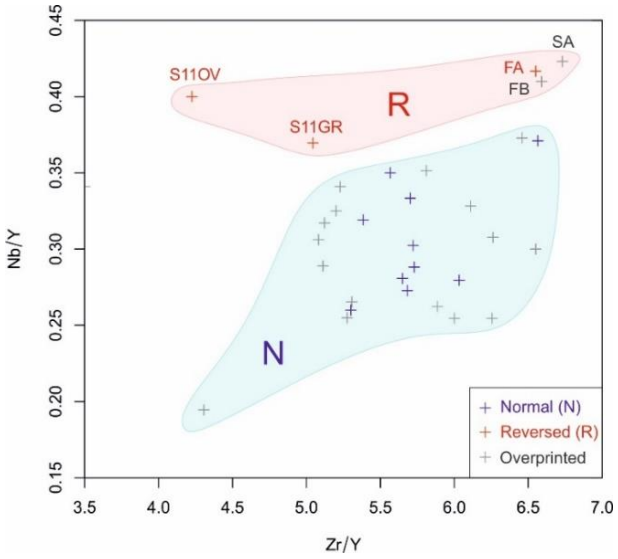

Figure 20. Variation of Nb/Y vs. Zr/Y for the normal and reversed polarity Group SK1 dykes (Satakunta).

In Häme, Groups H1 and H2 contain both N and R polarity dykes (Figure 18). Group H3 only has one dyke with a primary (R polarity) magnetization component (dyke H20). The Suomenniemi dykes do not show correlation between the magnetic polarity and geochemistry either (Figure 18). This means the mafic intrusions have emplaced during a long enough time period for the magnetic field reversal to have occurred at least once in Häme and in Suomenniemi. However, the data do not facilitate assessment of possible age differences between Groups H1, H2 and H3 in the Häme swarm.

As described by Mertanen and Pesonen (1995), the only N polarity dyke in Sipoo (the dyke SF) has probably obtained its N polarity magnetization direction as an overprint by the felsic intrusions in the area. It possibly originally contained also the R polarity magnetization direction. Thus, the Sipoo dykes are homogeneous in geochemistry and most likely have the same magnetic polarity (Figure 18), which implies they formed during the same magmatic event.

6.2. Comparison between VGPs and geochemistry

If the secular changes of the Earth's magnetic field are averaged out, coeval VGPs from same sampling site should be overlapping. Thus, dykes that record distinct VGPs

probably have an age difference. Within the studied dykes there is geochemical variation that could indicate age differences between the dykes. Therefore, the VGPs are compared with the geochemistry of the dykes.

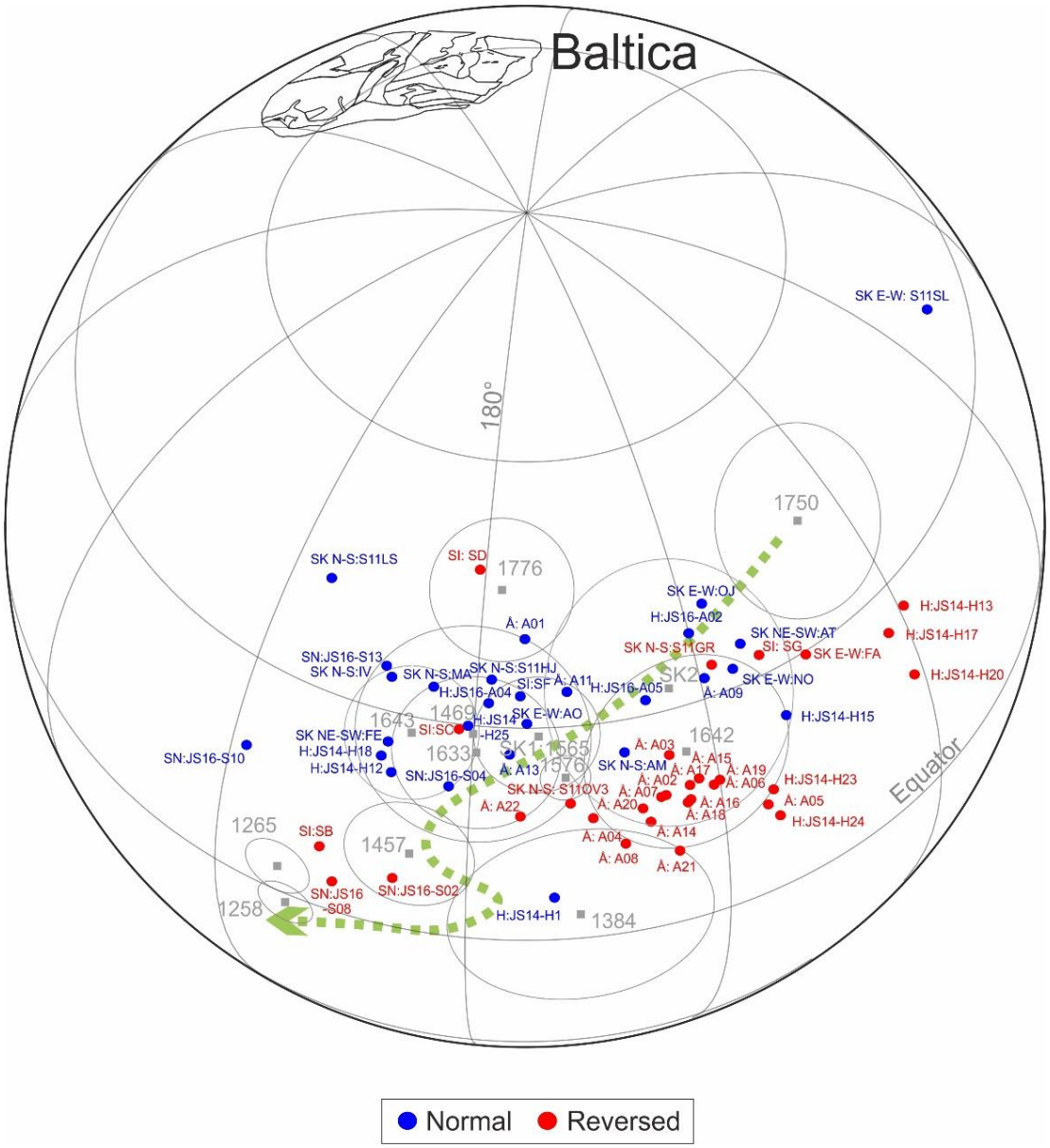

Figure 21. The virtual geomagnetic poles of the Subjotnian mafic dykes used in this study. VGP data from Mertanen and Pesonen (1995) and Salminen et al. (2014; 2016; 2017; 2018). Baltica is at its present-day location. The reversed polarity poles have been inverted. The grey squares with error circles and ages in Ma are paleomagnetic poles for Proterozoic Baltica: see references in Figure 3. The APWP for Proterozoic Baltica (green dashed line) is drawn after Salminen et al. (2017). Å = Åland, SK = Satakunta, H = Häme, SN = Suomenniemi, SI = Sipoo. The Satakunta dykes are divided into three groups based on their strike directions (N-S, NE-SW and E-W). The VGP of the dyke S11SL was interpreted to be of Svecofennian age by Salminen et al. (2014) based on its position.

This study uses the VGPs from the previous publications by Mertanen and Pesonen (1995) and Salminen et al. (2014; 2016; 2017; 2018). The VGPs are plotted in Figure 21. The geochemical analyses of this study are made from the same samples from which the paleomagnetic studies were made. The number of dykes showing primary magnetization (and a VGP) in this study is lower than the number of dykes used for geochemical analyses due to weak remanent magnetization components and/or strong secondary components, or due to scattered paleomagnetic results. In general, the R polarity VGPs seem to plot at lower latitudes than the N polarity VGPs, which reflects the geomagnetic reversal asymmetry observed in some Subjotnian paleomagnetic results (Salminen et al. 2014; 2016; 2017).

6.2.1. The Åland dyke swarm

Figure 22 highlights the positions of the VGPs of the Åland dykes. The geochemistry of the Åland dykes correlates with the polarity of VGPs as discussed in Chapter 6.1. The N polarity VGPs of Åland comprise a scattered group at higher latitudes than the R polarity VGPs that form a coherent group near the Häme 1642 Ma mean pole (Figure 22). This may imply a possible age difference between the N and R polarity dykes as suggested in previous studies (Salminen et al. 2016). The geochemistry supports this as the dykes with N polarity VGPs have slightly different ratios of incompatible elements than the dykes with R polarity VGPs. This suggests that the N polarity and R polarity dykes represent separate magmatic events.

The Åland Group Å2 has similar Zr/Y and Nb/Y values to Satakunta Group SK1 (Figure 17), which raises the question whether these two dyke swarms are at least partially co-magmatic. Generalizing, the VGPs of Åland Group Å2 are also near the VGPs of Satakunta (Figures 21–22). On the other hand, this is expected for nearly coeval poles and does not mean they are co-magmatic. The VGP of the R polarity dyke A8 from Group Å2 also plots together with the other R polarity VGPs of Åland (i.e. Group Å1) (Figure 22). Based on these data, it cannot be said that the Åland swarm continues to Satakunta region.

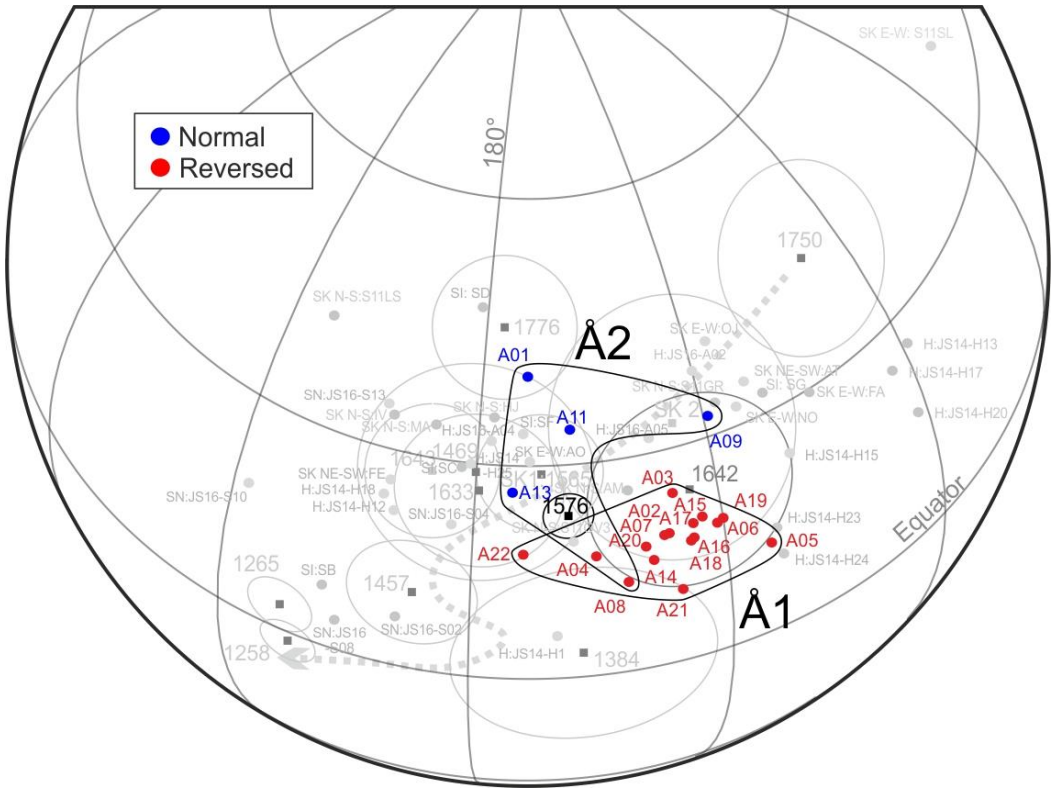

Figure 22. The highlighted normal and reversed polarity VGPs of Åland dykes. Other VGPs are shown for comparison (cf. Figure 21). The geochemical groups Å1 and Å2 are indicated. The paleomagnetic pole of the Åland swarm by Salminen et al. (2016) is indicated by black colour. Paleomagnetic data from Mertanen and Pesonen (1995) and Salminen et al. (2014; 2016; 2017; 2018).

6.2.2. The Satakunta dyke swarm

The variation of Nb/Y vs. Zr/Y and the VGPs of the Satakunta dykes are shown in Figure 23. For paleomagnetic studies, the Satakunta dykes were divided by Salminen et al. (2014) into three groups based on their strike directions (E-W, NE-SW and N-S). Salminen et al. (2014) obtained two paleomagnetic poles from Satakunta: Pole SK1 from the NE-SW and N-S trending dykes and Pole SK2 from the E-W trending dykes of Satakunta (Figures 3 and 23a). These poles are hereby referred to as "Pole SK1" and "Pole SK2" to separate them from the geochemical groups "Group SK1" and "Group SK2" defined in this study. Pole SK2 was interpreted to be older than Pole SK1 (but still Subjotnian) by Salminen et al. (2014). Additionally, one E-W trending dyke (dyke S11SL in this study) was interpreted to be Svecofennian (and was thus excluded from the Subjotnian pole calculations) by Salminen et al. (2014) based on its VGP position (Figures 21 and 23a).

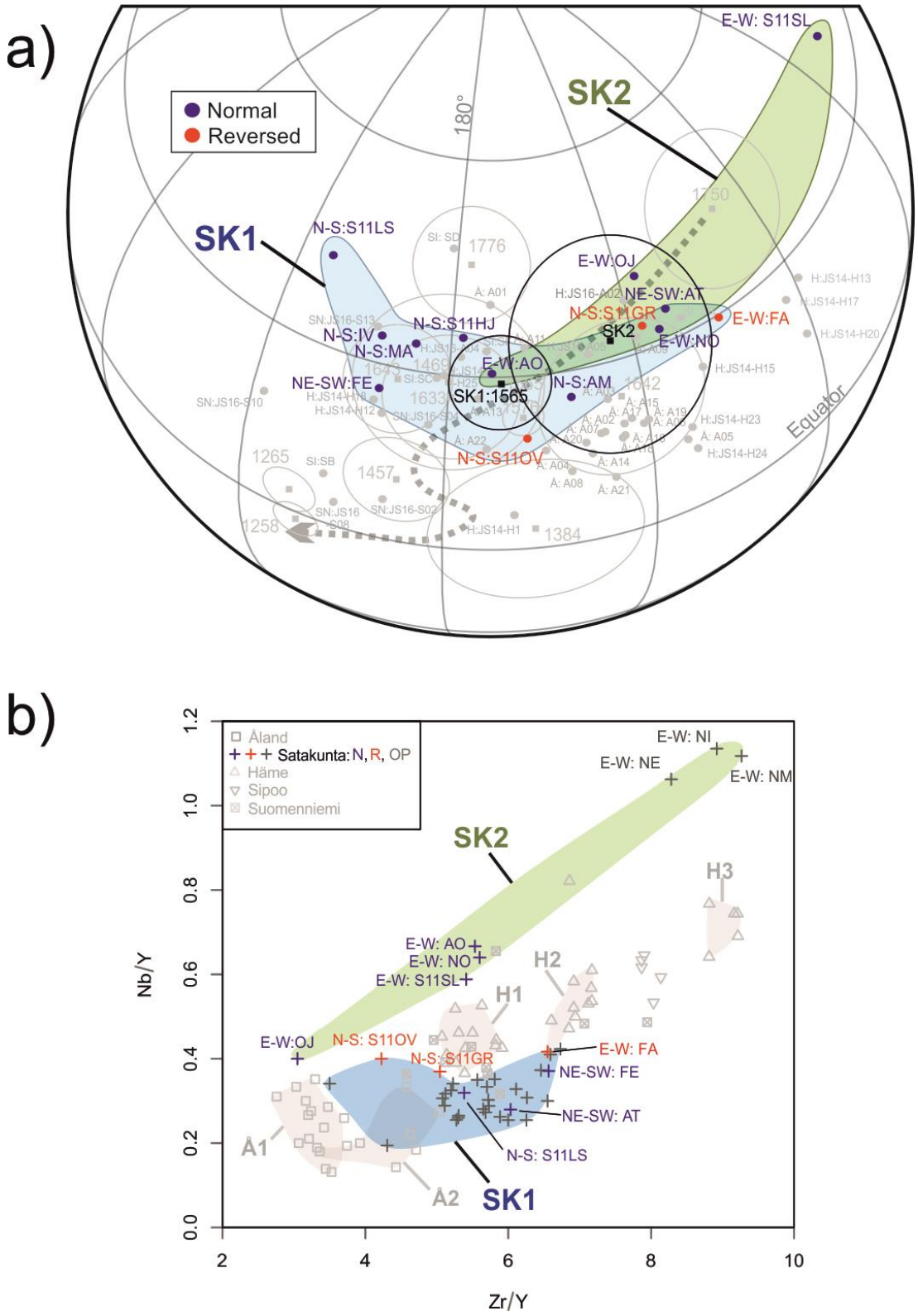

Figure 23. The highlighted a) positions of the VGPs (cf. Figure 21) and b) the variation of Nb/Y vs. Zr/Y of the Satakunta dykes (cf. Figure 17). The geochemical groups SK1 and SK2 of the Satakunta dykes (cf. Figure 17) are indicated in both figures. The paleomagnetic poles (SK1 and SK2) of Satakunta by Salminen et al. (2014) are indicated by black colour in a). N=normal polarity magnetization. R=reversed polarity magnetization. OP=overprinted (no primary component obtained). Paleomagnetic data from Mertanen and Pesonen (1995) and Salminen et al. (2014; 2016; 2017; 2018).

The geochemistry of this study mostly agrees with the division of the Satakunta dykes by Salminen et al. (2014) as Group SK2 consists only of E-W trending dykes (Table 4). In Group SK1, there is one E-W trending dyke that has a VGP (dyke FA). Group SK2 is discussed here first.

Based on petrography (Chapter 5.1.; Appendix III), dykes NI and NO from Group SK2 are metamorphic. The geochemical similarity (high Nb/Y) between the metamorphic dykes and other dykes belonging to Group SK2 suggests five Satakunta dykes (NO, S11SL, NI, NE, NM) are Svecofennian or at least older than Subjotnian (Figure 23b). Despite its similar geochemistry, dyke AO is not considered to be part of this presumably Svecofennian group, because it yielded a positive baked contact test (Salminen et al. 2014) and can be regarded as Subjotnian.

The VGP of the metamorphic dyke NO is located on the older side of the APWP for Baltica (Figure 23a), implying an older Subjotnian age than the 1.57 Ga Satakunta dykes [as suggested by Salminen et al. (2014) for the Pole SK2]. It is possible the Subjotnian magnetization component in dyke NO is a secondary component that has overprinted the possible Svecofennian primary magnetization direction.

Following the observations described above, the only dykes in Group SK2 that can be regarded as Subjotnian are dykes AO and OJ. They both have high Nb/Y at given Zr/Y and a *high* or a *very high* level of alteration (Appendix III). Additionally, the VGP of dyke OJ is on the older side of the APWP for Baltica (Figure 23a). Combined, the geochemical and paleomagnetic features imply that dykes AO and OJ have an older Subjotnian age than the 1.57 Ga age of Group SK1.

In Group SK1, there are three dykes that show VGPs on the older side of the APWP for Baltica (dykes FA, S11GR and AT; Figure 23a). The VGPs of these three dykes from Group SK1 thus imply they could belong to the presumably older group of Subjotnian dykes in Satakunta. One of them (dyke FA) has an E-W strike direction and was included in the calculation of the presumably older Pole SK2 by Salminen et al. (2014). Dyke FA is very altered (Appendix III) which supports it having an old age. It has also relatively high Nb/Y (0.4), connecting it with the >1.63 Ga dykes in Figure 17. The N-S trending dyke S11GR, however, apart from the differences related to the magnetic polarity of the

dykes (Chapter 6.1.), does not differ from the rest of the dykes of the Satakunta Group SK1 geochemically. The NE-SW trending dyke AT, on the other hand, has distinctively higher Ti, Zr, Y and Ce contents than all the other Satakunta dykes at the Mg number of 44.8 (Section 5.2.3.), but it does not stand out from Group SK1 dykes in Figure 23b. Dyke AT is also very altered (Appendix III). Although it cannot be concluded reliably without detailed chronological studies, dykes FA and AT have geochemical and paleomagnetic implications that they are part of the presumably older Subjotnian dykes of Satakunta.

The positions of the N and R polarity VGPs of Group SK1 (Figure 23a) do not support the speculation that the dykes of different polarities represent different magmatic events (as was discussed in Chapter 6.1). N and R polarity VGPs occur on both older and younger sides of the APWP for Baltica (Figure 23a).

6.2.3. The Häme dyke swarm

The VGPs of Häme swarm show a dispersion of VGPs comparable to that observed in the Satakunta swarm (Figures 23 and 24). The VGPs of the R polarity dykes of Häme plot near the older side of the APWP for Baltica, while the majority of the dykes with N polarity VGPs plot closer to the younger side (Figure 24a). Comparison of the three geochemical groups H1–H3 does not reveal correlation between geochemistry and VGPs (Figure 24). Häme Groups H1 and H2 show both N and R polarity and Group H3 only has one dyke with a primary magnetization component (dyke H20). Dyke H23 shows R polarity VGP but could not be assigned to any of the geochemical groups of Häme.

Several dykes from Häme have been dated, but only those age determinations that have error limits less than ±10 Ma are discussed in this section. The dated dykes that have N polarity VGPs are H12 and H25, and they show similar 1.64 Ga ages (J. Salminen, unpublished data). A dyke with a R polarity VGP (dyke H13) gives also an age of 1.64 Ga (J. Salminen, unpublished data). All these dated dykes belong to Group H1. These most reliable age determinations prove that some N polarity dykes are of same age as some R polarity dykes, but it does not necessarily mean that this applies to all the dykes of Häme. There is a ~60° difference in longitude between the VGPs of the nearly coeval dykes H12 (and H25) and H13 (Figure 24a). Therefore, it is likely that an age difference

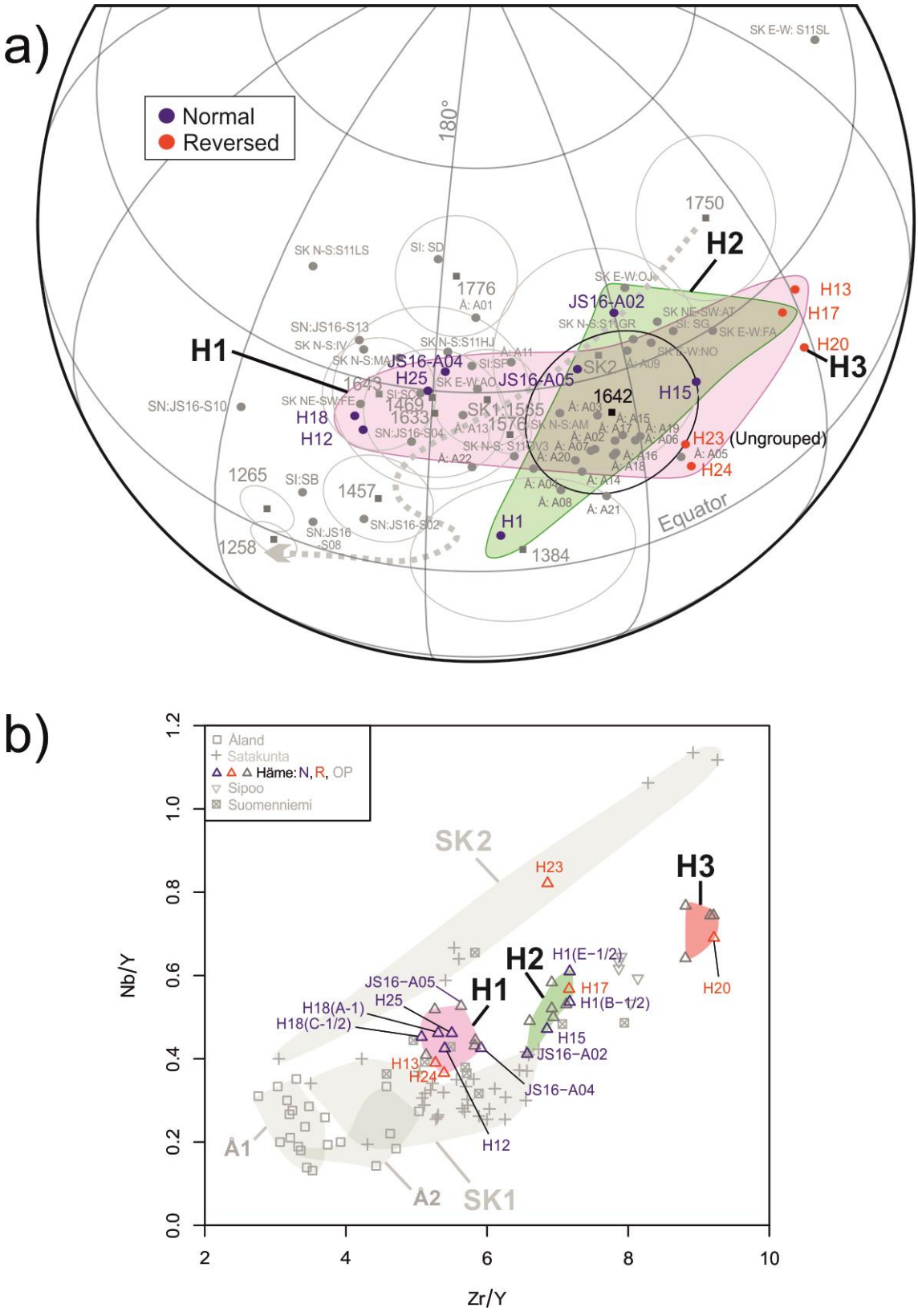

Figure 24. The highlighted a) positions of the VGPs (cf. Figure 21) and b) the variation of Nb/Y vs. Zr/Y of the Häme dykes (cf. Figure 17). The geochemical groups of the Häme dykes H1, H2 and H3 (as in Figure 17) are indicated in both figures. The paleomagnetic pole of the Häme swarm by Salminen et al. (2017) is indicated by black colour in a). N=normal polarity magnetization. R=reversed polarity magnetization, OP=overprinted (no primary component obtained). Paleomagnetic data from Mertanen and Pesonen (1995) and Salminen et al. (2014; 2016; 2017; 2018).

between the N and R polarity dykes does not explain the distinct VGPs of different polarities and the scatter in Häme paleomagnetic data.

There are no well-defined ages for the dykes of Häme Groups H2 and H3. However, dykes H17 and H20 from Groups H2 and H3 respectively, have VGPs near the dated dyke H13 (Figure 24a). This implies their ages are also similar to that of dyke H13 and that all the geochemical groups in Häme have roughly the same age: 1635–1640 Ma (J. Salminen, unpublished data). Geochemical variation can occur rapidly, and the differences observed between the geochemical groups of Häme can be explained with the age range of 5 Ma. There is however no reason for the purposes of paleomagnetism to separate different magma pulses if they are roughly the same age.

There are no implications in geochemistry that would explain the scattered VGPs of the Häme dykes. Thus, the VGPs may show scatter due to paleosecular variation of the geomagnetic field or due to other problems in paleomagnetic data that are beyond the scope of this study.

6.2.4. The Suomenniemi dyke swarm

The Suomenniemi VGPs are relatively scattered, but they tend to settle near the younger side of the APWP for Baltica (Figures 21 and 25a). The Suomenniemi dykes are also geochemically relatively variable. Some dykes resemble the Häme dykes while others resemble the Satakunta dykes (Figure 25b). One dyke (S10) from Suomenniemi has similar Zr/Y and Nb/Y values to the Sipoo dykes (Figure 25b). Dyke S13 from Suomenniemi shows similarity in geochemistry with the Häme Group H1 dykes and has a VGP near them (Figure 25). Dykes S02 and S08 have also geochemical affinities to the Häme dykes, but their VGPs are a bit off from the Häme VGPs (Figure 25). The positions of the R polarity VGPs of Suomenniemi near the younger side of the APWP for Baltica, however, imply that the Suomenniemi dykes were emplaced during an igneous event distinct from the Häme event(s).

Based on the presence of composite dykes as well as mafic dykes cutting 1644–1640 Ma rapakivi granites, Rämö (1991) and Vaasjoki et al. (1991) suggested that some of the Suomenniemi dykes are ~10 Ma younger than the 1643 Ma intrusion in Lovasjärvi (sheet-

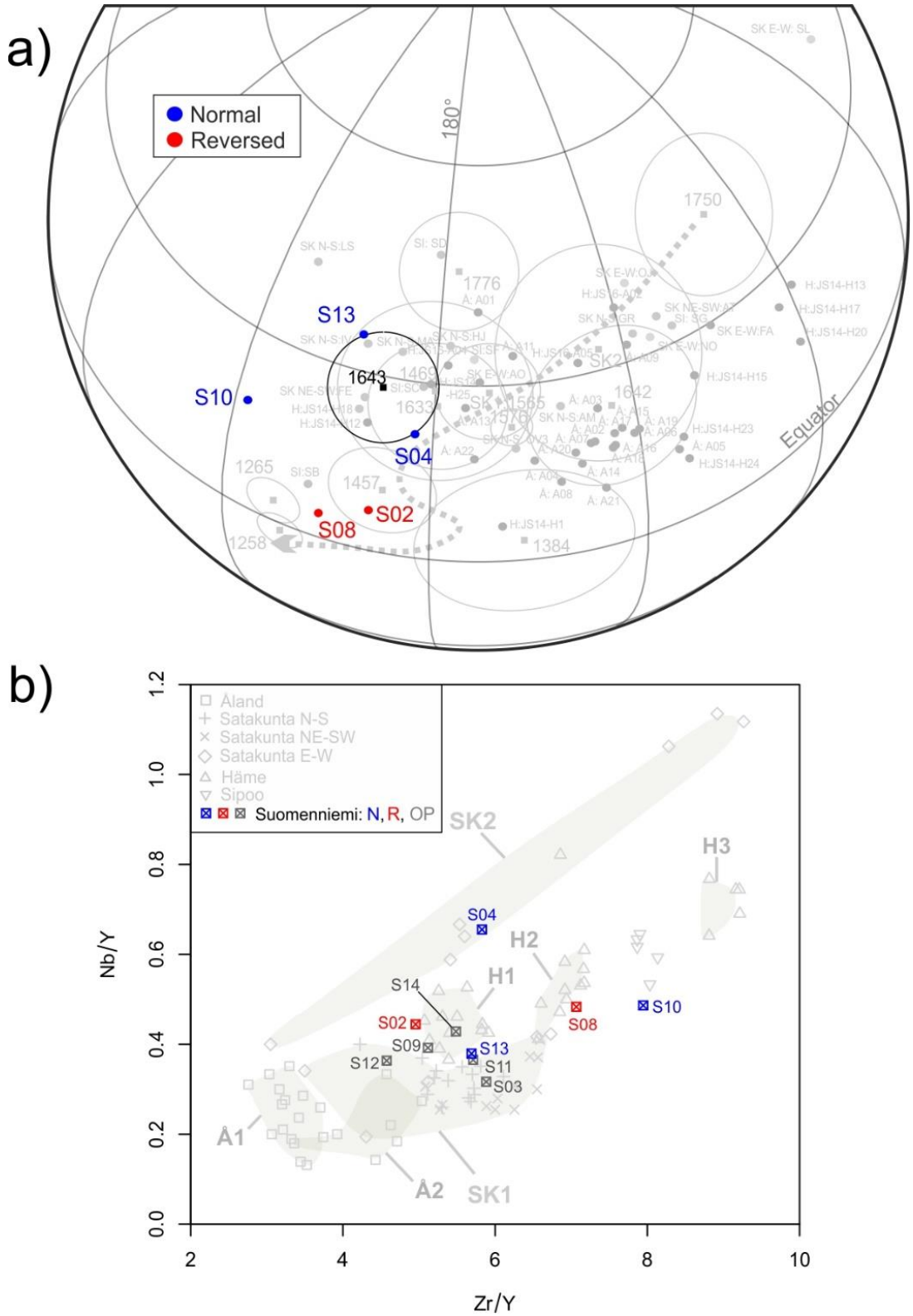

Figure 25. The highlighted a) positions of the VGPs and the paleomagnetic pole for the Suomenniemi swarm (cf. Figure 21) and b) the variation of Nb/Y vs. Zr/Y of the Suomenniemi dykes (cf. Figure 17). The paleomagnetic pole of the Suomenniemi swarm by Salminen et al. (2018) is indicated by black colour in a). N=normal polarity magnetization. R=reversed polarity magnetization. OP=overprinted (no primary component obtained). Paleomagnetic data from Mertanen and Pesonen (1995) and Salminen et al. (2014; 2016; 2017; 2018).

like intrusion S04 in this study). The intrusion S04 has a distinctively higher Nb/Y at given Zr/Y than the dykes of Suomenniemi in this study (Figure 25b). This feature cannot be explained by an accumulation of minerals, since the intrusion was petrographically observed to have a subophitic texture (Appendix III). The distinct Nb/Y values at given Zr/Y imply that the dykes in Suomenniemi formed in a different magmatic pulse than the Lovasjärvi intrusion (S04). The VGPs of dykes S02 and S08 are of different polarity and ~20°S from the VGP of intrusion S04. This could support the idea of younger ages at least for the dykes S02 and S08. It should, however, be noted that the quality of the paleomagnetic data from Suomenniemi is relatively poor due to scattered data and low number of samples.

6.2.5. The Sipoo dyke swarm

The Sipoo dykes are very homogenic in their geochemistry but their VGPs are very scattered (Figure 26). The number of samples is small, which makes the interpretation of the scattered data challenging. Based on their distinctive geochemistry, especially their higher TiO_2 contents at given Mg numbers (Figure 15), the Sipoo swarm represents a separate igneous event from those that generated the roughly coeval Häme and Suomenniemi swarms. This, however, does not mean that the emplacement ages are significantly different. The reason for the distinct paleomagnetic poles of the coeval swarms of Häme, Suomenniemi and Sipoo cannot be explained by the geochemical data.

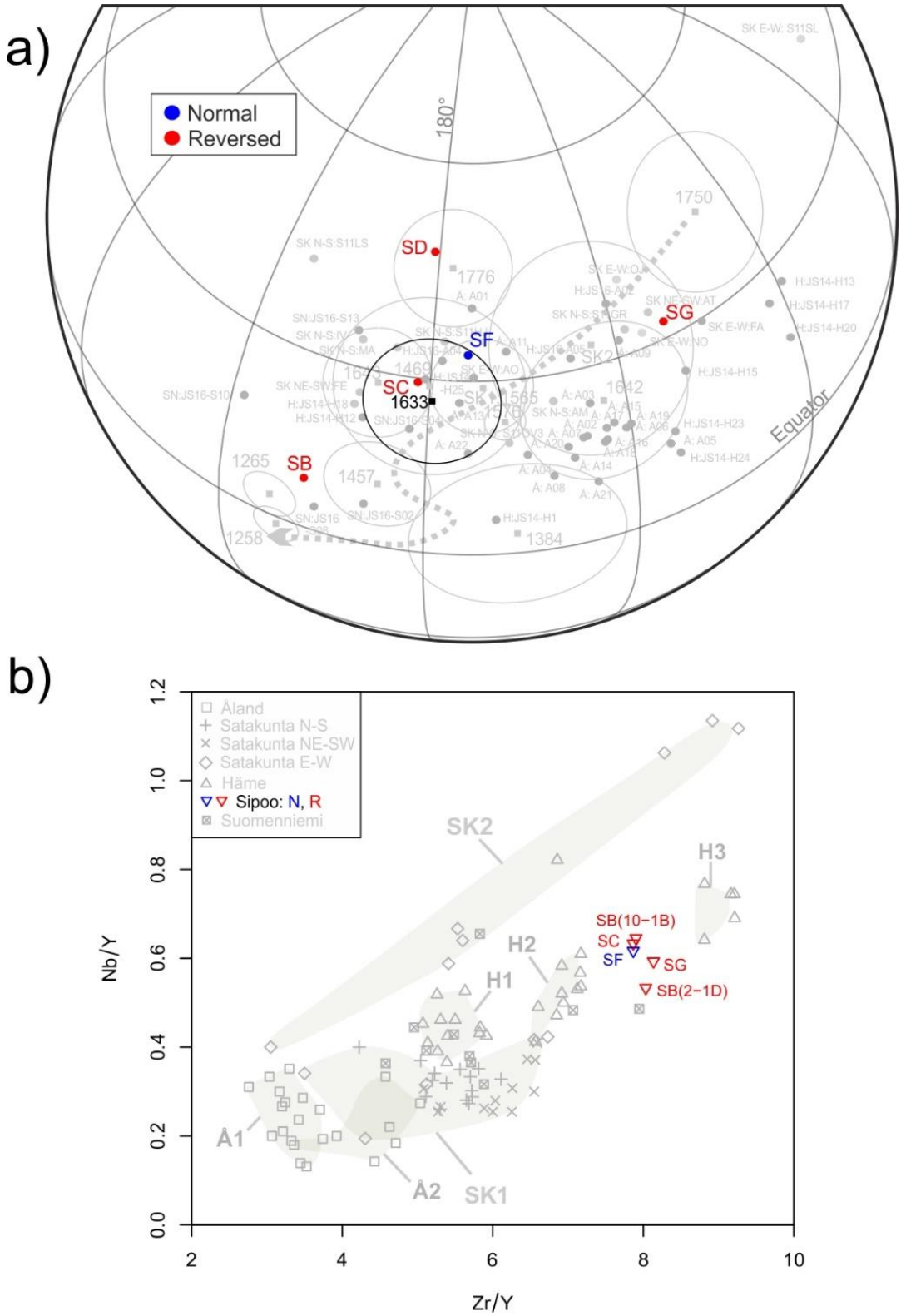

Figure 26. The highlighted a) positions of the VGPs (cf. Figure 21) and b) the variation of Nb/Y vs. Zr/Y (cf. Figure 17) of the Sipoo dykes. The paleomagnetic pole of the Sipoo swarm by Mertanen and Pesonen (1995) is indicated by black colour in a). N=normal polarity magnetization. R=reversed polarity magnetization. Geochemical data for dyke SD [VGP indicated in a)] are not available. Paleomagnetic data from Mertanen and Pesonen (1995) and Salminen et al. (2014; 2016; 2017; 2018).

6.3. Comparison with previous geochemical data

Comparison with previously published geochemical data (Figure 27) shows that the data of this study are generally compatible with the data from previous studies. The Åland-Åboland data from Lindberg et al. (1991) support the geochemical division defined in this study for the Åland dykes (Figure 27a). The Satakunta Group SK1 data of this study have some differences with the data of Salminen et al. (2014), but both show relatively low Nb/Y values for the dykes of Group SK1 (Figure 27a). It remains speculative whether the possibly older Subjotnian dykes (AO and OJ) of Satakunta Group SK2 have formed later than the 1.57 Ga Satakunta dykes. The dyke AO of Salminen et al. (2014) shows similar Nb/Y and Nb values to dyke OJ of this study (Figure 27b).

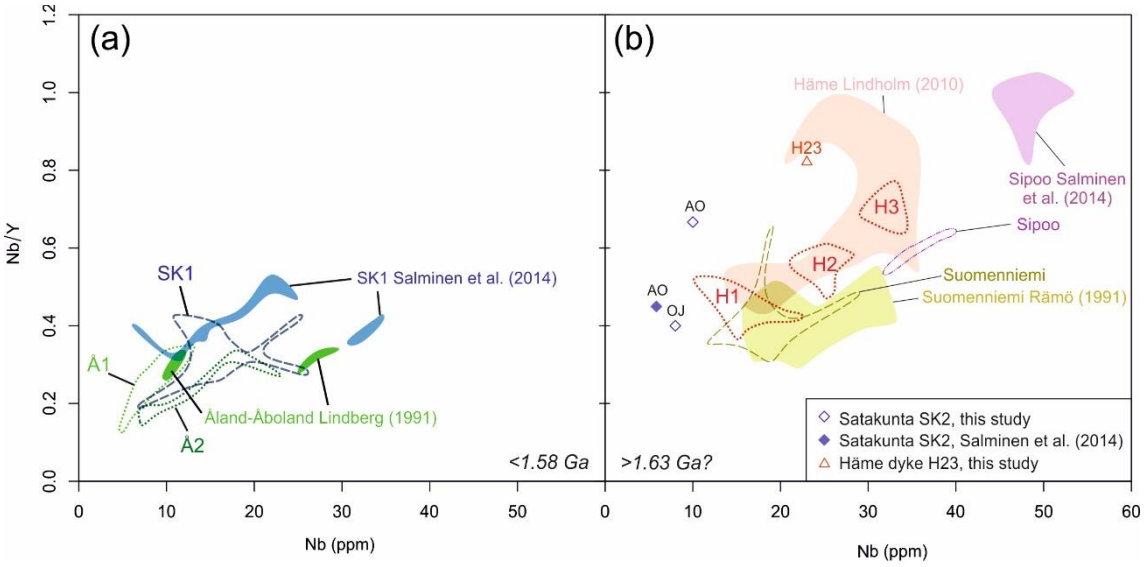

Figure 27. Variation of Nb/Y vs. Nb of a) Åland and Group SK1 Satakunta dykes and b) Group SK2 Satakunta (excluding the presumably Svecofennian dykes), Häme, Suomenniemi and Sipoo dykes. The geochemical groups (cf. Figure 17) of Åland (Å1 and Å2), Satakunta (SK1 and SK2) and Häme (H1–H3) are indicated. Data from previous studies are shown for comparison. Data without reference are from this study. Grouping of the Satakunta dykes from Salminen et al. (2014) is according to the grouping defined in this study of the Satakunta dykes. Data sources: Lindberg et al. (1991), Rämö (1991), Lindholm (2010), Salminen et al. (2014), this study.

The Häme data of this study show similar Nb/Y and Nb values to those of Lindholm (2010) (Figure 27b). Dyke H23 of this study and the data from Lindholm (2010), however, imply there is a set of high Nb/Y dykes in the Häme swarm which is not well represented by the data of this study (Figure 27b). Comparison with geochemical data of

Rämö (1991) shows that the sample material of this study also lacks examples of Nb-rich intrusions of the Suomenniemi swarm (Figure 27b). The Sipoo data of this study show lower Nb/Y values and Nb contents than the Sipoo data from Salminen et al. (2014) but they show overlap with the field of Häme dykes reported by Lindholm (2010) (Figure 27b). These features could imply that there is a connection between the roughly coeval Häme and Sipoo events.

The transition from high Nb/Y to low Nb/Y compositions during Subjotnian magmatism was briefly mentioned in Section 5.2.7. and shown in Figure 17. This transition is also seen in Figure 27, as the dyke swarms that are believed to have emplacement ages of <1.58 Ga plot at low Nb/Y values (Figure 27a) and those that probably intruded before 1.63 Ga show high Nb/Y values (Figure 27b).

There are no clear geochemical indicators that some of the Satakunta dykes would be part of, or the same age as the Häme swarm as has been discussed in previous studies (Pihlaja 1987; Salminen et al. 2014). Some of the Satakunta dykes in this study have, however, shown geochemical and paleomagnetic features that imply those dykes may have an older Subjotnian age than the 1.57 Ga age defined for the Satakunta swarm. The extension of the ~1.6 Ga magmatism to SW Finland is supported by the dating of the Vehmaa rapakivi granite at 1.63 Ga (Shebanov et al. 2000). The data of this study suggests that younger, possibly <1.58 Ga, emplacement events produced magmas with low Nb/Y (and Zr/Y) values showing higher degrees of partial melting or different mantle sources than the older events. Possibly due to the structural separation of Åland from the Vehmaa batholith in mainland Finland (Karell et al. 2009), the igneous activity did not manifest itself in Åland before ~1.58 Ga. Further, high-precision geochronological work at least on the Satakunta swarm is required to verify the regional scale of the ~1.6 Ga Subjotnian magmatism.

6.4. Geochemistry of the dykes with pervasive overprint

The B-component is thought to originate from hydrothermal alteration and crystallization of secondary magnetic minerals. To study if the B-component is related to the composition of the melt of which the dykes were crystallized, the Nb/Y vs. Zr/Y diagram was examined in the light of the B-component in the paleomagnetic data. Four groups

were assigned based on the possible existence of the B-component in the dyke (Figure 28): 1) “B” (n=16): dykes that show the B-component (B), but they do not show a primary component (P); 2) “P+B” (n=41): dykes that show a primary component and the B-component; 3) “P+S” (n=23): dykes that show a primary component and a secondary (S) component(s) other than the B-component; 4) “S” (n=30): dykes that show only a secondary component(s) other than the B-component.

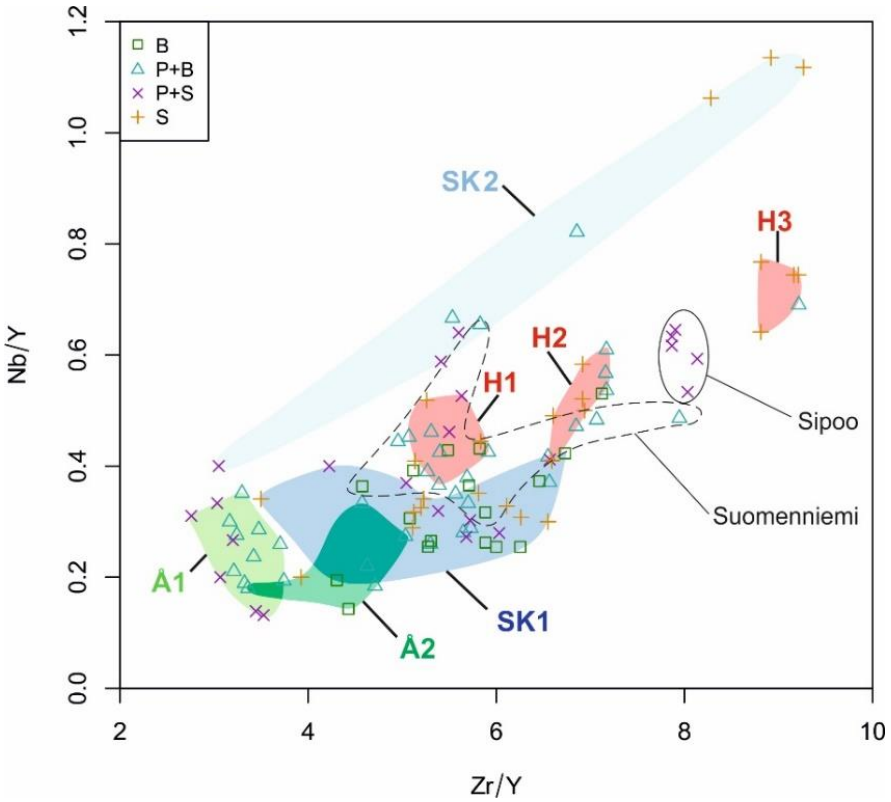

Figure 28. The variation of Nb/Y vs. Zr/Y in terms of the existence of the paleomagnetic B-component in the dykes (n=104). The geochemical groups (cf. Figure 17) of Åland (Å1 and Å2), Satakunta (SK1 and SK2) and Häme (H1–H3) are indicated as well as the areas where Suomenniemi and Sipoo samples are plotted. P=primary magnetization component. B=B-component. S=secondary component other than the B-component.

There is no correlation between the existence of a B-component and the source magma: the B-component occurs in dykes of all types of magmas (Figure 28). Therefore, it does not seem to be related to a specific composition of the melt from which the rocks were crystallized, i.e. the origin of the rock. The low total % -values and petrography (Chapter 5.1.) indicate the rocks with the B-component are usually more altered than the rocks without it, although alteration is not limited only to the processes that formed the B-

component. The physical properties, such as vesicularity, cracks and volatile content as well as mineralogy may have a bigger impact on the alteration of the rock than the geochemical composition of the rock. Indeed, most samples that were observed to contain vesicles and/or cracks (Appendix III), also showed the B-component. The results support the previous conclusions by Preeden et al. (2009) and Salminen et al. (2014), that the B-component overprint was formed by hydrothermal alteration of the rocks. The geochemistry does not explain what was the event that caused the B-component.

7. CONCLUSIONS

This study indicates variability in the geochemistry of Åland, Satakunta and Häme dyke swarms. The data are, however, compatible with previous data and are thus representative for the Subjotnian mafic dykes in southern Finland.

Within the Åland swarm, there is a geochemical division into two groups accompanied with a switch in magnetic polarity. This implies that two separate magmatic events/pulses that have an age difference have taken place in Åland. The geochemistry indicates that the Åland and Satakunta swarms are separate igneous events and that the Åland swarm does not continue to Satakunta region.

The Satakunta dykes form two geochemical groups. Group SK1 is dated to be <1.58 Ga and shows low Nb/Y (and Zr/Y) values. Group SK2 includes five presumably Svecofennian dykes and two Subjotnian dykes.

The geochemical data of this study from the Häme swarm forms three groups (H1–H3). The combined geochemical and paleomagnetic data as well as unpublished chronological data indicate the Groups H1–H3 are roughly coeval.

Although some Suomenniemi dykes show geochemical affinities to the Häme dykes, they probably represent a distinct igneous event of Häme.

The Sipoo dykes are very homogeneous in their geochemistry and can be distinguished from the emplacement event that formed the Häme and Suomenniemi swarms.

The Subjotnian dyke swarms in southern Finland that are believed to have emplacement ages of >1.63 Ga (Häme, Suomenniemi and Sipoo swarms) generally have higher Nb/Y (and Zr/Y) values than the dyke swarms that are believed to record younger magmatic events at <1.58 Ga (Åland and Satakunta swarms). Some Satakunta dykes, however, show geochemical and/or paleomagnetic implications that suggest these dykes could have an older Subjotnian age than the dated 1.57 Ga dyke in Satakunta. Further, high-precision chronological work on the Satakunta swarm is required to verify the ages of the dykes.

The origin of the paleomagnetic B-component is related to the alteration of rocks and is not associated with a certain magma type. The high level of alteration of the dykes that contain the B-component supports previous assumptions that it forms by hydrothermal alteration of the rocks.

8. ACKNOWLEDGEMENTS

I want to thank my supervisor Johanna Salminen for providing the thesis topic and samples, supporting and commenting the work in an encouraging way and for introducing me to the world of paleomagnetism. I also want to thank my other supervisor, Arto Luttinen for sharing his expertise in geochemistry and his valuable comments which greatly improved the quality of the thesis. I am thankful for Satu Mertanen for providing the Sipoo samples. I also want to acknowledge Pasi Heikkilä for instructing and teaching me the XRF method from scratch. The laboratory personnel and other staff at the University of Helsinki, Department of Geosciences and Geography were always very helpful which is greatly appreciated. Lastly, I would like to thank my family for support and my partner Hassan Blasim for his patience, support and cooking services during the busy stages of the work.

9. REFERENCES

Åhäll, K.-I., Brewer, T.S. and Connelly, J.N. 2000. Episodic rapakivi magmatism due to distal orogenesis?: Correlation of 1.69–1.50 Ga orogenic and inboard, “anorogenic” events in the Baltic Shield. Geology 28: 823–826.

Aigner-Torres, M., Blundy, J., Ulmer, P. and Pettke, T., 2007. Laser Ablation ICPMS study of trace element partitioning between plagioclase and basaltic melts: an experimental approach. Contributions to Mineralogy and Petrology, 153: 647–667.

Arndt, N.T. Czamanske, G.K., Wooden, J.L. and Fedorenko, V.A., 1993. Mantle and crustal contributions to continental flood volcanism. Tectonophysics, 223: 39–52.

Bergman, L. 1981. Berggrunden inom Signilskär, Mariehamn och Geta kartblad. Summary: Pre-Quaternary rocks of the Signilskär, Mariehamn and Geta map-sheet areas. Geological map of Finland 1:100 000; Sheets 0034+0043, 1012 and 1021. Explanation to the maps of Pre-Quaternary rocks, 72 p.

Bleeker, W. 2004. Taking the Pulse of Planet Earth: A Proposal for a New Multi-disciplinary Flagship Project in Canadian Solid Earth Sciences. Geoscience Canada 31, 179–190.

Bleeker, W. and Ernst, R. 2006. Short-lived mantle generated magmatic events and their dyke swarms: the key unlocking Earth's paleogeographic record back to 2.6 Ga. In: Hanski, E., Mertanen, S., Rämö, O.T., and Vuollo, J. (Eds.) Dyke Swarms - Time Markers of Crustal Evolution. Taylor and Francis Group, London, 3–26.

Bryan, S.E. and Ernst, R.E. 2008. Revised definition of Large Igneous Provinces (LIPs). Earth-Science Reviews 86: 175–202.

Buchan, K., Mertanen, S., Park, R., Pesonen, L., Elming, S.-Å., Abrahamsen, N. and Bylund, G. 2000. Comparing the drift of Laurentia and Baltica in the Proterozoic: the importance of key palaeomagnetic poles. Tectonophysics 319: 167–198.

Buchan, K.L. 2013. Key paleomagnetic poles and their use in Proterozoic continent and supercontinent reconstructions: A review. Precambrian Researc, 238: 93–110.

Butler, R.F. 1992. Paleomagnetism: Magnetic domains to geologic terranes. Blackwell Scientific Publications cop., Boston, 319 p.

Courtillot, V., Jaupart, C., Manighetti, I., Tapponnier, P. and Besse, J. 1999. On causal links between flood basalts and continental breakup. Earth and Planetary Science Letters, 166: 177–195.

Cox, K.G., Bell, J.D. and Pankhurst, R.J. 1981. The interpretation of igneous rocks. George Allen & Unwin Ltd, London, 450 p.

Earthref.org, GERM Partition coefficient (Kd) Database, site visited 02.10.2018. https://earthref.org/KDD/

Ehlers, C. and Ehlers, M. 1977. Shearing and multiple intrusion in the diabases of Åland archipelago, SW Finland. Geological Survey of Finland Bulletin 289: 42 p.

Eklund, O., Fröjdö, S. and Lindberg, B. 1994. Magma mixing, the petrogenetic link between anorthositic suites and rapakivi granites, Åland, SW Finland. Mineralogy and Petrology 50: 3–19.

Elming, S., Moakhar, M., Layer, P. and Donadini, F. 2009. Uplift deduced from remanent magnetization of a proterozoic basic dyke and the baked country rock in the Hoting area, Central Sweden: a palaeomagnetic and 40Ar/39Ar study. Geophysical Journal International 179: 59–78.

Ernst, R.E. and Buchan, K.L. 1997. Giant radiating dyke swarms: their use in identifying pre-Mesozoic large igneous provinces and mantle plumes. Geophysical Monograph -American Geophysical Union 100: 297–334.

Ernst, R.E. and Buchan, K.L. 2001. Large mafic magmatic events through time and links to mantle-plume heads. In: R.E. Ernst and K.L. Buchan (Eds.), Mantle plumes: Their identification through time, Geological Society of America Special Paper, pp. 483–575.

Ernst, R.E., Wingate, M.T.D., Buchan, K.L. and Li, Z.X. 2008. Global record of 1600–700Ma Large Igneous Provinces (LIPs): Implications for the reconstruction of the proposed Nuna (Columbia) and Rodinia supercontinents. Precambrian Research 160: 159–178.

Evans, D.A.D. 2013. Reconstructing pre-Pangean supercontinents. GSA Bulletin 125: 1735–1751.

Everitt, C.W.F. and Clegg, J.A. 1962. A Field Test of Palaeomagnetic Stability. Geophysical Journal of the Royal Astronomical Society 6: 312–319.

Gallagher, K. and Hawkesworth, C. 1992. Dehydration melting and the generation of continental flood basalts. Nature 358: 57–59.

Haapala, I. and Rämö, O.T. 1990. Petrogenesis of the Proterozoic rapakivi granites of Finland. Geological Society of America Special Paper 246: 275–286.

Heinonen, A. 2010. Ahvenisto AMCG complex - updates and recent discoveries. In: A. Heinonen, S. Lukkari and T. Rämö (Eds.) Guide to the IGCP-510 (A-type Granites and Related Rocks Through Time) Field Trip, Southeastern Finland, August 14-18, 2010. Department of Geosciences and Geology, University of Helsinki C3, pp. 18–21.

Heinonen, A.P., Andersen, T. and Rämö, O.T. 2010a. Re-evaluation of Rapakivi Petrogenesis: Source Constraints from the Hf Isotope Composition of Zircon in the Rapakivi Granites and Associated Mafic Rocks of Southern Finland. Journal of Petrology 51: 1687–1709.

Heinonen, A.P., Rämö, O.T., Mänttäri, I., Johanson, B. and Alviola, R. 2010b. Formation and fractionation of high-Al tholeiitic magmas in the Ahvenisto rapakivi granite massif-type anorthosite complex, southeastern Finland. The Canadian Mineralogist 48: 969–990.

Heinonen, J.S., Luttinen, A.V. and Bohrson, W.A. 2016. Enriched continental flood basalts from depleted mantle melts: modeling the lithospheric contamination of Karoo lavas from Antarctica. Contributions to Mineralogy and Petrology, 171: 9.

Hospers, J. 1954. Rock Magnetism and Polar Wandering. Nature 173: 1183–1184.

Idman, H. 1989. The Siipyy granite-a new rapakivi occurrence in Finland. Bulletin of the Geological Society of Finland 61: 123–127.

Karell, F., Ehlers, C., Airo, M.-L. and Selonen, O. 2009. Intrusion mechanisms and magnetic fabrics of the Vehmaa rapakivi granite batholith in SW Finland. Geotectonic Research 96: 53–68.

Laitakari, I. 1969. On the set of olivine diabase dikes in Häme, Finland. Bulletin de la Commission Géologique de Finlande 241, 65 pp.

Laitakari, I. 1987. Hämeen subjotuninen diabaasijuoniparvi. In: K. Aro and I. Laitakari (Eds.), Suomen diabaasit ja muut mafiset kivilajit. Geological Survey of Finland Report of Investigation 76., pp. 99–116.

Laitakari, I. and Leino, H. 1989. A New Model for the Emplacement of the Häme Diabase Dyke Swarm, Central Finland. In: S. Autio (Ed.), Current Research 1988. Geological Survey of Finland, Special Paper 10, pp. 7–8.

Laitala, M. 1984. Pellingin ja Porvoon kartta-alueiden kallioperä. Summary: Pre-Quaternary rocks of the Pellinki and Porvoo map-sheet areas. Geological map of Finland 1:100 000: Sheets 3012 and 3021. Explanation to the maps of pre-Quaternary rocks. Geological Survey of Finland, Espoo, 53 p.

Le Bas, M.J., Le Maitre, R.W., Streckeisen, A. and Zanettin, B. 1986. IUGS Subcommission on the Systematics of Igneous Rocks; A Chemical Classification of Volcanic Rocks Based on the Total Alkali-Silica Diagram. Journal of Petrology 27: 745–750.

Lehtonen, M., Kujala, H., Kärkkäinen, N., Lehtonen, A., Mäkitie, H., Mänttäri, I., Virransalo, P. and Vuokko, J. 2003. Etelä-Pohjanmaan liuskealueen kallioperä. Summary: Pre-Quaternary rocks of the South Osthrobothnia Schist Belt. Geological Survey of Finland, Report of Investigation 158: 1–125.

Lindberg, B., Eklund, O. and Suominen, V. 1991. Middle Proterozoic Subjotnian diabases and related mafic rocks in the archipelago of southwestern Finland. In: I. Laitakari (Ed.), Fennoscandian meeting and excursion on Precambrian dyke swarms, June 10-15, 1991, Finland. IGCP Technical Report 4, 18–30.

Lindberg, B. and Eklund, O. 1992. Mixing between basaltic and granitic magmas in a rapakivi related quartz-feldspar porphyry, Åland, SW Finland. Geologiska Föreningen i Stockholm Förhandlingar 114: 103–112.

Lindholm, T. 2010. Hämeen diabaasijuonien geokemia. Master's Thesis, University of Helsinki, 50 p.

Lubnina, N. 2009. The East European Craton in the Mesoproterozoic: new key paleomagnetic poles. Doklady Earth Sciences 428: 1174–1178.

Lubnina, N.V., Mertanen, S., Söderlund, U., Bogdanova, S., Vasilieva, T.I. and Frank-Kamenetsky, D. 2010. A new key pole for the East European Craton at 1452 Ma: Palaeomagnetic and geochronological constraints from mafic rocks in the Lake Ladoga region (Russian Karelia). Precambrian Research 183: 442–462.

Luosto, U., Tiira, T., Korhonen, H., Azbel, I., Burmin, V., Buyanov, A., Kosminskaya, I., Ionkis, V. and Sharov, N. 1990. Crust and upper mantle structure along the DSS Baltic profile in SE Finland. Geophysical Journal International 101: 89–110.

Luttinen, A.V. 2018. Bilateral geochemical asymmetry in the Karoo large igneous province. Scientific Reports 8: 5223.

Luttinen, A.V. and Kosunen, P.J. 2006. The Kopparnäs dyke swarm in Inkoo, southern Finland: New evidence for Jotnian magmatism in the SE Fennoscandian Shield. In: Hanski, E., Mertanen, S., Rämö, O.T., and Vuollo, J. (Eds.) Dyke Swarms - Time Markers of Crustal Evolution. Taylor and Francis Group, London, pp. 85–98.

McElhinny, M.W. 1973. Palaeomagnetism and plate tectonics. Cambridge University Press, New York, 358 p.

McElhinny, M.W. and McFadden, P.L. 2000. Paleomagnetism: Continents and Oceans. International Geophysics Series. Academic Press, San Diego, 386 p.

Meert, J.G. 2002. Paleomagnetic Evidence for a Paleo-Mesoproterozoic Supercontinent Columbia. Gondwana Research 5: 207–215.

Meert, J.G. 2012. What's in a name? The Columbia (Paleopangaea/Nuna) supercontinent. Gondwana Research 21: 987–993.

Merle, R., Marzoli, A., Reisberg, L., Bertrand, H., Nemchin, A., Chiaradia, M., Callegaro, S., Jourdan, F., Bellieni, G., Kontak, D., Puffer, J. and McHone, J.G. 2014. Sr, Nd, Pb and Os Isotope Systematics of CAMP Tholeiites from Eastern North America (ENA): Evidence of a Subduction-enriched Mantle Source. Journal of Petrology 55: 133–180.

Merrill, R.T. and McElhinny, M.W. 1983. The Earth's Magnetic Field: Its History, Origin, and Planetary Perspective. International Geophysics Series. Academic Press, London, 401 p.

Mertanen, S. and Pesonen, L.J. 1995. Palaeomagnetic and rock magnetic investigations of the Sipoo Subjotnian quartz porphyry and diabase dykes, southern Fennoscandia. Physics of the Earth and Planetary Interiors 88: 145–175.

Neymark, L.A., Yu. Amelin, V. and Larin, A.M. 1994. Pb-Nd-Sr isotopic and geochemical constraints on the origin of the 1.54–1.56 Ga Salmi rapakivi granite—Anorthosite batholith (Karelia, Russia). Mineralogy and Petrology 50: 173–193.

Pearce, J.A. and Cann, J. 1973. Tectonic setting of basic volcanic rocks determined using trace element analyses. Earth and planetary science letters 19: 290–300.

Pearce, J.A. 1996. A user's guide to basalt discrimination diagrams. Trace element geochemistry of volcanic rocks: applications for massive sulphide exploration. Geological Association of Canada, Short Course Notes 12: pp. 79–113.

Pesonen, L., Elming, S.-Å., Mertanen, S., Pisarevsky, S., D'Agrella-Filho, M., Meert, J., Schmidt, P., Abrahamsen, N. and Bylund, G. 2003. Palaeomagnetic configuration of continents during the Proterozoic. Tectonophysics 375: 289–324.

Pihlaja, P. 1987. The Subjotnian diabases of the Pori region, southwestern Finland. Geological Survey of Finland, Report of Investigation 76: 133–150.

Pisarevsky, S. and Bylund, G. 2010. Paleomagnetism of 1780–1770 Ma mafic and composite intrusions of Småland (Sweden): implications for the Mesoproterozoic supercontinent. American Journal of Science 310: 1168–1186.

Pisarevsky, S.A., Elming, S.-Å., Pesonen, L.J. and Li, Z.-X. 2014. Mesoproterozoic paleogeography: supercontinent and beyond. Precambrian Research 244: 207–225.

Pokki, J., Kohonen, J., Lahtinen, R., Rämö, T.O. and Andersen, T. 2013. Petrology and provenance of the Mesoproterozoic Satakunta formation, SW Finland, 204. Geological Survey of Finland, Report of Investigation 204: 61 p.

Preeden, U., Mertanen, S., Elminen, T. and Plado, J. 2009. Secondary magnetizations in shear and fault zones in southern Finland. Tectonophysics 479: 203–213.

Rämö, O.T. 1991. Petrogenesis of the Proterozoic rapakivi granites and related basic rocks of southeastern Fennoscandia: Nd and Pb isotopic and general geochemical constraints. Geological Survey of Finland Bulletin 355: 1–161.

Rämö, O.T. and Haapala, I. 1995. One hundred years of rapakivi granite. Mineralogy and Petrology 52: 129–185.

Rämö, O.T. and Haapala, I. 2005. Rapakivi Granites. In: M. Lehtinen, P.A. Nurmi and O.T. Rämö (Eds.), Precambrian Geology of Finland - Key to the Evolution of the Fennoscandian Shield. Elsevier, pp. 533–562.

Rämö, O.T. and Mänttäri, I. 2015. Geochronology of the Suomenniemi rapakivi granite complex revisited: Implications of point-specific errors on zircon U-Pb and refined λ87 on whole-rock Rb-Sr. Bulletin of the Geological Society of Finland 87: 25–45.

Rämö, O. T., Heinonen, A., Lahaye, Y., Larjamo, K., Mänttäri, I. and Turkki, V. 2014. Age and isotopic fingerprints of some plutonic rocks in the Wiborg rapakivi granite batholith with special reference to the dark wiborgite of the Ristisaari Island. Bulletin of the Geological Society of Finland 86, 71–91.

Rogers, J.J.W. and Santosh, M. 2002. Configuration of Columbia, a Mesoproterozoic Supercontinent. Gondwana Research 5: 5–22.

Salminen, J. and Pesonen, L.J. 2007. Paleomagnetic and rock magnetic study of the Mesoproterozoic sill, Valaam island, Russian Karelia. Precambrian Research 159: 212–230.

Salminen, J., Mertanen, S., Evans, D.A.D. and Wang, Z. 2014. Paleomagnetic and geochemical studies of the Mesoproterozoic Satakunta dyke swarms, Finland, with implications for a Northern Europe – North America (NENA) connection within Nuna supercontinent. Precambrian Research 244: 170–191.

Salminen, J., Klein, R., Mertanen, S., Pesonen, L.J., Fröjdö, S., Mänttäri, I. and Eklund, O. 2016. Palaeomagnetism and U–Pb geochronology of c. 1570 Ma intrusives from Åland archipelago, SW Finland – implications for Nuna. Geological Society, London, Special Publications 424: 95–118.

Salminen, J., Klein, R., Veikkolainen, T., Mertanen, S. and Mänttäri, I. 2017. Mesoproterozoic geomagnetic reversal asymmetry in light of new paleomagnetic and geochronological data for the Häme dyke swarm, Finland: Implications for the Nuna supercontinent. Precambrian Research 288: 1–22.

Salminen, J., Klein, R. and Mertanen, S. 2018. New rock magnetic and paleomagnetic results for the 1.64 Ga Suomenniemi dyke swarm, SE Finland. Precambrian Research, in press.

Salters, V.J.M. and Longhi, J., 1999. Trace element partitioning during the initial stages of melting beneath mid-ocean ridges. Earth and Planetary Science Letters, 166: 15–30.

Shebanov, A.D., Savatenkov, V., Eklund, O., Andersson, U.B., Annersten, H. and Claesson, S. 2000. Regional mineralogical correlation linking post- and anorogenic magmatic events: evidences from unusual barian biotites in the Järppilä rapakivi porphyries, Vehmaa batholith (s. Finland), In: Advances On Micas - Problems, Methods, Application in Geodynamics. Rome 2.-3.11.2000.

Siivola, J. 1987. The mafic intrusion of Lovasjarvi. Geological Survey of Finland, Report of Investigation 76: 121–128.

Suominen, V. 1991. The Chronostratigraphy of South-Western Finland with Special Reference to Postjotnian and Subjotnian Diabases. Geological Survey of Finland Bulletin 356: 100 p.

Törnroos, R. 1984. Petrography, mineral chemistry and petrochemistry of granite porphyry dykes from Sibbo, southern Finland. Geological Survey of Finland Bulletin 326: 1–43.

Vaasjoki, M. 1977. Rapakivi granites and other postorogenic rocks in Finland: their age and the lead isotopic composition of certain associated galena mineralizations. PhD Thesis, Geological Survey of Finland, Espoo, 74 p.

Vaasjoki, M. and Sakko, M. 1989. The radiometric age of the Virmaila diabase dyke: Evidence for 20 Ma of continental rifting in Padasjoki, southern Finland. Geological Survey of Finland, Special Paper 10: 43–44.

Vaasjoki, M., Rämö, O. T. and Sakko, M. 1991. New U-Pb ages from the Wiborg rapakivi area: constraints on the temporal evolution of the rapakivi granite-anorthosite-diabase dyke association of southeastern Finland. Precambrian Research 51: 227–243.

Wang, X.-C., Wilde, S.A., Li, Q.-L. and Yang, Y.-N. 2015. Continental flood basalts derived from the hydrous mantle transition zone. Nature Communications 6: 7700.

Winchester, J.A. and Floyd, P.A. 1976. Geochemical magma type discrimination: application to altered and metamorphosed basic igneous rocks. Earth and Planetary Science Letters 28: 459–469.

Winter, J.D. 2001. An Introduction to Igneous and Metamorphic Petrology. Prentice Hall, New Jersey, 697 p.

Zhao, G., Sun, M., Wilde, S.A. and Li, S. 2004. A Paleo-Mesoproterozoic supercontinent: assembly, growth and breakup. Earth-Science Reviews 67: 91–123.

10. APPENDICES

Appendix I. The coordinates of the dykes and other information.

Appendix II. The XRF results and C.I.P.W. norms.

Appendix III. Petrographic observations.

APPENDIX I. The locations and coordinates of the sampling sites, paleomagnetic polarity (N=normal, R=reversed) of virtual geomagnetic poles (VGPs) and other information on the samples. SVF=Svecofennian. On the "Paleomagnetic components" -column: P=primary magnetization component. B=B-component. S=secondary component other than the B-component.

SAMPLE/DYKE	LOCATION	LAT (°)	LONG (°)	POLARITY OF VGP	PALEO-MAGNETIC COMPO-NENTS	WIDTH OF DYKE (m)	STRIKE/ DIP (°)	SAMPLING NOTES
Åland								
A1E-2/**A1**	Enklinge	60.32501	20.73659	N	P+B	3	045/80	4 cm to dyke margin
A2F-2/**A2**	Korsö	60.41191	20.98899	R	P+B		170/-	cutting A2G-2
A2G-2/**A2**	Korsö	60.41191	20.98899	R	P+B	100-300	170/-	big dyke cut by narrower, fine-grained dykes (A2F-2), ~5 cm from the contact of the two varieties
A3C-2/**A3**	Korsö	60.42021	20.99369	R	P+B	>100	170/-	
A4D-2/**A4**	Brändö-s-tip	60.40367	21.03527	R	P+B	0.2	045/60	from margin
A5C-2/**A5**	Brändö-s-tip	60.40352	21.03536	R	P+B	0.3	045/90	from margin
A6A-2/**A6**	Brändö-s-tip	60.40349	21.03542	R	P+S	0.05-0.1	045/90	from margin
A7C-2/**A7**	Brändö-s-tip	60.40349	21.03542	R	P+S	0.15	045/90	from margin
A8C-2/**A8**	Brändö-s-tip	60.42021	20.99397	R	P+B	0.3	045/90	from margin
A9A-2/**A9**	Keistiö	60.3678	21.33001	N	P+B	0.12	020/80	
A10A-2/**A10**	Keistiö	60.36783	21.32999	-	S	0.1-0.6		15 cm from margin
A11B-2/**A11**	Keistiö	60.3741	21.29178	N	P+B	0.35	035/ 80	
A12C-2/**A12**	Keistiö	60.3741	21.29178	-	S	0.3	030/75	10 cm from margin
A13E-2/**A13**	Keistiö	60.37411	21.29178	N	P+B	5	025/ 85	from margin
A14F-2/**A14**	Torsholma-Barkholm	60.35017	21.06314	R	P+B	1.5	040/85	4 cm from margin
A15F-2/**A15**	Torsholma-Barkholm	60.35021	21.06291	R	P+S	0.8	040/80	
A16D-2/**A16**	Torsholma-Barkholm	60.35018	21.06307	R	P+B	0.5	040/80	
A17B-2/**A17**	Torsholma-Barkholm	60.35016	21.06313	R	P+S	1.5	025/80	
A18B-2/**A18**	Torsholma-Barkholm	60.35015	21.06316	R	P+B	1	040/90	
A19C-2/**A19**	Torsholma-Barkholm	60.35015	21.06316	R	P+S	1.5	030/90	
A20A-2/**A20**	Torsholma-Barkholm	60.35015	21.06316	R	P+B	1.5	025/85	5 cm from margin
A21C-2/**A21**	Torsholma-Barkholm	60.35011	21.06317	R	P+B	1.5	035/80	10 cm from margin
A22A-2/**A22**	Brändö-s-tip	60.42021	20.99397	R	P+S	>5		
Satakunta								
AM-1AB/2AB/**AM**	Ämttöö	61.662	21.62	N	P+B	>20	000/90	close to margin
AM7-1B/**AM**	Ämttöö	61.662	21.62	N	P+B	>20	000/90	3 m from margin
S11HJ 10.1/**S11HJ**	Heikinjärvi	62.05921	21.67	N	P+S	>6-10	020/90	close to margin
S11HJ 14.1/**S11HJ**	Heikinjärvi	62.05921	21.67	N	P+S	10	020/90	25 cm from margin
IV6-1A/**IV**	Ilvesmäki-Pori-Toukari	61.5419	21.7524	N	P+B	>20	170/90	2.15 m from margin
IV15-1A/**IV**	Ilvesmäki-Pori-Toukari	61.5419	21.7524	N	P+B	>20	170/90	center of dyke
S11GR 4.1/**S11GR**	Grötgrund	62.2404	21.37973	R	P+S	1.5	000/60	15 cm from margin
S11LS 5.1/**S11LS**	Lillsund	62.20588	21.42881	N	P+S	>60	000/-	
HH2-1B/**HH**	Holmberginhaka	61.687	21.594	-	S		005/80	sample covers the whole width of the dyke

S11KA 4.1/**S11KA**	Karlstrand	62.30109	21.37854	-	S	1.5	145/60	10 cm from margin
S11VA 1.1/**S11VA**	Västerängen	62.26948	21.43409	-	S	10-15	160/90	3 cm from margin
S11PL 1.1/**S11PL**	Powerline-Kristiinankaupunki	62.27918	21.43138	-	S	~4	165/70	4 cm from margin
S11VR 2.1/**S11VR**	Vargöskatan	62.22967	21.38082	-	S	0.5	160/-	7 cm from margin
S11SG 1.1/**S11SG**	Smultrongrung	62.19736	21.44071	-	S	7-10	000/-	middle of dyke
S11OV 3.1/**S11OV**	Överträsket	62.15448	21.39492	R	P+S	<0.15	010/60	5 cm from margin
MA1-1D/**MA**	Mäntymäki	61.7262	21.6094	N	P+B	15	170/90	closer to margin than MA9
MA9-1D/**MA**	Mäntymäki	61.7262	21.6094	N	P+B	15	170/90	MA1 is closer to margin than MA9
AT2-1B/**AT**	Ämttöö-Riisivilja	61.644	21.635	N	P+S	0.1	035/90	from margin
SO3-1A/**SO**	Söörmarkku	61.5681	21.81511	-	S			
FB5-1B/**FB**	Fiskee	61.683	21.55	-	S	~1	060/-	7 cm from margin
FE-1AB/1B/**FE**	Fiskee	61.679	21.545	N	P+B	0.3	060/72	center of dyke
FF3-1B/**FF**	Fiskee	61.687	21.594	-	S		040/90	6-8 cm from margin
FI1-1B/**FI**	Fiskee	61.68004	21.54199	-	B	<0.3	040/90	
FK2-3C/**FK**	Fiskee	61.68004	21.54199	-	B	0.7	058/90	center of dyke
FS3-1B/**FS**	Fiskee	61.68004	21.54199	-	B	0.35	050/ 90	center of dyke
FT10-1A/**FT**	Fiskee	61.68	21.553	-	S		047/90	
FC1-1D/**FC**	Fiskee	61.6802	21.5451	-	B	~7	060/90	~3 m from margin
FC5-1A/**FC**	Fiskee	61.6802	21.5451	-	B	~7	060/90	20 cm from margin
FD6-1D/**FD**	Fiskee	61.6804	21.5461	-	B	<0.3	060/50	~10 cm from margin
FH7-1AB/**FH**	Fiskee	61.6807	21.5462	-	B	0.3	060/ 80	
LK8-1B/**LK**	Fläksholma	61.687	21.587	-	S		055/90	~12 cm from margin
NE1-1B/**NE**	Niemi	61.74803	21.5541	-	S			
NI6-1B/**NI**	Niemi	61.74803	21.5541	-	S		100/75	
NM1-1C/**NM**	Niemi	61.74803	21.5541	-	S			
SA8-1B/**SA**	Salmela	61.744	21.616	-	B		090/75	
FA9-1C/**FA**	Fiskee	61.679	21.545	R	P+B	0.35	090/90	3 cm from margin
OJ2-2B/**OJ**	Ojala	61.744	21.616	N	P+S	0.1	090/90	
NO2-1B/**NO**	Söörrmarkuntie	61.56	21.82	N	P+S	0.6	150/65	15 cm from margin
NR6-1A/**NR**	Söörrmarkuntie	61.56	21.82	-	B	0.2	095/85	center of dyke
S11BR 5.1/**S11BR**	Brändön	62.19396	21.44967	-	S	<0.5	075/90	15 cm from margin
S11SL 5.1/**S11SL**	Strandlund	62.19736	21.44071	N (SVF)	P+S	1.5	090/90	1 cm from margin
AO3-1A/**AO**	Ämttöö-Riisivilja	61.6068	21.7833	N	P+B	0.25	115/60	3 cm from margin
JS16-A01B-1/**JS16-A01**	Karlstrand	62.30115	21.37869	-	S	<2	130/90	~50 cm from margin
Häme								
JS16-A02C/D-1/**JS16-A02**	Iso Niinilammi	61.2969	25.73298	N	P+S	1.9	135/75	20-30 cm from margin
JS16-A03F-1/**JS16-A03**	Soidinkallio	61.29261	25.78074	-	B	8	125/-	
JS16-A04A-1/**JS16-A04**	Kurjeniemi	61.26891	25.88807	N	P+B	24	140/90	
JS16-A05C-1/**JS16-A05**	Heinola	61.2554	25.07348	N	P+S	>250	135/-	
JS14-H1B-1/2/**H1**	Orivesi: Tre-Jklä road	61.66022	24.2579	N	P+B	5	090/90	
JS14-H1E-1/2/**H1**	Orivesi: Tre-Jklä road	61.66022	24.2579	N	P+B	5	090/90	close to margin
JS14-H2F-1/**H2**	Orivesi: Tre-Jklä road	61.6633	24.2652	-	S	1.5	100/-	10 cm from margin
JS14-H3A-1/**H3**	Kasiniemi	61.45257	24.89912	-	S	20	120/-	
JS14-H4B-1/2/**H4**	Kasiniemi/Ansio	61.44028	24.91873	-	S	30	120/-	

JS14-H6C-1/**H6**	Karivuori	61.49417	24.78237	-	S	>70	100/-	
JS14-H7B-1/**H7**	Vehkajärvi	61.50682	24.83713	-	S	3.1	100/90	from margin
JS14-H7L-1/**H7**	Vehkajärvi	61.50682	24.83713	-	S	3.1	100/90	20 cm from margin
JS14-H11A/**H11**	Hirtniemi	61.3335	25.3992	-	B	6-8	135/90	
JS14-H12A/**H12**	Hirtniemi	61.3397	25.3951	N	P+B	12	095/90	
JS14-H13A1/**H13**	Hirtniemi	61.3396	25.4095	R	P+B	>60	135/90	from margin
JS14-H14C-1/**H14**	Myllylahti	61.4781	25.1485	-	S	>40	140/ 00	from margin
JS14-H15C-1/2/**H15**	Harmoistenkaivo	61.4896	25.125	N	P+B	45	140/90	from margin
JS14-H16E-1/2/**H16**	Torittu	61.4515	25.1431	-	S	0.6	100/90	5 cm from margin
JS14-H17A-1/**H17**	Torittu	61.4515	25.1431	R	P+B	~60	090/90	from margin
JS14-H18A-1/**H18**	Tuomasvuori	61.3605	25.2903	N	P+B	~50	135/-	
JS14-H18C-1/2/**H18**	Tuomasvuori	61.3605	25.2903	N	P+B	~50	135/-	
JS14-H19A-3/**H19**	Koukkujärvi	61.442	25.2183	-	S	24	130/-	from margin
JS14-H19H-2/**H19**	Koukkujärvi	61.442	25.2183	-	S	24	130/-	
JS14-H20F-1/2/**H20**	Koukkujärvi	61.4411	25.2168	R	P+B	2.5-3	110/90	
JS14-H21a-1A/2A/**H21**	Koukkujärvi	61.4419	25.2173	-	S	0.5	040/45	forms network with host rock
JS14-H22B-1a/1d/**H22**	Koukkujärvi	61.4409	25.2177	-	S	>12	110/90	~2 m from margin
JS14-H23A1/**H23**	Partakorpi	61.4568	25.0548	R	P+B	30	110/-	
JS14-H24A1/**H24**	Romo	61.4041	25.0316	R	P+B	>50	130/-	
JS14-H25B/E-1/**H25**	Muorinkallio	61.4201	24.9873	N	P+S	>80	130/-	from margin
Suomenniemi								
JS16S02F-1/2/**S02**	Syväjärvi	61.38741	27.37468	R	P+B	10	120/-	
JS16S03F-1/2/**S03**	Kirkkovuori	61.4179	27.24749	-	B	15	120/-	~10 cm from margin
JS16S04A-1/**S04**	Lovasjärvi	61.15562	27.14392	N	P+B	~800	120/-	sheet-like intrusion
JS16S08E-2/3/**S08**	Pellosniemi	61.46265	27.26889	R	P+B	3	135/90	~1m from margin
JS16S09E-1/**S09**	Viiru	61.34045	27.18698	-	B	5	120/-	~2m from margin
JS16S10I-1/**S10**	Korpijärvi	61.33423	27.18958	N	P+B	>20	130/90	diabase and quartz-porphyry mingled dyke, sample from diabase close to quartz-porphyry
JS16S11D-1/**S11**	Lehtoniemi/Lehtojärvi	61.33242	27.1269	-	B	>20	120/-	
JS16S12A/B-1/**S12**	Riippa	61.35487	27.11097	-	B	<0.2	090/90	
JS16S13A/C-1/**S13**	Hujala	61.35692	27.3414	N	P+B	20		
JS16S14E-2/**S14**	Joutsa	61.69276	26.24243	-	B			
Sipoo								
SB10-1B/**SB**	Sipoo, Kerava, Ahjo	60.4	25.15	R	P+S	<3	~090/-	
SB2-1D/**SB**	Sipoo, Kerava, Ahjo	60.4	25.15	R	P+S	<3	~090/-	
SC1-1D/**SC**	Sipoo, Hästberget	60.4	25.23	R	P+S	<3	~090/-	
SD	Sipoo, Kalkstrand	60.25	25.4	R	P+S		~090/-	
SF2-1B/**SF**	Sipoo, railway	60.37	25.38	N	P+S	~0.3	~020/-	
SG2-1C/**SG**	Sipoo, Paipis	60.42	25.22	R	P+S	<3	~135/-	

APPENDIX II. Major and trace element concentrations by XRF at the Department of Geosciences and Geography, University of Helsinki. < denotes result below detection limit. CIPW norm calculated from major elements normalized to 100% with Fe^{3+}/total Fe at 0.1.

ÅLAND	A1E-2	A2F-2	A2G-2	A3C-2	A4D-2	A5C-2	A6A-2	A7C-2	A8C-2	A9A-2	A10A-2	A11B-2	A12C-2	A13E-2
SiO_2, wt.%	46.41	58.25	47.53	50.53	47.90	48.10	47.54	47.82	46.34	46.10	50.51	50.28	51.04	50.28
TiO_2	2.61	1.56	1.14	1.33	1.41	1.41	1.35	1.38	4.45	1.98	1.54	2.82	1.75	2.70
Al_2O_3	15.82	13.03	20.38	16.26	16.86	16.88	16.90	16.84	13.69	13.94	16.02	15.27	15.33	14.66
FeO	13.17	10.01	9.97	10.90	11.83	11.94	11.61	11.85	15.05	13.33	10.32	10.87	12.13	12.01
MnO	0.17	0.16	0.13	0.22	0.19	0.18	0.18	0.18	0.18	0.17	0.11	0.10	0.14	0.22
MgO	6.69	1.56	4.03	6.44	6.36	6.39	6.26	6.40	4.44	6.53	3.52	5.27	4.68	4.18
CaO	3.80	4.70	9.63	8.68	9.16	9.17	9.27	9.24	8.03	4.76	6.74	5.23	6.63	7.98
Na_2O	3.98	2.98	2.99	2.66	2.80	2.81	2.71	2.73	2.33	1.38	2.09	1.99	2.62	2.50
K_2O	1.38	3.40	1.26	0.55	0.48	0.47	0.45	0.45	1.59	2.23	2.09	1.53	0.99	0.91
P_2O_5	0.29	0.50	0.30	0.29	0.23	0.23	0.22	0.22	1.19	0.45	0.36	0.73	0.48	0.70
Sum	**94.32**	**96.15**	**97.36**	**97.89**	**97.22**	**97.58**	**96.49**	**97.11**	**97.29**	**90.87**	**93.30**	**94.09**	**95.79**	**96.14**
Ba, ppm	286	846	354	205	245	252	237	239	774	254	492	425	404	440
Ce	38	207	39	34	33	42	33	38	135	44	56	85	85	96
Cu	23	21	29	37	55	52	57	55	45	35	15	28	29	38
Cr	13	11	22	72	74	67	73	70	129	159	27	74	41	74
La	10	99	<10	12	19	<10	15	18	44	<10	20	43	24	40
Nb	7	28	7	6	9	8	10	6	23	9	8	13	7	18
Ni	43	5	43	48	83	84	81	81	45	70	21	28	31	27
Rb	82	142	37	26	14	14	12	12	53	171	51	92	80	31
Sr	156	172	278	243	256	257	256	258	284	56	266	205	355	246
U	<2	3	2	<2	<2	4	3	2	2	<2	<2	<2	<2	<2
V	141	76	78	158	192	196	186	188	127	188	254	137	258	150
Y	38	99	27	31	30	29	30	30	84	50	40	59	49	54
Zn	135	232	116	126	113	105	110	109	219	270	66	123	119	132
Zr	179	431	100	116	95	94	91	92	423	168	157	273	217	247
CIPW														
Q	0.00	13.01	0.00	0.85	0.00	0.00	0.00	0.00	0.82	2.96	6.43	10.75	5.51	6.33
C	1.66	0.00	0.00	0.00	0.00	0.00	0.00	0.00	0.00	1.85	0.00	2.74	0.00	0.00
Or	8.65	20.90	7.65	3.32	2.92	2.85	2.76	2.74	9.66	14.50	13.24	9.61	6.11	5.59
Ab	35.71	26.23	25.99	23.00	24.37	24.37	23.77	23.79	20.27	12.85	18.96	17.90	23.14	22.00
An	17.98	12.62	39.51	31.48	32.93	32.85	33.81	33.33	22.82	22.75	30.18	22.51	28.34	27.14
Di	0.00	7.09	6.32	8.75	10.16	10.14	10.25	10.27	8.51	0.00	2.64	0.00	2.28	7.77
Hy	7.53	14.37	0.52	27.73	13.97	14.33	14.67	14.81	24.18	37.68	22.93	27.34	28.16	22.34
Ol	20.49	0.00	15.61	0.00	10.59	10.42	9.83	10.08	0.00	0.00	0.00	0.00	0.00	0.00
Mt	2.03	1.51	1.49	1.62	1.76	1.77	1.75	1.77	2.24	2.13	1.60	1.68	1.84	1.81
Il	5.26	3.08	2.23	2.58	2.76	2.75	2.66	2.70	8.69	4.14	3.14	5.70	3.47	5.34
Ap	0.73	1.23	0.73	0.70	0.56	0.56	0.54	0.54	2.90	1.17	0.91	1.84	1.19	1.73
Sum	100.03	100.04	100.03	100.03	100.02	100.02	100.02	100.02	100.08	100.04	100.03	100.05	100.04	100.05

ÅLAND, cont.	A14F-2	A15F-2	A16D-2	A17B-2	A18B-2	A19C-2	A20A-2	A21C-2	A22A-2
SiO_2, wt.%	46.97	46.78	47.29	47.22	47.23	47.23	46.94	47.00	48.15
TiO_2	1.76	1.38	1.74	1.80	1.72	1.71	1.72	1.95	1.39
Al_2O_3	16.00	17.06	16.23	15.92	16.2	16.14	16.05	16.06	16.80
FeO	12.96	12.70	12.31	12.56	12.38	12.52	12.58	12.15	11.90
MnO	0.19	0.18	0.18	0.18	0.18	0.18	0.18	0.16	0.18
MgO	6.82	6.58	6.88	6.86	6.97	7.07	7.00	6.67	6.45
CaO	9.24	9.12	9.59	9.47	9.57	9.53	9.52	9.24	9.33
Na_2O	2.45	2.63	2.37	2.37	2.52	2.55	2.50	2.59	2.70
K_2O	0.60	0.35	0.58	0.70	0.53	0.52	0.58	0.59	0.45
P_2O_5	0.29	0.16	0.33	0.33	0.31	0.31	0.30	0.37	0.22
Sum	**97.28**	**96.94**	**97.50**	**97.41**	**97.61**	**97.76**	**97.37**	**96.78**	**97.57**
Ba, ppm	270	191	306	312	295	300	281	322	245
Ce	53	33	49	30	30	39	30	55	20
Cu	67	58	55	61	58	61	70	67	60
Cr	174	46	200	200	195	187	196	215	71
La	11	10	11	11	<10	26	19	19	13
Nb	8	9	9	5	7	5	13	12	8
Ni	91	80	109	104	109	111	107	101	83
Rb	15	12	18	20	13	18	14	20	16
Sr	221	241	226	222	226	225	220	224	268
U	<2	<2	2	3	3	2	2	<2	<2
V	230	229	205	218	218	213	217	228	192
Y	38	29	38	38	37	36	37	42	30
Zn	127	111	116	118	122	116	116	128	105
Zr	122	80	130	134	123	124	122	146	96
CIPW									
Q	0.00	0.00	0.00	0.00	0.00	0.00	0.00	0.00	0.00
C	0.00	0.00	0.00	0.00	0.00	0.00	0.00	0.00	0.00
Or	3.65	2.13	3.52	4.25	3.21	3.14	3.52	3.60	2.73
Ab	21.31	22.96	20.57	20.59	21.85	22.07	21.73	22.65	23.42
An	31.75	34.78	32.75	31.55	32.09	31.77	31.69	31.47	33.20
Di	11.12	8.98	11.44	11.97	11.97	12.01	12.24	11.08	10.58
Hy	14.56	12.55	16.23	15.26	13.16	12.47	11.84	14.39	15.93
Ol	11.56	13.63	9.50	10.23	11.82	12.63	13.05	10.30	9.17
Mt	1.93	1.90	1.83	1.87	1.84	1.86	1.87	1.82	1.77
Il	3.44	2.71	3.39	3.51	3.35	3.32	3.36	3.83	2.71
Ap	0.71	0.39	0.80	0.80	0.75	0.75	0.73	0.91	0.53
Sum	100.03	100.02	100.03	100.03	100.03	100.03	100.03	100.03	100.02

SATAKUNTA	AM1-1AB/2AB	AM7-1B	S11HJ 10.1	S11HJ 14.1	IV15-1A	IV6-1A	S11GR 4.1	S11LS 5.1	HH2-1B	S11KA 4.1	S11VA 1.1	S11PL-1.1	S11VR 2.1	S11SG 1.1	S11OV 3.1	MA9-1D	MA1-1D
SiO_2, wt.%	52.34	50.79	50.09	49.69	51.84	51.99	51.13	50.31	51.93	50.91	51.28	50.34	50.90	57.83	49.24	51.95	52.14
TiO_2	2.98	2.85	2.65	2.63	3.03	3.04	2.32	2.63	1.74	2.09	3.19	2.28	2.29	1.90	2.32	3.03	3.04
Al_2O_3	12.66	13.49	14.02	14.01	13.45	13.24	14.65	14.04	14.56	14.94	13.16	14.48	14.62	14.11	14.68	13.44	13.28
FeO	12.96	13.30	13.20	13.29	12.73	12.85	11.95	12.39	10.95	11.62	13.93	12.89	11.94	7.26	13.25	12.65	12.91
MnO	0.18	0.18	0.18	0.18	0.17	0.17	0.17	0.17	0.15	0.16	0.18	0.18	0.17	0.10	0.18	0.17	0.17
MgO	4.63	3.90	4.45	4.58	3.57	3.52	5.23	5.26	5.00	5.50	3.46	5.17	5.20	2.59	5.78	3.62	3.55
CaO	3.70	6.78	8.18	8.41	7.30	7.54	7.88	7.55	7.42	8.01	7.20	7.96	7.96	5.08	8.42	7.46	7.52
Na_2O	3.74	2.30	2.49	2.47	2.38	2.34	2.51	2.32	2.58	2.48	2.31	2.38	2.47	3.57	2.48	2.31	2.29
K_2O	0.79	1.66	1.13	0.95	1.76	1.44	1.45	1.47	1.35	1.33	2.26	1.45	1.40	4.02	1.02	1.79	1.78
P_2O_5	0.74	0.67	0.62	0.60	0.76	0.78	0.58	0.74	0.44	0.50	0.91	0.55	0.58	1.38	0.47	0.75	0.76
Sum	**94.72**	**95.92**	**97.01**	**96.81**	**96.99**	**96.91**	**97.87**	**96.88**	**96.12**	**97.54**	**97.88**	**97.68**	**97.53**	**97.84**	**97.84**	**97.17**	**97.44**
Ba, ppm	202	945	655	537	756	744	604	917	605	543	868	598	593	3632	471	773	784
Ce	84	84	65	64	93	95	78	110	89	67	118	70	79	495	55	104	95
Cr	60	55	47	51	57	53	162	170	144	169	49	138	165	32	171	53	55
Cu	19	32	31	32	37	34	44	29	57	46	42	50	50	34	48	31	38
La	34	31	16	25	38	43	33	62	30	26	57	31	25	287	18	54	40
Nb	10	13	12	13	16	17	17	15	13	13	21	15	13	27	16	19	21
Ni	38	37	42	43	33	32	86	61	96	94	42	85	84	15	97	32	34
Rb	32	64	25	22	40	37	37	39	59	36	71	41	38	148	30	44	43
Sr	152	418	453	418	369	326	316	495	358	308	247	282	308	1595	268	327	326
U	<2	2	2	3	3	4	3	3	2	<2	4	<2	2	5	4	2	<2
V	223	240	231	239	230	234	202	187	174	194	229	222	207	103	227	233	229
Y	50	50	44	43	57	59	46	47	37	40	64	44	45	36	40	57	60
Zn	146	176	162	164	163	170	138	153	134	132	194	152	141	156	143	168	170
Zr	267	265	250	246	322	338	232	253	215	208	391	230	230	860	169	325	334
CIPW																	
Q	8.07	7.04	4.16	3.89	7.97	9.27	3.42	4.33	5.32	2.97	5.95	2.60	3.52	8.37	0.47	8.12	8.39
C	0.74	0.00	0.00	0.00	0.00	0.00	0.00	0.00	0.00	0.00	0.00	0.00	0.00	0.00	0.00	0.00	0.00
Or	4.93	10.23	6.88	5.80	10.72	8.78	8.76	8.97	8.30	8.06	13.65	8.77	8.48	24.28	6.16	10.89	10.80
Ab	33.41	20.29	21.72	21.59	20.76	20.43	21.70	20.26	22.71	21.51	19.97	20.62	21.43	30.88	21.45	20.12	19.89
An	14.28	22.50	24.47	25.14	21.46	22.05	24.96	24.31	25.14	26.35	19.27	25.13	25.30	10.84	26.48	21.63	21.24
Di	0.00	6.74	11.06	11.66	9.07	9.52	9.25	7.79	8.46	9.16	9.43	9.70	9.41	4.77	10.89	9.61	10.08
Hy	28.82	23.94	23.07	23.34	20.37	20.21	24.29	25.57	23.93	24.96	21.33	25.54	24.26	12.85	26.98	20.05	19.96
Ol	0.00	0.00	0.00	0.00	0.00	0.00	0.00	0.00	0.00	0.00	0.00	0.00	0.00	0.00	0.00	0.00	0.00
Mt	1.98	2.01	1.97	1.99	1.90	1.92	1.77	1.85	1.65	1.73	2.06	1.91	1.78	1.08	1.96	1.89	1.92
Il	5.98	5.65	5.19	5.16	5.94	5.96	4.50	5.16	3.44	4.07	6.19	4.44	4.46	3.69	4.51	5.93	5.93
Ap	1.85	1.65	1.51	1.47	1.86	1.91	1.40	1.81	1.08	1.21	2.20	1.33	1.41	3.34	1.14	1.83	1.85
Sum	100.05	100.05	100.05	100.04	100.05	100.05	100.04	100.05	100.04	100.04	100.06	100.04	100.04	100.08	100.04	100.05	100.05

SATAKUNTA, cont.	AT2-1B	SO3-1A	FB5-1B	FE5-1AB/1B	FF3-1B	FI1-1B	FK2-3C	FS3-1B	FT10-1A	FC1-1D	FC5-1A	FD6-1D	FH7-1AB	LK8-1B
SiO_2, wt.%	44.55	60.71	48.85	49.14	39.84	47.05	48.60	47.07	49.22	46.31	46.62	47.36	46.32	48.80
TiO_2	4.37	0.88	3.20	3.15	3.95	2.41	3.08	2.34	3.26	3.27	3.17	2.45	3.34	3.12
Al_2O_3	14.19	13.29	14.39	14.64	10.60	15.36	14.70	15.28	14.92	15.87	15.52	15.34	15.36	14.58
FeO	14.61	8.92	13.64	13.47	12.83	12.88	13.35	12.68	12.54	12.19	12.64	12.93	13.28	13.49
MnO	0.24	0.08	0.18	0.18	0.20	0.18	0.17	0.18	0.15	0.14	0.16	0.18	0.16	0.18
MgO	5.98	5.23	4.25	4.23	9.60	6.13	4.18	6.20	4.48	5.09	5.17	6.19	5.55	4.19
CaO	4.46	1.32	7.97	8.15	12.97	9.28	8.03	9.25	6.97	7.44	7.77	9.29	8.21	7.96
Na_2O	1.30	1.28	2.57	2.61	0.49	2.48	2.60	2.37	2.61	2.58	2.59	2.45	2.68	2.60
K_2O	2.96	4.28	1.35	1.33	1.94	0.83	1.29	0.75	1.39	1.38	1.27	0.84	1.10	1.34
P_2O_5	1.35	0.15	1.04	1.02	2.99	0.67	0.99	0.65	1.06	0.84	0.80	0.68	0.86	1.02
Sum	**94.01**	**96.14**	**97.44**	**97.92**	**95.41**	**97.27**	**96.99**	**96.77**	**96.60**	**95.11**	**95.71**	**97.71**	**96.86**	**97.28**
Ba, ppm	905	365	802	786	378	485	769	461	807	635	600	486	582	808
Ce	183	34	151	122	370	102	136	86	147	97	119	94	96	137
Cr	78	24	66	62	258	171	66	172	62	244	245	170	227	57
Cu	50	80	40	46	64	46	41	50	45	44	46	54	51	44
La	71	10	67	72	147	46	62	35	66	51	39	49	46	69
Nb	26	11	25	23	35	13	22	15	20	14	14	13	16	18
Ni	60	20	35	40	217	90	36	94	39	87	83	92	93	35
Rb	61	85	44	46	92	29	41	26	43	51	44	32	41	43
Sr	178	70	297	323	646	231	302	222	298	275	271	236	275	303
U	<2	<2	3	<2	<2	2	4	4	2	<2	3	<2	<2	4
V	205	143	190	182	247	200	182	206	192	162	159	210	161	185
Y	93	36	61	62	50	49	59	49	65	55	55	51	61	60
Zn	157	278	190	184	163	151	180	143	190	229	172	153	176	184
Zr	561	146	402	407	396	260	381	249	407	344	330	269	359	393
CIPW														
Q	3.87	21.74	2.78	2.67	0.00	0.00	2.49	0.00	4.20	0.00	0.00	0.00	0.00	2.62
C	4.22	4.69	0.00	0.00	0.00	0.00	0.00	0.00	0.00	0.00	0.00	0.00	0.00	0.00
Or	18.61	26.31	8.19	8.03	12.02	5.04	7.86	4.58	8.50	8.58	7.84	5.08	6.71	8.14
Ab	11.70	11.27	22.32	22.55	4.35	21.57	22.68	20.72	22.86	22.95	22.90	21.22	23.41	22.62
An	14.16	5.79	24.37	24.82	22.00	29.12	25.39	29.80	25.77	29.07	28.18	29.04	27.50	24.83
Di	0.00	0.00	7.76	8.12	20.30	11.37	7.57	10.97	2.39	3.30	5.52	11.26	7.27	7.49
Hy	33.04	26.76	23.86	23.31	9.38	17.86	23.62	21.51	25.46	23.62	23.00	19.33	18.09	23.78
Ol	0.00	0.00	0.00	0.00	14.88	6.81	0.00	4.38	0.00	2.06	2.43	5.79	6.43	0.00
Mt	2.25	1.35	2.03	2.00	1.95	1.92	2.00	1.90	1.88	1.86	1.92	1.92	1.99	2.01
Il	8.83	1.74	6.24	6.11	7.87	4.71	6.03	4.60	6.41	6.53	6.29	4.76	6.55	6.09
Ap	3.40	0.37	2.53	2.47	7.42	1.63	2.42	1.59	2.60	2.09	1.98	1.65	2.10	2.48
Sum	100.09	100.02	100.07	100.07	100.18	100.05	100.06	100.05	100.07	100.06	100.06	100.05	100.06	100.07

SATAKUNTA, cont.	NE1-1B	NI6-1B	NM1-1C	SA8-1B	FA9-1C	OJ2-2B	NO2-1B	NR6-1A	S11BR 5.1	S11SL 5.1	AO3-1A	JS16-A01B-1
SiO_2, wt.%	48.37	49.11	49.00	47.79	48.73	42.86	48.73	46.52	46.34	49.06	52.91	50.96
TiO_2	2.65	3.05	2.96	1.85	3.14	1.01	1.47	2.07	3.68	3.29	0.73	2.11
Al_2O_3	12.22	13.45	12.97	14.67	14.74	17.91	14.33	16.27	12.92	13.89	15.68	14.85
FeO	10.58	11.02	10.58	11.97	13.27	10.77	9.52	13.30	16.41	13.44	9.10	11.61
MnO	0.14	0.17	0.18	0.17	0.17	0.21	0.16	0.18	0.29	0.19	0.13	0.16
MgO	9.78	7.64	7.97	6.15	4.15	9.67	9.73	6.14	3.69	4.94	6.74	5.48
CaO	7.61	8.27	8.78	9.31	7.88	4.88	9.42	8.48	7.78	8.81	8.07	8.01
Na_2O	0.39	0.52	0.47	2.22	2.67	2.33	0.58	2.91	1.89	2.78	2.98	2.51
K_2O	2.26	1.67	1.65	1.63	1.36	1.56	2.10	0.44	2.01	0.89	0.57	1.34
P_2O_5	1.03	1.42	1.26	0.38	1.02	0.13	0.73	0.32	1.45	0.68	0.11	0.50
Sum	**95.03**	**96.32**	**95.82**	**96.14**	**97.13**	**91.33**	**96.77**	**96.63**	**96.46**	**97.97**	**97.02**	**97.53**
Ba, ppm	567	620	565	454	777	339	553	224	758	420	240	545
Ce	134	180	187	36	138	33	119	27	106	47	21	75
Cr	501	348	405	232	65	340	576	88	16	64	255	172
Cu	26	40	12	86	42	149	44	62	59	36	67	49
La	54	81	80	16	73	13	57	<10	37	25	11	22
Nb	34	42	38	11	25	8	16	7	15	20	10	13
Ni	249	164	205	69	39	219	172	87	12	62	151	92
Rb	88	71	70	52	46	38	86	13	106	28	25	37
Sr	300	903	755	247	301	216	539	296	487	532	375	309
U	3	<2	<2	2	5	2	<2	<2	<2	2	2	2
V	158	146	144	245	184	233	221	176	314	191	149	198
Y	32	37	34	26	60	20	25	36	44	34	15	41
Zn	147	158	168	122	189	100	103	127	233	160	87	135
Zr	265	330	315	175	393	61	140	155	154	184	83	210
CIPW												
Q	5.37	9.72	9.20	0.00	2.38	0.00	1.42	0.00	2.24	1.45	2.89	2.95
C	0.00	0.00	0.00	0.00	0.00	4.19	0.00	0.00	0.00	0.00	0.00	0.00
Or	14.05	10.25	10.18	10.02	8.28	10.09	12.83	2.69	12.31	5.37	3.47	8.12
Ab	3.47	4.57	4.15	19.54	23.26	21.59	5.07	25.48	16.58	24.01	25.99	21.78
An	26.22	30.56	29.65	26.26	24.93	25.58	31.31	31.08	21.60	23.27	28.58	25.94
Di	5.21	1.97	5.88	15.91	7.10	0.00	9.78	8.56	7.30	14.04	9.81	9.51
Hy	36.26	31.86	30.44	13.93	23.51	10.03	33.55	12.26	26.79	21.90	26.22	24.69
Ol	0.00	0.00	0.00	7.97	0.00	24.40	0.00	13.10	0.00	0.00	0.00	0.00
Mt	1.61	1.66	1.60	1.81	1.98	1.71	1.43	2.00	2.47	1.99	1.36	1.73
Il	5.30	6.02	5.87	3.66	6.14	2.10	2.89	4.07	7.25	6.38	1.43	4.11
Ap	2.57	3.49	3.12	0.94	2.49	0.34	1.79	0.78	3.56	1.64	0.27	1.21
Sum	100.07	100.09	100.08	100.03	100.07	100.02	100.05	100.03	100.09	100.05	100.02	100.04

HÄME	JS16-A02C/D-1	JS16-A03F-1	JS16-A04A-1	JS16-A05C-1	JS14-H1B-1/2	JS14-H1E-1/2	JS14-H2F-1	JS14-H3A-1	JS14-H4B-1/2	JS14-H6C-1	JS14-H7B-1	JS14-H7L-1	JS14-H11A	JS14-H12A	JS14-H13A1
SiO_2, wt.%	49.51	48.11	48.42	44.11	47.37	47.28	49.34	47.80	48.72	47.99	49.39	49.44	49.53	47.43	47.63
TiO_2	3.07	3.07	2.96	1.11	2.68	2.70	3.04	1.76	1.51	2.59	3.03	3.01	3.03	2.69	2.59
Al_2O_3	14.46	14.24	15.12	11.25	15.13	15.18	14.49	18.19	16.82	16.06	14.44	14.43	14.28	16.01	16.12
FeO	14.06	14.79	14.02	19.01	14.29	14.10	13.86	11.65	12.77	13.64	13.88	13.85	14.02	14.03	13.97
MnO	0.18	0.20	0.18	0.23	0.19	0.18	0.18	0.15	0.16	0.18	0.18	0.18	0.18	0.18	0.18
MgO	3.77	4.73	4.23	15.42	4.20	4.14	3.79	5.55	6.03	5.02	3.76	3.73	3.73	5.16	5.15
CaO	6.89	7.57	7.48	5.31	7.43	7.44	6.89	8.25	7.23	8.20	6.89	6.94	6.71	7.84	7.92
Na_2O	2.75	2.68	2.85	1.78	2.93	2.81	2.83	3.01	3.09	2.88	2.83	2.61	2.74	2.87	2.93
K_2O	1.85	1.73	1.77	0.80	1.91	1.91	1.97	1.10	1.50	1.43	2.00	2.06	1.92	1.41	1.38
P_2O_5	0.89	0.74	0.77	0.26	0.87	0.88	0.87	0.40	0.47	0.60	0.87	0.87	0.88	0.59	0.56
Sum	**97.43**	**97.86**	**97.80**	**99.28**	**97.00**	**96.62**	**97.26**	**97.86**	**98.30**	**98.59**	**97.27**	**97.12**	**97.02**	**98.21**	**98.43**
Ba, ppm	837	743	734	373	804	786	868	467	568	599	875	863	829	590	581
Ce	117	101	100	38	107	129	125	38	74	81	107	106	119	78	74
Cr	42	76	60	107	48	43	44	62	40	70	45	50	46	84	67
Cu	38	53	33	20	41	45	37	20	18	43	35	38	37	32	33
La	45	40	41	25	49	39	54	26	37	41	58	46	57	27	32
Nb	21	22	20	10	22	25	28	14	16	18	25	24	26	17	16
Ni	22	40	32	225	32	30	22	49	68	42	23	23	22	46	45
Rb	50	54	51	22	56	58	61	29	41	40	53	56	58	40	36
Sr	366	358	369	272	422	409	361	447	399	402	364	372	354	384	382
U	4	<2	3	2	3	<2	<2	3	3	<2	3	3	2	5	<2
V	190	201	179	78	151	146	195	112	95	167	190	191	191	178	161
Y	51	51	47	19	41	41	48	27	36	44	48	48	49	40	41
Zn	187	180	175	182	164	165	188	122	143	161	190	188	185	163	159
Zr	335	297	278	107	294	294	332	142	210	226	332	333	349	216	216
CIPW															
Q	2.18	0.00	0.00	0.00	0.00	0.00	1.26	0.00	0.00	0.00	1.27	2.22	2.38	0.00	0.00
C	0.00	0.00	0.00	0.00	0.00	0.00	0.00	0.00	0.00	0.00	0.00	0.00	0.00	0.00	0.00
Or	11.22	10.45	10.70	4.76	11.64	11.68	11.97	6.64	9.02	8.57	12.15	12.54	11.70	8.49	8.29
Ab	23.88	23.17	24.66	15.17	25.56	24.61	24.62	26.03	26.60	24.72	24.62	22.74	23.90	24.73	25.19
An	22.22	22.19	23.76	20.49	23.19	23.98	21.61	33.59	28.07	27.05	21.37	22.21	21.64	27.12	27.18
Di	5.83	9.45	7.61	3.55	7.55	6.98	6.49	4.62	4.41	8.57	6.69	6.24	5.70	7.16	7.55
Hy	24.49	20.86	20.25	9.54	12.93	15.68	23.98	9.47	11.12	12.84	23.85	24.03	24.57	12.61	11.61
Ol	0.00	3.99	3.38	40.99	9.69	7.55	0.00	13.57	14.89	9.86	0.00	0.00	0.00	11.24	11.82
Mt	2.09	2.19	2.08	2.78	2.14	2.12	2.07	1.73	1.88	2.01	2.07	2.07	2.10	2.07	2.06
Il	5.99	5.96	5.75	2.12	5.25	5.31	5.94	3.42	2.92	4.99	5.92	5.89	5.93	5.20	5.00
Ap	2.16	1.79	1.87	0.62	2.12	2.16	2.12	0.97	1.13	1.44	2.12	2.12	2.15	1.42	1.35
Sum	100.06	100.05	100.05	100.03	100.06	100.06	100.06	100.03	100.04	100.04	100.06	100.06	100.06	100.04	100.04

HÄME, cont.	JS14-H14C-1	JS14-H15C-1/2	JS14-H16E-1/2	JS14-H17A-1	JS14-H18A-1	JS14-H18C-1/2	JS14-H19A-3	JS14-H19H-2	JS14-H20F-1/2	JS14-H21a-1A/2A	JS14-H22B-1a/1d	JS14-H23A1	JS14-H24A1	JS14-H25B/E-1
SiO_2, wt.%	50.25	50.59	50.30	47.58	47.51	47.43	47.97	49.14	51.14	51.47	52.16	45.56	46.50	48.09
TiO_2	3.18	3.13	3.13	2.94	2.55	2.65	3.51	3.17	3.08	1.02	3.03	2.31	2.48	1.66
Al_2O_3	13.99	13.91	14.19	16.39	16.78	16.24	14.52	14.27	14.01	17.31	13.86	13.93	14.20	18.53
FeO	14.21	13.68	13.96	13.66	13.11	13.67	12.34	13.60	13.71	9.26	13.45	16.19	16.24	11.44
MnO	0.19	0.18	0.18	0.18	0.17	0.18	0.10	0.17	0.17	0.19	0.17	0.20	0.21	0.14
MgO	3.60	3.32	3.22	4.09	4.72	4.90	3.58	3.25	3.17	6.38	3.15	8.22	6.55	5.49
CaO	6.81	6.49	6.16	8.29	8.43	8.33	5.71	6.50	5.99	7.66	5.90	7.13	7.08	8.45
Na_2O	2.53	2.81	2.74	3.14	2.99	2.95	3.53	2.64	2.61	0.74	2.62	2.60	2.71	2.99
K_2O	2.22	2.50	2.59	1.71	1.34	1.36	2.43	1.86	2.63	2.74	2.71	1.33	1.41	1.07
P_2O_5	0.92	0.94	0.94	0.68	0.56	0.61	1.06	0.94	0.93	0.14	0.90	0.51	0.58	0.40
Sum	**97.90**	**97.55**	**97.41**	**98.66**	**98.16**	**98.32**	**94.75**	**95.54**	**97.44**	**96.91**	**97.95**	**97.98**	**97.96**	**98.26**
Ba, ppm	883	929	1086	749	551	574	816	1071	1158	274	1146	594	578	460
Ce	131	133	139	94	68	81	151	137	122	58	145	47	71	55
Cr	48	40	25	38	57	60	27	31	22	47	22	41	58	50
Cu	40	36	42	36	34	33	30	40	39	14	35	29	35	22
La	59	55	68	34	27	36	73	62	60	11	62	24	34	19
Nb	26	25	32	21	18	19	34	32	29	8	33	23	15	12
Ni	22	19	16	20	41	42	17	17	16	64	18	82	68	59
Rb	68	90	75	44	34	36	67	54	69	153	72	36	39	29
Sr	357	346	395	472	403	389	177	391	395	257	395	383	342	462
U	<2	3	<2	<2	4	2	<2	4	<2	<2	<2	<2	<2	2
V	194	186	162	178	161	174	170	163	162	140	162	157	149	104
Y	53	53	43	37	39	42	53	43	42	23	43	28	41	26
Zn	190	184	183	157	152	157	133	191	183	115	182	161	188	124
Zr	350	363	394	265	207	213	467	396	387	90	379	192	221	143
CIPW														
Q	3.44	2.71	2.61	0.00	0.00	0.00	0.00	4.23	4.50	5.58	5.54	0.00	0.00	0.00
C	0.00	0.00	0.00	0.00	0.00	0.00	0.00	0.00	0.00	0.00	0.00	0.00	0.00	0.00
Or	13.40	15.15	15.71	10.24	8.07	8.18	15.16	11.51	15.95	16.71	16.35	8.02	8.51	6.44
Ab	21.87	24.38	23.80	26.93	25.78	25.39	31.53	23.38	22.67	6.46	22.63	22.45	23.41	25.75
An	20.69	18.41	19.27	25.92	28.94	27.52	17.52	22.60	19.24	36.96	18.43	22.87	22.88	34.58
Di	6.49	7.03	4.92	9.48	8.32	8.76	4.26	4.00	4.26	1.08	4.62	8.15	7.61	4.51
Hy	23.66	21.98	23.27	4.88	8.89	9.62	14.91	23.65	23.14	29.50	22.44	5.52	11.57	10.08
Ol	0.00	0.00	0.00	13.29	11.82	11.98	5.13	0.00	0.00	0.00	0.00	24.91	17.45	12.82
Mt	2.11	2.03	2.08	2.01	1.94	2.02	1.89	2.06	2.04	1.39	1.99	2.40	2.40	1.69
Il	6.17	6.10	6.11	5.66	4.94	5.12	7.04	6.30	6.01	2.00	5.88	4.48	4.81	3.21
Ap	2.23	2.28	2.29	1.63	1.35	1.47	2.65	2.33	2.26	0.34	2.18	1.23	1.40	0.96
Sum	100.06	100.06	100.06	100.05	100.04	100.04	100.07	100.06	100.06	100.02	100.06	100.04	100.04	100.03

SUOMEN-NIEMI	JS16S02F-1/2	JS16S03F-1/2	JS16S04A-1	JS16S08E-2/3	JS16S09E-1	JS16S10I-1	JS16S11D-1	JS16S12A/B-1	JS16S13A/C-1	JS16S14E-2
SiO_2, wt.%	47.29	52.43	49.13	51.04	45.77	52.44	47.33	46.39	52.25	49.43
TiO_2	2.66	2.51	2.81	3.21	2.99	1.48	2.97	1.72	2.40	1.99
Al_2O_3	16.09	13.75	19.06	13.09	14.78	16.09	16.31	16.97	13.93	17.00
FeO	13.85	12.49	10.73	14.32	16.01	10.36	14.26	12.10	12.21	12.27
MnO	0.18	0.18	0.12	0.19	0.21	0.15	0.18	0.16	0.18	0.17
MgO	4.35	3.34	3.09	3.08	4.75	4.52	3.16	6.05	3.57	4.84
CaO	8.28	6.99	7.85	6.70	7.04	6.95	7.29	8.55	6.54	8.27
Na_2O	2.97	2.77	3.33	2.48	2.98	2.83	3.22	2.60	2.72	3.03
K_2O	1.36	1.82	1.22	2.26	1.32	1.96	1.74	0.92	2.02	1.35
P_2O_5	0.56	0.75	0.41	0.97	0.62	0.23	0.66	0.26	0.68	0.45
Sum	**97.59**	**97.03**	**97.75**	**97.34**	**96.47**	**97.01**	**97.12**	**95.72**	**96.50**	**98.80**
Ba, ppm	525	1050	493	839	591	688	701	296	1004	533
Ce	99	167	63	108	95	103	94	33	155	73
Cr	32	35	41	23	62	54	23	72	45	38
Cu	30	28	60	38	57	29	51	35	25	34
La	34	70	22	63	38	41	31	16	71	29
Nb	20	19	19	29	20	18	19	12	22	15
Ni	32	12	28	14	45	28	20	40	14	39
Rb	36	65	47	81	46	72	59	48	81	42
Sr	370	595	473	321	333	369	392	356	516	435
U	<2	2	2	3	3	4	2	<2	<2	<2
V	149	202	185	175	176	138	97	169	196	161
Y	45	60	29	60	51	37	52	33	58	35
Zn	155	182	114	192	164	131	180	119	189	139
Zr	223	353	169	424	261	294	297	151	330	192
CIPW										
Q	0.00	6.69	0.00	5.87	0.00	2.80	0.00	0.00	6.19	0.00
C	0.00	0.00	0.00	0.00	0.00	0.00	0.00	0.00	0.00	0.00
Or	8.24	11.09	7.38	13.72	8.09	11.94	10.59	5.68	12.37	8.08
Ab	25.75	24.16	28.83	21.56	26.14	24.69	28.06	22.98	23.85	25.95
An	27.21	20.31	34.23	18.40	23.90	26.19	25.65	33.34	20.55	29.15
Di	9.37	8.77	2.42	7.86	6.84	6.50	6.08	7.63	7.14	7.86
Hy	10.27	20.42	18.46	21.90	10.90	22.90	10.41	11.39	21.72	15.20
Ol	10.61	0.00	0.68	0.00	14.38	0.00	9.72	13.10	0.00	7.09
Mt	2.06	1.87	1.59	2.13	2.41	1.55	2.13	1.83	1.84	1.80
Il	5.18	4.92	5.46	6.27	5.89	2.90	5.81	3.41	4.73	3.83
Ap	1.36	1.83	0.99	2.36	1.52	0.56	1.61	0.64	1.67	1.08
Sum	100.04	100.05	100.03	100.06	100.05	100.02	100.05	100.03	100.05	100.04

SIPOO	SB10-1B	SB2-1D	SC1-1D	SF2-1B	SG2-1C
SiO_2, wt.%	45.35	45.13	45.24	44.69	45.09
TiO_2	4.11	4.07	4.13	4.11	4.08
Al_2O_3	14.13	14.08	14.13	14.00	14.09
FeO	15.56	15.83	16.14	15.85	15.94
MnO	0.19	0.20	0.20	0.20	0.20
MgO	4.27	4.24	4.33	4.33	4.26
CaO	7.49	7.43	7.62	7.28	7.47
Na_2O	2.81	2.86	2.88	2.79	2.90
K_2O	1.69	1.63	1.65	1.85	1.67
P_2O_5	1.16	1.14	1.15	1.13	1.13
Sum	**96.76**	**96.61**	**97.47**	**96.23**	**96.83**
Ba, ppm	786	789	780	782	796
Ce	129	143	132	125	131
Cr	44	47	50	36	50
Cu	48	47	43	41	42
La	63	60	57	67	58
Nb	40	32	38	37	35
Ni	32	32	33	33	35
Rb	56	46	50	56	50
Sr	356	356	359	349	353
U	3	2	<2	2	2
V	127	116	125	127	121
Y	62	60	60	60	59
Zn	143	190	201	158	202
Zr	490	482	472	472	480
CIPW					
Q	0.00	0.00	0.00	0.00	0.00
C	0.00	0.00	0.00	0.00	0.00
Or	10.32	9.97	10.00	11.36	10.19
Ab	24.57	25.05	25.00	24.53	25.34
An	21.65	21.50	21.29	21.00	21.17
Di	7.51	7.55	8.25	7.46	8.00
Hy	13.88	12.71	10.49	10.07	10.52
Ol	8.89	10.13	11.79	12.36	11.70
Mt	2.33	2.38	2.40	2.39	2.39
Il	8.07	8.01	8.05	8.12	8.01
Ap	2.84	2.80	2.80	2.78	2.76
Sum	100.08	100.07	100.07	100.07	100.07

APPENDIX III. Petrographic observations. Percentages are vol.%. ppl=plane polarized light, plg=plagioclase, ol=olivine, cpx=clinopyroxene, hbl=hornblende, bio=biotite, q=quartz, kfs=alkali feldspar, zr=zircon, ap=apatite, carb=carbonate, amp=amphibole, chl=chlorite, opx=orthopyroxene, sil=sillimanite, spi=spinel, serp=serpentine, op=opaque, ser=sericite, gar=garnet, musc=muscovite, saus=saussurite.

SAMPLE/DYKE	plg	ol	cpx	Other	Accessory minerals	Opaques	(Primary) Texture	Alteration level (low, moderate, high, very high)
ÅLAND								
A2F-3/A2	middle parts are more altered	-	-	hbl + bio + q not a diabase but andesitic	kfs + zr + ap + carb	elongated	granular, fine-grained	-
A2G-1/A2	60%, An45, <1,5cm compositional zoning	-	-	40% of secondary interstitial minerals (amp, chl, bio, carb)	ap+q	some elongated, some anhedral interstitial	subophitic	moderate
A3F-2/A3	50%, An35, euhedral, <2mm	5%, interstitial, altered to bio + op	40%, augite, interstitial, some cpx may be opx	metasedimentary xenolith (sil + spi)	secondary bio + amp + serp + chl + carb	10%, mainly anhedral interstitial, some elongated euhedral grains inside secondary mica (alteration of ol)	subophitic-ophitic	moderate
A5C-1/A5	50%, subhedral, mainly <<1mm, micro-phenocrysts <2mm, swallow tails & skeletal	-	5%, subhedral micro-phenocrysts <1mm	20% microcrystalline matrix, cracks and vesicles filled with op + carb + bio		25%, interstitial	preferred orientation of plg, glomerophyric (plg + cpx)	moderate
A8C-3/A8	50%, subhedral, mainly <<1mm, micro-phenocrysts <1mm, swallow tails	-	-	35% microcrystalline matrix + vesicles (<<1 mm) filled with bio + carb		15%, micro-phenocrysts (<1mm) + a lot in the matrix (+bio), mostly elongated euhedral grains (ilmenite)	preferred orientation of plg	moderate

A9A-3/A9	50%, subhedral, mainly <<1mm, microphenocrysts <1mm	-		45% matrix of secondary minerals	secondary bio+ carb	5%, anhedral spots	too altered to see	very high
A12B-3/A12	40%, mainly <1mm, microphenocrysts <4mm, swallow tails & skeletal, altered	-	-	40% microcrystalline matrix + vesicles (<1mm) filled with carb + q (no reaction rims)		20%, mainly euhedral elongated + in cracks anhedral reddish	preferred orientation of plg	high
A13E-1/A13	50%, mainly <<1mm, microphenocrysts <3mm, swallow tails and spherulites	-	-	45% microcrystalline matrix + vesicles (<1mm) filled with carb + q + bio + chl (round, no reaction rims)		5%, mainly euhedral elongated in matrix + in cracks	preferred orientation/flow texture of plg 70% of the thin section + 30% spheluritic	high
A14E-1/A14	45%, An30, subhedral, mainly <1mm, microphenocrysts 2mm	-	-	35% matrix of secondary minerals (chl + ser + bio)		20%, anhedral intergranular, some euhedral elongated	subophitic	high
A15E-1/A15	50%, An50, subhedral, mainly <<1mm, microphenocrysts <3mm, spherulites	-	-	45% matrix of secondary minerals (chl + amp + ser + bio)		5%, anhedral intergranular, a few subhedral enclosed by plg	ophitic	high
A19C-1/A19	50%, mainly <<1mm, microphenocrysts <1mm, swallow tails	10%, subhedral <<1mm grains	30%, interstitial, almost completely altered		secondary bio + chl + ser	10%, subhedral intergranular	subophitic	high
SATAKUNTA								
AM7-2AB/AM	50%, subhedral, <3mm, also very altered	-	40%, almost completely chloritized (+ possibly amp)	completely altered xenolith (3mm) of feldspar +op+ bio + chl + q	secondary amp+ chl + ser + carb + op	10%, anhedral interstitial + euhedral elongated	subophitic	very high

S11HJ 10.3/ S11HJ	50%, An45, subhedral, <3mm	-	40%, almost completely chloritized (+ possibly amp)		q + secondary carb + chl + ser	10%, anhedral interstitial + euhedral elongated	subophitic	high
S11HJ 16.1/ S11HJ	40%, subhedral, <1mm,	-	-	30% interstitial secondary minerals + 10% completely chloritized microphenocrysts (<1mm)		20%, anhedral interstitial + euhedral cubic & elongated	preferred orientation of plg	high
IV/IV	50%, An35, subhedral, <2mm, some are zonal	-	30%, almost completely chloritized (+ possibly amp)	secondary bio+ser		10%, anhedral interstitial/inter-granular	subophitic	high
S11GR 4.3/ S11GR	40%, mostly <<1mm, microphenocrysts ~1mm	-	-	30% microcrystalline matrix + 5% completely altered phenocrysts (<1mm)		25%, anhedral interstitial + euhedral cubic & elongated	preferred orientation of plg	moderate
MA9-1A/MA	55%, An60, subhedral, <3mm, altered (ser+ saus)	-	30% augite, interstitial and elongated	three “clots” of q + carb + bio + musc, reaction rims, vesicle-like	secondary: chl + bio + carb+ ser+ saus	15%, anhedral interstitial + euhedral cubic & elongated	subophitic, elongated crystal shapes	high
AT2-1AB/AT	35%, <1mm, subhedral, also very altered	-	-	30%, interstitial secondary matrix, 10% vesicles filled with q (mostly) + carb + secondary minerals (very round, no reaction rims)		25%, crack-filling+ mainly elongated intergranular	preferred orientation of plg	high
FE1-1B/FE	40%, An45, subhedral, mostly <1mm, microphenocrysts <3mm	-	-	30% microcrystalline matrix + 5% opx + 5% vesicles filled with q + carb + bio (no reaction rims)		25%, dendritic	could be ophitic	high

FK2-2B/FK	50%, An45, subhedral, <3mm, compositional zoning in some	-	-	10% opx, 10% secondary inter-stitial minerals + vesicles filled with bio+ carb+ musc	secondary musc + carb	30%, dendritic mainly between plg-laths	could be ophitic	high
NI6-1AB/NI	anhedral			amphibolite: amphibole (hbl)+ bio + plg + q + op	musc + ap	10%, anhedral interstitial	metamorphic: foliated, recrystallized	
FA5-1C/FA	40% mainly <1mm subhedral with swallow tails, some zonal ~2mm microphenocrysts	-	-	10% vesicles filled with q + carb + bio + op (no reaction rims), 30% microcrystalline matrix	-	20%, dendritic, possibly crystallized at the same time as plg	preferred orientation of plg, spherulitic,	high
OJ4-3AB/OJ	50% <<1mm, microphenocrysts ~1mm, almost completely altered to ser + carb	-	-	40% matrix: secondary chl + carb + ser + op + other alteration products	-	10%, in cracks and in matrix	too altered to see	very high
NO2-2B/NO	anhedral			amphibolite: amphiboles (hbl+ ortho-amp) + bio+plg	ap + q + cpx + zr	10%, anhedral interstitial	metamorphic: foliated, recrystallized	
NR6-1F/NR	50%, ~An40, euhedral, <2mm	-	-	20% microcrystalline matrix	-	30%, in cracks and in ground mass	could be primary ophitic	moderate
AO4-1A/AO	30% sub-/euhedral microphenocrysts of <1mm, swallow tails	-	-	50% spherulitic matrix, 20% opx-microphenocrysts	op	accessory, in cracks and in ground mass	microphenocrysts+ spherulitic/ feathery matrix	high

HÄME								
JS16-A02A-1/ JS16-A02	40%, mainly <<1mm, microphenocrysts <1mm, swallow tails, spherulites	-	-	35% microcrystalline matrix + vesicles (<1mm) filled with carb + q + bio		25%, intergranular, euhedral elongated and anhedral	spherulitic	high
JS16-A05B/ JS16-A05	40%, ~An55, mainly anhedral interstitial between ol with ol inclusions, also eu-/subhedral grains	45%, subhedral, forsteritic	10%, interstitial: ol, plg & op inclusions			5%, anhedral interstitial, crystall. before cpx	ol cumulate with plg and cpx intercumulus	low
JS14-H1A-1/ H1	55%, An45, mainly <2mm, microphenocrysts ~5mm	15%, euhedral and interstitial, very altered to op + serp	20%, interstitial, altered to amp		secondary carb + ser + amp + chl + bio	10%, anhedral interstitial + euhedral	subophitic-ophitic	high
JS14-H11D-2/ H11	40%, An40, subhedral, <2mm	-	40%, interstitial, almost completely altered	vesicles filled with q + carb + chl (no reaction rims)	secondary bio, amp,chl, ser	20%, mainly anhedral interstitial, also euhedral elongated	subophitic-ophitic	high
H12/H12	50%, An50, subhedral, <3mm	25%, anhedral interstitial	15%, anhedral interstitial		ap + zr + secondary: bio + op + serp + ser + chl	10%, anhedral interstitial, before cpx	nesophitic, subophitic domains	moderate
JS14-H13E-2/ H13	55%, mainly subhedral <1mm, also euhedral microphenocrysts <5mm with ol +op inclusions and compositional zoning	20%, eu-/subhedral and anhedral interstitial	20%, augite			10%, both euhedral (crystallized before cpx) and interstitial ones	nesophitic, subophitic domains	low

H13/H13	50%, euhedral + interstitial domains, <3mm	20%, interstitial with plg inclusions	20%, interstitial, reddish in ppl		secondary ser + bio + chl	10%, anhedral interstitial	nesophitic, subophitic domains, adcumulus-type plg growth	low
JS14-H14E-1/ H14	60%, An45, anhedral interstitial: poikilitic with cpx inclusions, <3mm	-	30%, augite twinning, subhedral		zr + ap + secondary bio	10%, elongated grains	intergranular dolerite, adcumulus-type plg growth	low
H14/H14	55%, An45, subhedral, <4mm, compositional zoning	15%, subhedral	20%, augite, interstitial		secondary bio + chl + ser	10%, anhedral interstitial + some elongated grains	nesophitic, subophitic domains	moderate
JS14-H15A-1/ H15	40%, <2mm, swallow tails and skeletal, spherulites	-	-	40% microcrystalline matrix + vesicles (<1mm) filled with carb + q + chl + bio (no reaction rims)	secondary carb + chl + bio + ser	20%, mainly elongated euhedral, also anhedral interstitial	spherulitic	high
JS14-H17D-1/ H17	45%, subhedral, <4mm, compositional zoning	20%, forsteritic, anhedral interstitial and subhedral, crystallized before cpx	20%, interstitial, possibly pigeonite		ap + secondary bio + chl,+ serp + op	15%, anhedral interstitial+ inclusions in plg	subophitic domains	high
JS14-H18B-1/ H18	55%, An45, subhedral, <2mm	25%, forsteritic, anhedral interstitial and subhedral , crystallized before cpx	35%, interstitial, reddish in ppl		secondary bio	10%, anhedral interstitial, large areas, crystall. after cpx	nes-/subophitic, ophitic domains	low
JS14-H20F-3/ H20	60%, An35, euhedral, mainly <<1mm, microphenocrysts <1mm	-	accessory, small spots (<<1mm), altered	10% vesicles of some kind filled with q + amp (<2mm)	secondary: amp + ser + chl + bio	30%, sub-/euhedral cubic and elongated, some anhedral	granular (plg + cpx + op), could be nesophitic	high

JS14-H23B-1/ H23	50%, An45, subhedral, <5mm	25%, forsteritic, anhedral interstitial and subhedral, crystallized before cpx	20%, interstitial	secondary bio + idd + ser	ap	5%, anhedral interstitial, crystallized before cpx	nesophitic	low
JS14-H24B-2/ H24	45%, An60, subhedral, up to 7mm	25%, forsteritic, anhedral interstitial and subhedral , crystallized before cpx	25%, augite, interstitial, reddish in ppl	secondary bio + ser	ap	5%, euhedral inclusions in cpx +anhedral interst., before cpx	ophitic	low
H24/H24	45%, An55, subhedral, <3mm	10%, subhedral	35%, augite, almost completely altered to amp, interstitial	secondary bio + amp + ser + chl + idd + op	ap	10%, anhedral interstitial + euhedral elongated(big)	ophitic	high
H25/H25	55%, An45, subhedral, up to 8mm, compositional zoning	20%, interstitial, also as inclusions in plg	20%, interstitial		ap, secondary idd	5%, anhedral interstitial, crystallized before cpx	nesophitic, subophitic domains	low
SUOMENNIEMI								
JS16S02G-2/ S02	40%, An55, subhedral, <5mm, some are zonal, relatively unaltered	15%, subhedral granular and anhedral interstitial	30%, reddish in ppl	secondary bio+chl	ap	15%, anhedral interstitial + subhedral elongated	nesophitic, subophitic domains	moderate
JS16S04C-3/ S04	50%, subhedral, up to 2cm, also very altered	-	40% altered cpx (chl + amp)	secondary: amp + chl + bio + ser		10%, anhedral interstitial	subophitic	very high

JS16S08F-1/ S08	50%, An45, subhedral, <1mm, relatively unaltered	-	40% almost completely altered cpx (amp), interstitial	secondary amp		10%, mainly elongated subhedral, some anhedral interstitial	ophitic	high
JS16S10I-2/ S10	50%, An30, subhedral, <2mm, relatively unaltered	-	45% completely altered cpx (amp), interstitial	secondary: amp + bio + ser		5%, elongated subhedral + anhedral interstitial	ophitic	high
JS16S12C-2/ S12	50%, subhedral, mostly <1mm, microphenocrysts <1,5mm	-	45%, completely altered cpx(amp), interstitial	secondary: amp + chl + ser		5%, mainly intergranular subhedral	ophitic	high
JS16S13E/ S13	50%, subheral, <1mm, also very altered	-	-	30% secondary interstitial minerals + q-xenocryst (4mm) with reaction rim		20%, euhedral + anhedral interstitial	could be subophitic/ophitic	very high
SIPOO								
SB1-1B/SB	60%, ~An45, subhedral <2mm, oriented, some are zonal	-	10%, interstitial	15% secondary bio	zr + ap	15% interstitial + euhedral, some inclusions in plg	preferred orientation of plg	high
SF2-1D/SF	plg 50%, sub-/euhedral, <2mm, quite altered	-	30%, no primary cpx: completely altered to amp, interstitial	secondary amp + bio + chl + ser		20%, elongated euhedral + interstitial /intergranular	subophitic	very high
SG9-1B/SG	50%, subhedral, <1mm	-	-	25% matrix: microcrystalline bio + other secondary minerals, 5% vesicles filled with bio+ carb + chl + op (no reaction rims),		25%, interstitial/-granular	could be intergranular or ophitic	very high